HETEROGENEOUS INTERACTION MODALITIES FOR SHAPE-SIMILAR FORMATIONS

A Dissertation
Presented to
The Academic Faculty

By

Ian Buckley

In Partial Fulfillment
of the Requirements for the Degree
Doctor of Philosophy in
Robotics

Georgia Institute of Technology

May 2020

HETEROGENEOUS INTERACTION MODALITIES FOR SHAPE-SIMILAR FORMATIONS

Dr. Magnus Egerstedt, Advisor
School of Electrical and Computer Engineering
Georgia Institute of Technology

Dr. Fumin Zhang
School of Electrical and Computer Engineering
Georgia Institute of Technology

Dr. Yorai Wardi
School of Electrical and Computer Engineering
Georgia Institute of Technology

Dr. Anirban Mazumdar
School of Mechanical Engineering
Georgia Institute of Technology

Dr. Michael West
Georgia Tech Research Institute
Georgia Institute of Technology

Date Approved: March 16, 2020

ACKNOWLEDGEMENTS

This work is the result of years of friendship, guidance, and support from a group of incredible people. I want to thank my advisor Dr. Magnus Egerstedt for challenging me to learn and encouraging me to grow as a researcher. I am grateful for the effort of my committee, which helped shape this work, and for the time that I spent working with Dr. Yorai Wardi and Dr. Michael West on exciting projects outside of this thesis. To Dr. Lauren Huie, thank you for your tutelage and tremendous words of advice. I want to thank the following educators for their critical and formative role in my life and work: Dr. Eric Johnson, Dr. Daniel Noneaker, Dr. Stephen Hubbard, Dr. Filiberto Mares, Lisa Norman, Jim Morris, Timothy McKnight, Robert Ellington.

My thanks goes to the members of the GRITSLab: Daniel Pickem, Matt Hale, Tina Setter, Li Wang, Sebastian Ruf, Siddarth Mayya, María Santos, Gennaro Notomista, Anqi Li, Chris Banks, Yousef Emam, Tatsuya Miyano, Soobum Kim, Pietro Pierpaoli, Sean Wilson, and the many visiting students we had the pleasure of working with—I am lucky to have been among these brilliant people. I want to thank my good friend Paul Glotfelter, with whom I shared an uncountable, but probably finite, number of fine coffee drinks as an excuse to share stray thoughts and big ideas, and my lifelong friend Patrick Reeves, with whom I've always been myself. Friends, even in the lean times, I wish that I had space to thank them individually: Andrew Fillingim, Kamil Saigol, Alex Chang, Chris Parker, William H. Attridge, Chase Frazelle, Zeyu Zhang, Sean Gorman, Josh Beste, Bastien Bacro-Duverger, George Seignious, Jake Riffle, Thad Moore, Conrad Bauknight.

I am blessed with a large, complicated, loving, and wonderful family, too many to name, and too precious not to. To my brother and best friend, Aidan; my father and stepmother, Claude and Elena; my mother and stepfather, Lala and Jim; my stepfathers, Rick and Peter; my grandparents, Tasa and Reid; my cousin, Adam; my godmother, Esther; my uncles, aunts, and cousins all; and a new family, Scott and Pam—thank you. And of course…

My erstwhile lab partner,

My companion,

My love,

Carley.

TABLE OF CONTENTS

LIST OF FIGURES

SUMMARY

Formation control of multi-robot teams is fundamentally influenced by the available sensing and communication capabilities of individual robots. The significance of these capabilities manifests in the network topology induced by interaction modalities present in the team, which may include maintenance of relative distances, bearings, or angles in the formation. To understand this significance and aid in design of effective control strategies, this thesis investigates the interplay between network topology and heterogeneous interaction modalities present in multi-robot formations. With regard to this investigation, each chapter of this thesis addresses a series of research questions that motivate and drive the results. The thesis begins by considering formations in which the relative angles between robots are maintained. To characterize such formations, infinitesimal shape-similarity is developed to describe frameworks in which angle maintenance renders the framework invariant to infinitesimal translations, rotations, and uniform scaling. After developing tools for assessing frameworks for this property, design of formation controllers for infinitesimally shape-similar frameworks reveals the sensing and communication requirements on the robots executing them. To explore relaxations of these requirements, a bearing-only self-assembly mechanism for a class of infinitesimally shape-similar frameworks is designed, and a formation-control strategy is developed to leverage a single distance measurement, suggesting that heterogeneity may be exploited at large. To relate heterogeneous distance, bearing, and angle constraints, the relationships between infinitesimal rigidity, bearing-rigidity, and shape-similarity are examined, espousing the coupling of network topology and interaction modalities in a team. The motions of formations specified by heterogeneous constraints are then characterized, and formation-control strategies are developed. Ultimately, this thesis demonstrates that the coupling of the network topology and heterogeneous interaction modalities of multi-robot teams should be accounted for explicitly to assess the tradeoffs between connectivity and information access in achieving effective formation control.

CHAPTER 1
INTRODUCTION

Inspired by naturally occurring multi-agent systems, where the global capabilities of a group, such as fish schooling or group transport by ants, can be studied through the local interactions between individual agents, this thesis considers motion coordination of mobile robot teams. Unlike their natural counterparts, multi-robot teams are engineered systems for which the interactions between individual robots, influenced by their available sensing and communication capabilities, must be designed; this design process necessitates a thorough understanding of the effects of inter-robot interactions on the ability of a team to accomplish a particular objective. To achieve this understanding and aid in design, this thesis explores the interplay between the interaction modalities between individual robots and the underlying network topology of multi-robot teams.

With regard to this exploration, multi-robot formations are used to expose the fundamental coupling of network topology and the interaction modalities of individual robots in a team. In terms of the potential impact and utility of this choice, justification for the use of multi-robot formations in furthering the purpose of this thesis is ample. At large, motion coordination of mobile robots, for which multi-robot formations are representative, has wide-ranging applications, both established and emerging, spanning a variety of domains such as undersea sensing network deployment [1], autonomous driving [2], autonomous warehousing [3], and environmental monitoring [4]. With regard to utility, control of multi-robot formations relies critically on exploiting both the network structure induced by the local interactions between robots and the information contained in those interactions.

Because of their centrality, the precise nature of the interaction modalities as they pertain to this thesis must be described. In a networked team, and in particular, in a multi-robot formation, individual robots typically have access to limited information about other robots,

a limitation that is imposed by the equipped sensing and communication mechanisms. These mechanisms can be used to measure functions of the relative robot states, and in this thesis, the interaction modalities between individual robots refer to maintenance of these functions, which include the relative distances, bearings, and angles in the formation. Because the capabilities of a multi-robot team are fundamentally impacted by the sensing and communication modalities available to the individual robots, the formation-control objectives that can be achieved by the team depend critically on the information that each robot has about its neighbors; this dependence is explored explicitly throughout this thesis.

For teams of robots that are not identically equipped, subsets of the team have access to different information that can give rise to *heterogeneous* interaction modalities, which can be leveraged when maintaining certain distances, bearings, and angles in the formation. In this thesis, consideration is given to the capabilities of individual robots in the context of formation control in order to characterize the mobility of the formation and to design controllers that exploit it. While introducing heterogeneity increases the complexity of developing tools for analyzing and controlling a multi-robot team, it is hypothesized that the heterogeneous interaction modalities that arise from the sensing and communication capabilities of individual robots broaden the capabilities of the team as a whole—this hypothesis is supported by the theoretical developments of this work and demonstrated in the design and deployment of formation controllers on teams of differential-drive robots.

Having broadly described the scope of this thesis and justified its purpose, the primary objective of this work and the driving research questions it seeks to answer are succinctly stated. *To aid in motion-coordination design, the objective of this thesis is to investigate the interplay between network topology and the heterogeneous interaction modalities available in multi-robot formations by addressing the following questions.*

- When the sensing modalities of a multi-robot team are restricted to bearing-only sensors, which are used to measure and maintain the relative angles between robots in formation, what types of formations can be achieved, and what are the available

motions of such formations? (Chapter 3)

- Through design of formation controllers for teams of robots described by infinitesimally shape-similar frameworks, how can the tools of infinitesimal shape-similarity be leveraged to achieve formation stabilization; what do these controllers require in terms of the sensing and communication modalities of the networked team; and what does this design process reveal about the necessity of heterogeneity in the available interaction modalities? (Chapter 4)

- In formation control of triangulations of robots, what is the result of limited incorporation of distance information to a multi-robot team that is otherwise restricted to bearing-only sensors? (Chapter 5)

- In terms of network topology as it relates to the interaction modalities of a networked team, what are the underlying relationships between infinitesimal rigidity, bearing-rigidity, and shape-similarity? (Chapter 6)

- When considering multi-robot formations characterized by the maintenance of distances, bearings, and relative angles, what types of formations can be achieved; what motions are available to such formations; and what control strategies can be employed to leverage the benefits of heterogeneity? (Chapter 7)

In brief summary of the approach taken to addressing these fundamental research questions, infinitesimal shape-similarity is developed to characterize formations in which the angles between robots are maintained; the theoretical underpinnings of this property are are readily amenable to formation control and highlight the importance of heterogeneity in the interaction modalities of a networked team. Infinitesimal shape-similarity is then connected to the related concepts of infinitesimal rigidity and infinitesimal bearing-rigidity, which, when taken together, provide a basis upon which the role of the heterogeneous interactions between robots in formation can be studied and exploited. Backed by these theoretical

developments, formation controllers are designed which leverage this understanding, and throughout this thesis, emphasis is placed on demonstration of the results using teams of differential-drive robots—the Robotarium, a remotely accessible swarm-robotics testbed at Georgia Tech, is used exclusively and repeatedly in this regard [5]. With these results and demonstrations, the thesis concludes having unequivocally substantiated the claim that network topology and the interaction modalities of a team are inextricably linked in the study and design of multi-robot formations.

In the following section, the technical contributions of this work are detailed in the order they are presented in this thesis, but before this summary, the following nuanced position must be made plain. The purpose of this work, reiterated for emphasis, is to explore the coupling between network topology and inter-robot interactions in the context of formation control. While the results of this work culminate in a series of formation controllers, the purpose of this work is not formation control, but rather to gain insight through design into the fundamental coupling of network topology and interaction modalities, a distinction that is evident from the research questions above. As such, discussion of the performance of the formation controllers is limited to narrow control-theoretic sense, rather than in broad comparison to the many established formation controllers in the literature, as this comparison does not further the objective of this thesis. Having described this important distinction in the research presented here, a summary of the technical contributions follows.

1.1 Summary of Contributions

The technical results of this thesis are partitioned into five chapters, each dedicated to addressing a specific set of research questions indicated in the previous section. Beginning in Chapter 3, infinitesimal shape-similarity is developed; this development follows the initialisms presented in [6] and [7], which are refined in [8]. First, infinitesimal shape-similarity is defined, and the shape-similarity matrix, the principle tool in assessing frameworks for infinitesimal shape-similarity, is derived. Conditions on the nullspace and rank of the

shape-similarity matrix are provided to certify infinitesimally shape-similar frameworks and identify pathological frameworks.

In Chapter 4, two controllers, based on the development of infinitesimal shape-similarity, are presented; these controllers appear in [9]. First, a controller is designed to stabilize a formation specified by desired angles; the stabilizing controller is simulated, and the limitations of this approach, as well as the sensing and communication requirements of the controller, are discussed. To improve upon this initial controller, a controller-synthesis approach to formation control is presented, which admits user-specified desired motion of the formation.

With revelations from the formation controllers for infinitesimally shape-similar frameworks in Chapter 4, Chapter 5 furthers the exploration of heterogeneous interaction modalities in formation control through design of formation controllers for a particular class of infinitesimally shape-similar frameworks, triangulations; this examination is based on work concerning the same subject in [7] and [10], which are united in [8]. Discussed in this chapter, certain triangulations are demonstrated to have a particular structure amenable to a leader-follower formation-control strategy in which all robots are equipped with bearing-only sensors, and a single robot is capable of additionally measuring distances.

With the case study in heterogeneity provided in Chapter 5, towards designing formation controllers to leverage heterogeneous interaction modalities in the networked team, Chapter 6 relates infinitesimal shape-similarity, rigidity, and bearing-rigidity. Algebraic relationships between the corresponding matrices of each framework property are first developed. Then, supported by these algebraic relationships, the implications of each framework property on the others, which varies with dimension, is described.

Continuing the investigation of the role of heterogeneous interaction modalities in design of formation controllers, Chapter 7 examines the available motions of frameworks specified by sets of distances, bearings, and angles. Then, a controller-synthesis formation-control strategy is presented for formations characterized by heterogeneous constraints to unite

the synthesis approach in Chapter 4 with the comparison of the framework properties in Chapter 6.

1.2 Organization

The thesis is structured as follows. Chapter 2 provides a detailed description of the background information relevant to the theoretical developments of this work; a description of the Robotarium is also provided in this chapter to support the demonstrations of the formation controllers provided throughout the text. In Chapter 3, the primary theoretical contribution of this work is presented; namely, the underpinnings of infinitesimal shape-similarity are discussed and tools for assessing frameworks for this property are developed. Chapter 4 applies the developments of the previous chapter on the design and implementation of formation controllers for infinitesimally shape-similar frameworks. In a particular instantiation, Chapter 5 examines control of triangulations to demonstrate the significance of heterogeneous interaction modalities in formation control. To further the examination of heterogeneous interaction modalities in formation control, Chapter 6 relates the framework properties of infinitesimal rigidity, bearing-rigidity, and shape-similarity; this comparison bears fruit in Chapter 7, which is concerned with control of formations specified by heterogeneous constraints. Finally, Chapter 8 concludes the examination of the interplay between network topology and the interaction modalities of a networked team. Appendix A includes several theorems regarding affine spaces that are critical in understanding the available motions of infinitesimally rigid and shape-similar frameworks in higher dimensions. For convenience to the reader, notation is introduced in situ, and Appendix B contains a glossary of notation used throughout the thesis.

CHAPTER 2
BACKGROUND

To support the exploration of the interplay between network topology and the heterogeneous interaction modalities of a multi-robot team, this section provides a summary of important background information that serves to support and contextualize the results of this thesis in the literature. With this regard, this section is divided according to the principle areas upon which the results draw. Read in sequence, these sections further develop the thesis argument and substantiate the approach taken as described previously in Chapter 1; read individually, each of these sections provides sufficient background information such that the significance of, and intuition behind, the results presented in subsequent chapters can be made clear.

To begin in Chapter 2.1, a description of graph theoretic methods in formation control is presented. As detailed in this section, the tools afforded by the graph theoretic approach immediately support the investigation into network topology and interaction modalities. Alongside the introduction of graphs and frameworks to represent multi-robot formations, several applications of these objects to formation control are presented in order to contrast the subject of these approaches with other formation control methods and to highlight their significance towards introducing the concepts of subsequent sections of this chapter, namely those of infinitesimal rigidity and bearing-rigidity.

Chapter 2.2 is dedicated to the introduction and description of the framework properties of infinitesimal rigidity and bearing-rigidity. The significance of these properties is made clear in the context of teams of robots equipped with particular sensing modalities capable of measuring distances and bearings.

In Chapter 2.3, background information on controller synthesis is provided; this approach, which yields controllers through solution of constrained optimization problems, is chosen to achieve formation control in Chapter 4 and Chapter 7. Details concerning the

structure and properties of the optimization problems are provided alongside examples of this approach in the greater context of robotics and autonomy, which supports the application of controller synthesis to formation control presented by this thesis.

Finally, Chapter 2.4 is devoted to a thorough description of the Robotarium, the swarm robotics testbed used throughout this thesis to demonstrate the theoretical results on teams of real robots.

2.1 Graph Theoretic Approaches in Formation Control

In this section, formation control, the medium through which the interplay between network topology and the sensing modalities of a networked team is investigated, is briefly introduced. While there are many approaches to the motion coordination problem of achieving and maintaining multi-robot formations, a few methods are highlighted to contrast with the graph theoretic approach to formation control pursued by this thesis. Because of the diverse and extensive literature available on multi-robot systems and formation control, the references provided here are not intended to be exhaustive, rather, the contrast with methods not necessarily relying on graphs highlights the natural application of graph theoretic approaches to formation control as considered in this thesis.

Formation control involves the design of appropriate coordinated control strategies for assembling and maintaining desired relative inter-robot states. Many approaches to formation control are surveyed by [11] and [12]. These references describe a variety of successful formation-control strategies that have been developed for a wide range of platforms and performance objectives, and while the techniques applied to this problem are varied, it is evident that formation control of multi-robot teams is fundamentally impacted by factors such as the sensing and communication capabilities of the robots, mobility considerations, and interactions with the environment; the impact of these factors is a primary driver in the choice of formation control as the means by which the interplay between network topology and the available interaction modalities is investigated.

As noted in [12], various classifications of approaches to formation control exist; for example, that of [13] classifies formation control methods under the following three categories: leader-follower, behavioral, and virtual structure. The leader-follower approach to formation control typically designates a single robot as the leader, which is controlled to achieve some task, while the remaining robots execute controllers to maintain the formation about the leader; for example, [14] adopts this approach, as do [15], [16], [17], and [18]. Behavioral approaches to formation control design controllers to execute certain behaviors, that when composed, result in coordinated motion; see [19] for an example. Finally, virtual structure approaches to formation control consider the formation as a whole, designing controllers for individual robots based on the desired motion of the structure; this approach is showcased in [20]. Other geometric approaches include the use of Jacobi shape space, as in [21], [22], and [23], which model formations as particles in a deformable body for which coordinate motion controllers can be designed.

In contrast with the aforementioned approaches to formation control and irrespective of the particular taxonomy introduced in [13] and used in [12], the following discussion highlights works that rely fundamentally on the use of graphs to drive the investigation and design of multi-robot formation controllers. As will be demonstrated by the literature in the remainder of this chapter, graph theoretic approaches are of particular relevance because they can be used to abstractly model the interactions between robots and because established graph-theoretic tools can be brought to bear in the study of multi-robot formation control.

Recognizing the centrality of network topology and robot interactions, many works, e.g., [24], [25], [26], etc., explore the dual issue of control design and determining what information should be shared between robots in a team. Notable for the direct influence of the graph topology and the admission of distributed implementations, the consensus protocol, described extensively in the previously cited references and cohesively presented in [27], serves as the foundation for many approaches to formation control, including recent examples such as [28] and [29]. Evident in the techniques described in [30] and

[27], approaches to multi-agent control benefit from the use of graphs to represent robot interactions, enabling the union of graph and control theoretic techniques to achieve desired collective behavior. As suggested by the surveys [11] and [12], characterization and control of multi-robot formations, a subject which is intimately related to the purpose of this thesis of exploring the interplay between network topology and the available interaction modalities, squarely fits the archetype of using graphs to represent robot teams; e.g., [25][31][32][33].

The breadth of literature espousing the graph theoretic approach to formation control demonstrates the relevance of these approaches to the exploration of the interplay between network topology and interaction modalities. Having introduced a spectrum of such works, the most relevant of the graph theoretic approaches to formation control, namely the topics of infinitesimal rigidity and bearing-rigidity as they apply to multi-robot formations, can be discussed to contextualize the results of this thesis with established results in the literature. However, prior to the description of these important properties, the following subsection explicitly defines graph and frameworks, the central objects used to abstractly represent multi-robot formations.

2.1.1 Graphs and Frameworks

Here, a concise introduction of graphs and frameworks is presented to support the results of this thesis; a thorough exposition of graph theoretic techniques is found in [34].

The graph $\mathcal{G} = (\mathcal{V}, \mathcal{E})$ consists of the vertex-set $\mathcal{V} = \{1, ..., n\}$ and the edge-set $\mathcal{E} = \{(i, j) | i, j \in \mathcal{V}, i \neq j\}$; let ϵ be the number of edges. The incidence matrix $H \in \mathbb{R}^{\epsilon \times n}$ is formed by: assuming an arbitrary orientation of the graph $\mathcal{G}$; and then assigning 1 to the element corresponding with i^{th} edge in row i and the j^{th} vertex in column j if j is the head of edge i, -1 if j is the tail of edge i, and 0 otherwise. The graph Laplacian $L \in \mathbb{R}^{n \times n}$ is given by $L = H^\top H$. Define $H_d = H \otimes I_d$, where $\otimes$ denotes the Kronecker product, and $L_d = L \otimes I_d$. Consider the incidence matrix of $\mathcal{G}$, which has $\text{rank}(H) = n - 1$, and $\ker(H) = \text{span}\{\mathbf{1}_n\}$; thus, $\text{rank}(H_d) = d(n - 1)$.

An embedding of the graph $\mathcal{G}$ in $\mathbb{R}^d$ is denoted by $G(x) = (\mathcal{G}, x)$, where $x = \left[x_1^\top, x_2^\top, ..., x_n^\top\right]^\top \in \mathbb{R}^{dn}$ is a vector of the d-dimensional positions of the vertices; $G(x)$ is conventionally referred to as a *framework*. The corresponding *complete framework* to $G(x)$ is $G^\kappa(x) = (\mathcal{G}^\kappa, x)$, where $\mathcal{G}^\kappa$ is the complete graph. Frameworks for which any of the vertex positions are the same are referred to as *degenerate frameworks.* For frameworks in which the positions of the vertices are functions of time, the framework is denoted $G(x(t))$; the *infinitesimal motion* of $G(x(t))$ is $\dot{x}(t) = [\dot{x}_1^\top(t), \dot{x}_2^\top(t), ..., \dot{x}_n^\top(t)]^\top$. For notational clarity, time dependence of the vertex positions is omitted when the presentation is unambiguous.

Restricting graphs and frameworks to the plane, the following definitions are particularly relevant to the results presented in Chapter 5.

Definition 2.1 ([34, pg. 243])**.** *A graph $\mathcal{G}$ is* planar *if it can be drawn in the plane so that its edges intersect only at their ends. The planar embedding of the graph $\mathcal{G}$ is a* plane graph*.*

In other words, plane graphs are frameworks $G(x)$ in which the vertices are embedded in the plane, i.e. $x \in \mathbb{R}^{2n}$, and the graph $\mathcal{G}$ is planar.

Definition 2.2 ([34, pg. 249])**.** *The* faces *of a plane graph are the arc-wise connected open sets partitioned by the embedding of the edges and vertices.*

The *outer face* of a plane graph is the only unbounded face of the plane graph; all other faces are *inner faces.* The *boundary* of a face is the boundary of the associated open set, and faces are adjacent if their boundaries share an edge. The *degree* of a face is the number of adjacent faces.

Definition 2.3 ([34, pg. 258])**.** *An* outerplane graph *is a plane graph for which all vertices lie on the boundary of the outer face.*

The adjacency of the faces of a plane graph are described by the weak dual graph, defined as follows.

Definition 2.4 ([35]). *The* weak dual graph *of a plane graph is the geometric dual graph, in which vertices correspond to faces of the plane graph and edges correspond to adjacency of the faces, less the vertex corresponding to the outer face.*

The results of Chapter 5, particularly the method used to assemble maximally outerplane graphs, rely on the use of graph grammars. Following the conventions in [36] and [37], a *labeled graph* is denoted $g = (\mathcal{G}, \nu, \xi)$, where ν is the set of vertex labels, and ξ is the set of edge labels. A *graph grammar* Φ consists of rules, ordered pairs of labeled graphs of the form $r = (g_l, g_r)$; applying r transforms g_l to g_r. With an initial labeled graph g_0, Φ defines a non-deterministic dynamical system (g_0, Φ). The trajectory of (g_0, Φ) is the sequence of graphs attained by applying Φ, denoted $\tau = \{g_k\}_{k=0}^{\infty}$.

2.2 Framework Properties

In this section, the fundamental framework properties of infinitesimal rigidity and bearing-rigidity are introduced. These framework properties, and the methods by which given frameworks are assessed for them, serve as a critical component in the foundation of this thesis because they inform the approach taken in the development of infinitesimal shape-similarity in Chapter 3. Furthermore, taken together with infinitesimal shape-similarity, infinitesimal rigidity and bearing-rigidity address one of the fundamental investigations of this thesis, namely the types of formations that can be achieved and the available motions of those formations under a given interaction modality. Infinitesimal rigidity, as the name suggests, is based on the maintenance of inter-robot distances, and so requires that these quantities be measured, while infinitesimal bearing-rigidity is based on maintenance of inter-robot bearings. The following subsections detail the principle tools and results of each of these framework properties.

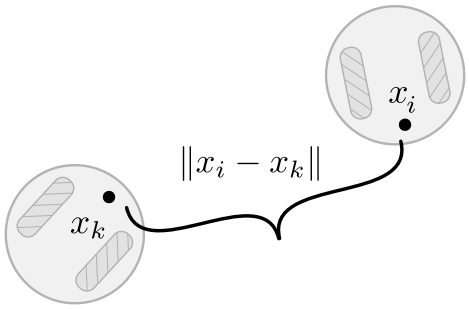

Figure 2.1: For multi-robot formations in which the distances between robots, pictured above as the norm of the difference of robot positions $\|x_i - x_k\|$, are maintained, infinitesimal rigidity indicates invariance of the formation to infinitesimal translation and rotation.

2.2.1 Infinitesimal Rigidity

When edges in a framework represent distances sensed between robots, as depicted in Figure 2.1, then the results of graph rigidity can be applied to multi-robot formations; this statement summarizes the relevance of graph rigidity to this thesis. The study of rigidity has a rich history, summarized in the first chapter of [38], and the development of many controllers for rigid formations draws from the results of [39], [40], [41], [42], and [43] on the rigidity of graphs. Motivated in a few words, rigidity is property of graphs for which almost all embeddings of the graph in $\mathbb{R}^n$ can be treated as rigid bodies by maintenance of the distances between the vertices [41].

Of particular relevance to formation control is the concept of infinitesimal rigidity presented in [42], which is a property of frameworks for which maintaining certain distances ensures invariance to translation and rotation. As discussed in works such as [44], questions of what distances need be specified to achieve a unique realization of the framework are related intimately to infinitesimal rigidity, but more importantly for this thesis, the property of infinitesimal rigidity gives conditions on the network topology for when the available motions of the framework are restricted to rigid body motions. To introduce infinitesimal rigidity in the parlance of this thesis, the following definition of infinitesimal rigidity is provided.

Definition 2.5. *A framework $G(x)$ is infinitesimally rigid if the only distance preserving*

motions are infinitesimal translations and rotations of the framework.

In Def. 2.5, a distance preserving motion is an infinitesimal motion of $G(x)$ for which

$$\frac{d}{dt}\frac{1}{2}\|x_i - x_j\|^2 = (x_i - x_j)^\top(\dot{x}_i - \dot{x}_j) = 0,\ \forall (i,j) \in \mathcal{E}; \tag{2.1}$$

if (2.1) implies that

$$\frac{d}{dt}\frac{1}{2}\|x_i - x_j\|^2 = (x_i - x_j)^\top(\dot{x}_i - \dot{x}_j) = 0,\ \forall (i,j) \in \mathcal{V} \times \mathcal{V}, \tag{2.2}$$

then the framework is infinitesimally rigid.

For assessing frameworks for infinitesimal rigidity, the condition in (2.1) can be written in matrix form. For a pair of vertices x_i and x_k, let $z_{ik} = x_i - x_k$. For a framework $G(x)$, let z_b, for $b = 1, \ldots, \epsilon$, be the vectors associated with each edge in $\mathcal{G}$ under arbitrary orientation; denote by $\mathrm{diag}(z_b) \in \mathbb{R}^{d\epsilon \times \epsilon}$ the matrix formed by arranging each vector z_b along the diagonal. Define the *distance-constraint function* $f_D : \mathbb{R}^{dn} \to \mathbb{R}^\epsilon$ to be

$$f_D(x) = \frac{1}{2}[\|z_1\|^2, \ldots, \|z_\epsilon\|^2]^\top.$$

The *rigidity matrix* is defined to be

$$R_D(x) = \frac{\partial f_D(x)}{\partial x} = \mathrm{diag}(z_b^\top) H_d. \tag{2.3}$$

Connecting the rigidity matrix to the condition in (2.2), a framework is infinitesimally rigid if the only $\dot{x} \in \ker(R_D(x))$ correspond with infinitesimal translations and rotations of the framework.

Having introduced $f_D(x)$ and developed the rigidity matrix $R_D(x)$, the definition of infinitesimal rigidity given in [42] can now be presented using the notation of this thesis:

Definition 2.6 ([42])**.** *Let $f_{D,\kappa}(x)$ be the distance constraint function of $G^\kappa(x)$, let $p =$*

$\dim(\text{aff}\{x\})$ *be the dimension of the affine hull of* x*, and let* $T(x)$ *be the tangent space to the* $d + \frac{1}{2}d(d-1) - \frac{1}{2}(d-p)(d-p-1)$ *dimensional smooth manifold* $f_{D,\kappa}^{-1}(f_{D,\kappa}(x))$*.* $G(x)$ *is infinitesimally rigid in* $\mathbb{R}^d$ *if* $T(x) = \ker(R_D(x))$*.*

Despite the apparent difference in the language, Def. 2.5 and Def. 2.6 are equivalent definitions of infinitesimal rigidity. Information on affine spaces is found in Appendix A.

Explicit use of the definition of infinitesimal shape-similarity is cumbersome to apply when determining whether a given framework has this property, so a rank condition on the rigidity matrix is used by [42] to assess frameworks for infinitesimal rigidity. The rank condition was presented in-text in [42], but is included here as a theorem for emphasis.

Theorem 2.1 ([41])**.** *Let* $p = \dim(\text{aff}\{x\})$ *be the dimension of the affine hull of* x*. A framework* $G(x)$ *is infinitesimally rigid if and only if the rank of the rigidity matrix is given by*

$$\text{rank}(R_D(x)) = nd - d - \frac{1}{2}\left(d(d-1) - (d-p)(d-p-1)\right).$$

Intuition behind this rank condition is drawn from the fact that a rigid body has d degrees of freedom due to translation and $\binom{d}{2} - \binom{d-p}{2}$ degrees of freedom due to rotation. The rank condition on the rigidity matrix allows for the quick assessment of a given framework for infinitesimal rigidity. When considering formations as in Chapter 3, for which the angles between vertices are maintained, inspiration from graph rigidity drives the development of infinitesimal shape-similarity and a rank condition on the shape-similarity matrix.

The study of graph rigidity, and that of infinitesimal rigidity in particular, has been leveraged extensively in formation control to reason about teams of robots capable of measuring inter-robot distances; for example, the authors of [45] describe an architecture in which graph theoretic techniques and rigidity can be applied to formation control of distance-measuring robots to achieve such tasks as merging and splitting. Here, a non-exclusive discussion of some specific works is included to highlight problems that have been addressed using rigidity-based methods for formation control.

Design of rigid frameworks, merging and splitting of formations, formation stabilization, and rigidity maintenance are among the many tasks considered in the application of graph rigidity to formation control. In particular, [46] considers the issue of determining which edges to include in the framework, an important issue when designing the structure of a formation for a particular task, assuming that robots are equipped with line-of-sight sensors capable of determining the relative positions of robots in formations; the authors propose Delaunay triangulations as an alternative to the Henneberg construction [47] for generating generically isostatic (i.e. generically minimally rigid) graphs. The choice of which edges to include in the framework is important not only for achieving rigidity of the underlying graph, but also in asymptotically stabilizing the robots to desired formations [32][48]; in [49] and [50], connections between formation stabilization and rigidity are explored. Similarly, [14] is concerned with formation stabilization, proving necessary and sufficient conditions on formation stabilization under a particular leader-follower architecture for formation control. In addition to formation stabilization, other works have designed strategies for rigidity maintenance [51] [52], allowing the topology of the underlying interaction graph to change as the formation moves.

2.2.2 Infinitesimal Bearing-Rigidity

As graph rigidity applies to formations of robots capable of measuring distances, infinitesimal bearing-rigidity, and in Chapter 3, infinitesimal shape-similarity, are motivated by considering teams of robots equipped with bearing-only sensors, which yield direction but not distance information as indicated in Figure 2.2.

Bearing-only approaches to formation control have recently received significant interest, resulting in a number of formation controllers designed around the limited sensing capabilities of the robots; e.g., [53], [54], [55], etc.. Infinitesimal bearing-rigidity, detailed in [56], [57], and [58], is a property of frameworks for inter-vertex bearing maintenance results in invariance to infinitesimal translation and uniform scaling.

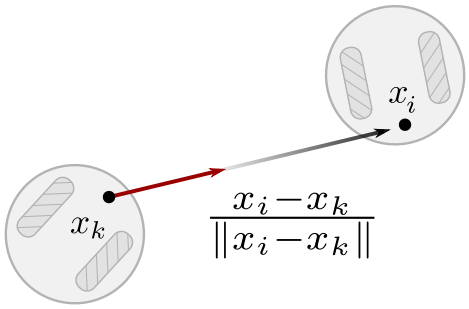

Figure 2.2: For multi-robot formations in which the bearings between robots, pictured above as the red unit vector $\frac{x_i - x_k}{\|x_i - x_k\|}$, are maintained, infinitesimal bearing-rigidity indicates invariance of the formation to infinitesimal translation and uniform scaling.

Definition 2.7 ([57, Defintion 5])**.** *A framework is infinitesimally bearing-rigid if all the infinitesimal bearing motions are trivial.*

To explain Def. 2.7, the following notation is introduced. The bearing from x_k to x_i is

$$\hat{z}_{ik} = \frac{z_{ik}}{\|z_{ik}\|}.$$

For a framework $G(x)$, let $\hat{z}_b$, for $b = 1, \ldots, \epsilon$, be the bearings associated with each edge in $\mathcal{G}$ under arbitrary orientation, and denote by $\mathrm{vec}(\hat{z}_b) \in \mathbb{R}^{d\epsilon}$ the concatenation of these bearings. Define the *bearing-constraint function* $f_B : \mathbb{R}^{dn} \to \mathbb{R}^{d\epsilon}$ to be

$$f_B(x) = [\hat{z}_1^\top, \ldots, \hat{z}_\epsilon^\top]^\top = \mathrm{vec}(\hat{z}_b).$$

The bearing-rigidity matrix is defined to be

$$R_B(x) = \frac{\partial f_B(x)}{\partial x} = \mathrm{diag}\left(\frac{Q_{z_b}}{\|z_b\|}\right) H_d, \tag{2.4}$$

where

$$Q_{z_b} = I_d - \frac{z_b z_b^\top}{\|z_b\|^2}$$

is the orthogonal projection matrix with respect to z_b.

Referring to Def. 2.7, $\dot{x}$ is a infinitesimal bearing motion if $\dot{x} \in \ker(R_B(x))$, and such

motions are trivial if they correspond with translations or uniform scalings of the framework. As with infinitesimal rigidity, the following rank condition on the bearing-rigidity matrix allows for arbitrary frameworks to be assessed for this property.

Theorem 2.2 ([57, Theorem 4])**.** *For a framework $G(x)$ in $\mathbb{R}^d$, $G(x)$ is infinitesimally bearing-rigid if and only if*

$$\operatorname{rank}(R_B(x)) = nd - d - 1.$$

The intuition behind this rank condition on the bearing-rigidity matrix is drawn from the fact that there are d degrees of freedom due to translations and one degree of freedom due to uniform scaling.

Infinitesimal bearing-rigidity has received interest for its application to multi-robot formations; e.g., [56][57][58][59][60]. Contrasting with rigid frameworks, where edges correspond with distances between robots, for bearing-rigid frameworks, edges represent inter-robot bearings, a sensing modality in which an angle between robots is measured relative to a reference frame. Resulting from this difference, infinitesimally bearing-rigid frameworks are invariant to translation and uniform scaling if certain inter-robot bearings are maintained, further highlighting the coupling between network topology and robot capabilities. Examples of bearing-rigidity-based formation-control strategies include [57], [61], [62], [63], and [64].

2.3 Controller Synthesis

The formation-control strategies for infinitesimally shape-similar frameworks in Chapter 4, and the strategies for controlling frameworks relying on heterogeneous interaction modalities in Chapter 7, feature the use of a particular optimization-based approach to synthesis of formation controllers. Various approaches to synthesis of controllers for multi-agent systems, such as [65] and [66], are represented in the literature. So too are examples of optimization-

based approaches to formation control, including approaches based on the Linear Quadratic Regulator (LQR) and Model Predictive Control (MPC); e.g., [67], [68], [69], [70], etc..

The decision to apply controller synthesis to formation control of infinitesimally shape-similar frameworks is motivated by observation of the formation controllers surveyed in [11] and [12]. Sampled approaches referenced by these surveys address formation stabilization, in which the origin of an error system characterizing the difference between desired and current functions of the relative robot states is made stable, while the formation moves (e.g., [14], [32], [71], etc.). Recognizing that formation stabilization is a constraint on the motion of the formation, controller synthesis can be used to arbitrate between potentially competing, high-level, user-designated objectives and the low-level constraint that the formation should be maintained. With this regard, this thesis applies controller synthesis to formation control.

Though not in the context of formation control, the particular optimization-based approach to controller synthesis used in this thesis has recently been demonstrated as an effective means of constraint satisfaction for robotic systems [72][73][74][75][76]. The referenced approaches to controller synthesis solve a Quadratic Program (QP) in which constraints on the solution are encoded through inequality constraints derived from Control Lyapunov Functions (CLFs) or Control Barrier Functions (CBFs).

Precisely, the controller-synthesis approach to formation control presented in this thesis relies on repeatedly solving, point-wise in time, quadratic programs of the following structure:

$$\begin{aligned} u^* = &\arg\min_{u\in\mathbb{R}^{dn}} \frac{1}{2}\|u-u^{\text{nom}}\|^2 \\ &\text{s.t.} \quad \frac{\partial V(x)}{\partial x}u \leq -\rho V(x), \\ &\qquad \frac{\partial h(x)}{\partial x}u \geq -\eta h^3(x). \end{aligned} \tag{2.5}$$

where $\rho, \eta \in \mathbb{R}_+$. In the QP of (2.5), u^{nom} is the nominal controller for the framework; the first inequality in (2.5) ensures that the Lyapunov function $V(x)$ is a CLF, and the second inequality ensures that $h(x)$ is a CBF. In this thesis, the CLF constraint will be used to achieve formation stabilization, while the CBF constraint will be used to achieve

collision avoidance; the nominal controller will be used to direct the motion of the formation according to a higher-level objective.

The benefits of this approach to controller synthesis are well documented in the referenced works, but in brief summary: QPs can be solved efficiently, supporting their use in real-time robotics applications; and CLFs and CBFs are implicit methods, which respectively guarantee stability or set invariance without requiring explicit knowledge of the state trajectory. The benefits of this approach to controller synthesis apply in the context of formation control; furthermore, this approach provides a structured way of incorporating user-designated objectives for the multi-robot formation.

2.4 The Robotarium

The Robotarium, a remotely-accessible swarm-robotics testbed at Georgia Tech [5], is described to support the clear demonstration of the formation-control algorithms of this thesis. The Robotarium is populated by small differential-drive robots, which drive on a flat surface, where demonstrations and experiments are performed. The positions of the robots are tracked using reflective IR markers by motion capture cameras arrayed above the testbed surface. A projector and webcam are mounted directly above the testbed surface, allowing information, such as adjacency information or virtual obstacles, to be visualized in real-time. The robots are not equipped with physical sensors and communicate only with a central server, which executes user-submitted MATLAB or Python code to control the robots; as such, communication and sensing constraints are enforced virtually and totally according to the user-submitted code.

In this thesis, formation controllers are designed to drive the motion of the positions of vertices in a framework rather than the positions of robots; as such, the controllers presented in this work are designed under the assumption that robots in formation have single-integrator dynamics of the form $\dot{x}_i = u_i$, i.e., that the velocities of the robots can be specified directly, whereas the differential-drive robots are modelled as unicycles. To

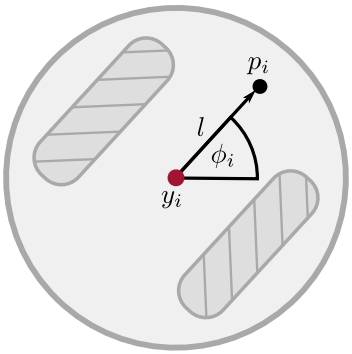

Figure 2.3: The differential-drive robots of the Robotarium are modelled by the unicycle model; by controlling the velocity of the point p a short distance l ahead of the position $[y_{1,i}, y_{2,i}]^\top$, orthogonal to the wheel axis, the differential-drive robots can execute controllers designed for single-integrators.

address this discrepancy, a mapping from single-integrator to unicycle dynamics is used.

The differential-drive robots of the Robotarium are modelled as unicycles:

$$\begin{bmatrix} \dot{y}_{1,i} \\ \dot{y}_{2,i} \\ \dot{\phi}_i \end{bmatrix} = \begin{bmatrix} \cos(\phi_i) & 0 \\ \sin(\phi_i) & 0 \\ 1 & 0 \end{bmatrix} \begin{bmatrix} v_i \\ \omega_i \end{bmatrix},$$

where, $[y_{1,i}, y_{2,i}]^\top$ is the position of robot i, ϕ_i is its heading, and its control inputs are v_i, the translational velocity, and ω_i, the rotational velocity.

Consider a point $p_i = [p_{1,i}, p_{2,i}]^\top$, with velocities $\dot{p}_i$, a short distance l ahead of the robot as shown in Figure 2.3. The following near-identity diffeomorphism, as in [77], maps from $\dot{p}_i$ to the control inputs of the unicycle:

$$\begin{bmatrix} v_i \\ \omega_i \end{bmatrix} = \begin{bmatrix} \cos(\phi_i) & \sin(\phi_i) \\ -\sin(\phi_i)/l & \cos(\phi_i)/l \end{bmatrix} \begin{bmatrix} \dot{p}_{1,i} \\ \dot{p}_{2,i} \end{bmatrix}. \tag{2.6}$$

Setting $p_i = x_i$ and $\dot{p}_i = u_i$, the mapping in (2.6) allows the differential-drive robots to execute formation controllers designed for single-integrators.

CHAPTER 3
ANGLE CONSTRAINED FORMATIONS AND INFINITESIMAL SHAPE-SIMILARITY

With respect to the overarching objective of exploring the interplay between network topology and the interaction modalities available in a multi-robot team, this chapter focusses on determining the types of formations that can be achieved and the motions available when robots in formation are restricted to bearing-only sensors that are used to measure and maintain the relative angles between robots in formation. Specifically, this chapter examines frameworks with a particular property, infinitesimal shape-similarity, which characterizes the types of formations that can be achieved by maintaining the relative angles between robots. Infinitesimal shape-similarity, and the tools described in this chapter to assess arbitrary frameworks for this property, were first introduced in [6] and [7], and were refined in [8].

This chapter is structured in the following way. Beginning in Chapter 3.1, infinitesimal shape-similarity is defined. In Chapter 3.2, the shape-similarity matrix, the primary tool for characterizing frameworks for infinitesimal shape-similarity, is developed. Chapter 3.3 examines the nullspace of the shape-similarity matrix, yielding a rank condition on the shape-similarity matrix for assessing frameworks for infinitesimal shape-similarity. Finally, the conclusions of this section as they pertain to the objective of this thesis are provided in Chapter 3.4.

3.1 Infinitesimal Shape-Similarity

Here, infinitesimal shape-similarity, a framework property, is defined. Consider a framework $G(x)$ with vertex positions $x = [x_1^\top, x_2^\top, \ldots, x_n^\top]^\top \in \mathbb{R}^{dn}$, and denote by Θ_S the angle-set, which contains all m angles formed between three distinct, connected vertices in the

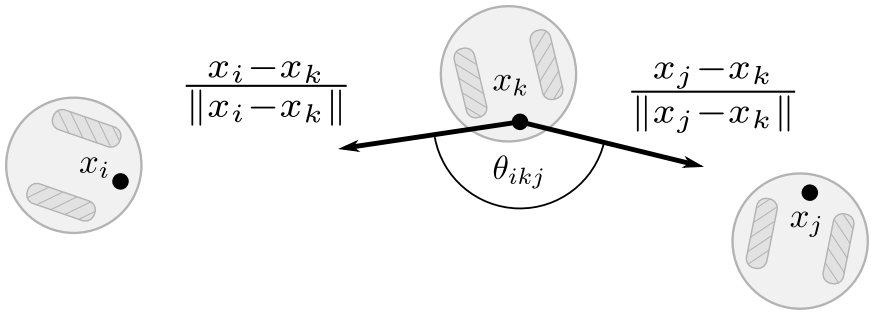

Figure 3.1: Inter-robot bearings capture direction relative to a coordinate frame and are represented as unit vectors. Pairs of bearings define angles independently of a coordinate frame; infinitesimal shape-similarity characterizes frameworks for which these angles are maintained.

framework; i.e., $\Theta_S = \{(i,k,j) | (i,k),(j,k) \in \mathcal{E}, i \neq j\}$. For $G(x)$, let

$$\theta(x) = [\ldots, \theta_{ikj}, \ldots]^\top \; \forall (i,k,j) \in \Theta_S$$

be the vector of angles formed between three distinct, connected vertices, where the angle between the vectors $z_{ik} = x_i - x_k$ and $z_{jk} = x_j - x_k$ centered on x_k, shown in Figure 3.1, is given by

$$\theta_{ikj} = \cos^{-1}\left(\frac{z_{ik}^\top z_{jk}}{\|z_{ik}\|\|z_{jk}\|}\right). \tag{3.1}$$

Having introduced the angles of $G(x)$ according to (3.1), consider infinitesimal motions of the framework under which these angles remain constant.

Definition 3.1. *Infinitesimal motions $\dot{x}$ of the framework $G(x)$ are* angle-consistent motions[1] *if $\frac{d}{dt}\theta(x(t)) = 0 \; \forall t \geq 0$; the trajectory $\{x(t)\}$ of the framework $G(x)$ is angle-consistent if $\dot{x}$ is angle-consistent.*

Of particular interest are angle-consistent infinitesimal motions that preserve the shape of $G(x)$, where the shape[2] refers to the initial angles of the corresponding complete framework $G^\kappa(x(0))$. Geometric intuition and parallels with rigidity and bearing-rigidity correctly

[1] Angle-consistency was stated in [6], defined in [7], and is clarified here.

[2] This notion of shape was used in [6] and is explicitly stated here using the notation of this work for cohesiveness and clarity.

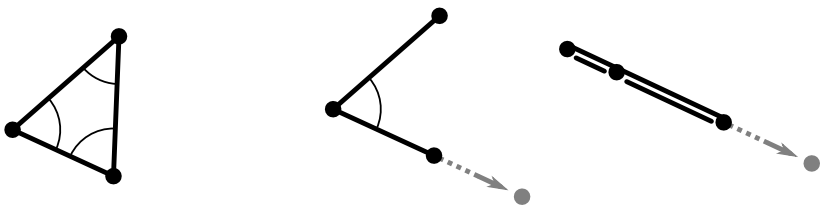

Infinitesimally Shape-Similar

Not Infinitesimally Shape-Similar

Figure 3.2: The left framework is infinitesimally shape-similar. In contrast, the right frameworks are not infinitesimally shape-similar because, due to network topology and pathological configuration, angle-consistent motion along the dotted lines is not a translation, rotation, or uniform scaling.

suggest that the shape of the framework will be maintained by only applying infinitesimal translations, rotations, and uniform scalings to the framework; however, depending on the underlying graph topology, there may exist angle-consistent motions of $G(x)$ that do not preserve its shape—infinitesimal shape-similarity captures this notion.

Definition 3.2. *The framework $G(x(t))$ is* infinitesimally shape-similar[3] *if all angle-consistent trajectories only result in translations, rotations, and uniform scalings of $G(x(0))$.*

Infinitesimal shape-similarity as defined in Def. 3.2 requires that all angle-consistent motions of the framework be shape-preserving, which is a property that depends on the underlying graph topology and does not hold for frameworks at large; for example, consider the frameworks of Figure 3.2. Furthermore, in order for frameworks to be infinitesimally shape-similar, the angles between vertices in the framework must be defined; thus, the frameworks under consideration must have at least three vertices and not be degenerate. The following sections develop analytical tools to determine whether a given framework is infinitesimally shape-similar, but before proceeding, reference to recent and related constructions should be made. Related to infinitesimal shape-similarity, infinitesimal angle-rigidity is described in [78]; the definition of infinitesimal angle-rigidity amounts to the definition of infinitesimal shape-similarity when restricted to the plane. The approach taken in [78] follows that of [42], and the results are compared against [57]. While the work

[3]Infinitesimal shape-similarity was originally defined in [6] with reference to the shape of the framework; here, the definition is clarified to include reference to the initial conditions $G(x(0))$.

of [78] is related to this thesis, there are many substantive differences between them in terms of the approaches taken and results achieved, for example, the use of an index set of angles rather than the set of all angles of the formation as used in this thesis; as such, [78] is complementary.

3.2 The Shape-Similarity Matrix

This section develops the shape-similarity matrix, the primary tool for investigating the infinitesimal shape-similarity of a given framework. To begin, consider angle-consistent motions of $G(x)$. Rather than considering the time derivatives of these angles directly as in [6] and [7], the time derivatives of the cosines of these angles are shown to be zero along angle-consistent trajectories of $G(x)$.

Proposition 3.1. *For angles θ_{ikj} as described in* (3.1)*, $\dot{\theta}_{ikj} = 0$ if and only if $\frac{d}{dt}\cos(\theta_{ikj}) = 0$.*

Proof. Suppose $\dot{\theta}_{ikj} = 0$; then,

$$\frac{d}{dt}\cos(\theta_{ikj}) = -\sin(\theta_{ikj})\dot{\theta}_{ikj} = 0. \tag{3.2}$$

Now, suppose $\frac{d}{dt}\cos(\theta_{ikj}) = 0$; this implies that $\cos(\theta_{ikj}) = c_1$, where $c_1 \in [-1, 1]$ is a constant. Thus, $\theta_{ikj} = \cos^{-1}(c_1) = c_2$, where $c_2 \in [0, \pi]$ is a constant, so $\dot{\theta}_{ikj} = 0$. □

The structure of the shape-similarity matrix is revealed by examining the time derivative of the cosine of an arbitrary angle θ_{ikj} along angle-consistent trajectories of $G(x)$:

$$\frac{d}{dt}\cos(\theta_{ikj}) = \frac{d}{dt}\left(\frac{z_{ik}^{\top} z_{jk}}{\|z_{ik}\|\|z_{jk}\|}\right) = \frac{\partial \cos(\theta_{ikj})}{\partial x}\dot{x}.$$

Because it depends only on x_i, x_j, and x_k, the partial derivatives of $\cos(\theta_{ikj})$ with respect to

all other vertex positions are zero; thus,

$$\frac{d}{dt}\cos(\theta_{ikj}) = \gamma_{ikj}\left(Q^{\top}_{z_{ik}}(z_{jk})\dot{x}_i + Q^{\top}_{z_{jk}}(z_{ik})\dot{x}_j - \left(Q^{\top}_{z_{ik}}(z_{jk}) + Q^{\top}_{z_{jk}}(z_{ik})\right)\dot{x}_k\right), \quad (3.3)$$

where $\gamma_{ikj} = (\|z_{ik}\|\|z_{jk}\|)^{-1}$, and $Q_{z_{jk}}(z_{ik})$ is the component of z_{ik} orthogonal to z_{jk} given by

$$Q_{z_{jk}}(z_{ik}) = \left(I_d - \frac{z_{jk}z_{jk}^{\top}}{\|z_{jk}\|^2}\right) z_{ik}.$$

Now, define the *angle-constraint function* $f_S : \mathbb{R}^{nd} \to [-1, 1]^m$, where

$$f_S(x) = \cos(\theta(x)) = [\ldots, \cos(\theta_{ikj}), \ldots]^{\top} \; \forall (i, k, j) \in \Theta_S$$

is the vector of the element-wise cosines of $\theta(x)$. Repeating the differentiation in (3.3) for all m angles in $\theta(x)$ specifying the framework of n vertices, (3.3) takes the form:

$$\frac{d}{dt} f_S(x) = \Gamma(x) R_S(x) \dot{x} = \mathbf{0}, \quad (3.4)$$

where $R_S(x) \in \mathbb{R}^{m \times dn}$ is the *shape-similarity matrix*, and $\Gamma(x) = \mathrm{diag}(\ldots, \gamma_{ikj}, \ldots) \in \mathbb{R}^{m \times m}$ is a diagonal matrix of positive scalars associated with rows of $R_S(x)$.

Each row of the expression in (3.4) corresponds with an angle. The element $m_{pq} \in \mathbb{R}^{1 \times d}$ of $R_S(x)$ corresponds to the component of the angle p contributed by vertex q; if vertex q is not one of the three vertices defining the angle p, then $m_{pq} = \mathbf{0}$. For example, the shape-similarity matrix of the triangle between x_i, x_j, and x_k shown in the leftmost and rightmost frameworks of Figure 3.2 is

$$\begin{bmatrix} Q^{\top}_{z_{ij}}(z_{kj}) & -Q^{\top}_{z_{ij}}(z_{kj}) - Q^{\top}_{z_{kj}}(z_{ij}) & Q^{\top}_{z_{kj}}(z_{ij}) \\ -Q^{\top}_{z_{ki}}(z_{ji}) - Q^{\top}_{z_{ji}}(z_{ki}) & Q^{\top}_{z_{ji}}(z_{ki}) & Q^{\top}_{z_{ki}}(z_{ji}) \\ Q^{\top}_{z_{ik}}(z_{jk}) & Q^{\top}_{z_{jk}}(z_{ik}) & -Q^{\top}_{z_{ik}}(z_{jk}) - Q^{\top}_{z_{jk}}(z_{ik}) \end{bmatrix}. \quad (3.5)$$

Referring to the frameworks depicted in Figure 3.2, the shape-similarity matrix of the rightmost framework is a matrix of zeros because the vertices are all collinear, which quantifies the description of this framework as not being infinitesimally shape-similar.

Along angle-consistent trajectories of $G(x)$, the time derivatives of each θ_{ikj} can be written using (3.2) and (3.3):

$$\dot{\theta}_{ikj} = \lambda_{ikj}\left(Q_{z_{ik}}^{\top}(z_{jk})\dot{x}_i + Q_{z_{jk}}^{\top}(z_{ik})\dot{x}_j - \left(Q_{z_{ik}}^{\top}(z_{jk}) + Q_{z_{jk}}^{\top}(z_{ik})\right)\dot{x}_k\right), \tag{3.6}$$

where $\lambda_{ikj} = -\gamma_{ikj}/\sin(\theta_{ikj})$. Repeated for m angles along angle-consistent trajectories, $\dot{\theta} = \Lambda(x)R_S(x)\dot{x} = \mathbf{0}$, where $\Lambda(x) = \mathrm{diag}(\ldots, \lambda_{ikj}, \ldots) \in \mathbb{R}^{m\times m}$.

The expression in (3.6) was originally used in [6] to develop the shape-similarity matrix. In this formulation, the behavior of $\dot{\theta}_{ikj}$ is unclear when θ_{ikj} is zero or π because of the division by $\sin(\theta_{ikj})$, which results in an indeterminate form; in contrast, the formulation in (3.3) does not suffer this limitation and enables the following observation.

Remark 3.1. *Consider* (3.3)*; when the angle θ_{ikj} formed between the three vertices is zero or π, $\frac{d}{dt}\cos(\theta_{ikj}) = 0$ regardless of $\dot{x}$. In effect, for certain configurations, all infinitesimal motions of $G(x)$ are angle-consistent, which is significant because a framework that is infinitesimally shape-similar in one configuration may not be in another; such pathologies are discussed in Chapter 3.3.*

3.3 Assessing Frameworks for Infinitesimal Shape-Similarity

This section develops tools for assessing arbitrary frameworks for infinitesimal shape-similarity; examination of the nullspace of the shape-similarity matrix is central in this development. Consider the following theorem, which follows from the construction of the shape-similarity matrix.

Theorem 3.1. *Infinitesimal motions $\dot{x}$ of the framework $G(x)$ are angle-consistent if and*

only if $\dot{x} \in \ker(R_S(x))$.[4]

Proof. Suppose $\dot{x}$ is an angle-consistent motion of $G(x)$; by Def. 3.1, $\dot{\theta}(x) = \mathbf{0}$. By Prop. 3.1 and the construction of $R_S(x)$, this implies that $\frac{d}{dt} f_S(x) = \Gamma(x) R_S(x) \dot{x} = \mathbf{0}$, so $\dot{x} \in \ker(R_S(x))$. Now, suppose that $\dot{x} \in \ker(R_S(x))$; $\frac{d}{dt} f_S(x) = \Gamma(x) R_S(x) \dot{x} = \mathbf{0}$, so by Prop. 3.1 and Def. 3.1, $\dot{x}$ is an angle-consistent motion of $G(x)$. □

From Thm. 3.1, $\ker(R_S(x))$ characterizes the angle-consistent motions of $G(x)$. By Def. 3.2, $G(x)$ is infinitesimally shape-similar if the only $\dot{x}$ in $\ker(R_S(x))$ are infinitesimal translations, rotations, and uniform scalings. The following presentation develops a basis for $\ker(R_S(x))$ of infinitesimally shape-similar $G(x)$. To facilitate this development, the following preliminaries are introduced.

Definition 3.3. *The points* $x = [x_1^\top, x_2^\top, \ldots, x_n^\top]^\top \in \mathbb{R}^{dn}$ *are* oriented *if the last* $(d - p)$ *coordinates of each point are zero where* $p = \dim(\text{aff}\{x\})$; *i.e. if*

$$x_i = [x_{i,1}, \ldots, x_{i,p}, 0, \ldots, 0]^\top \; \forall i = 1, \ldots, n.$$

A framework $G(x)$ *is oriented if the vertices* x *are oriented.*

Now, a description of vectors corresponding with infinitesimal translations, rotations, and uniform scaling is provided. Denote the standard basis vectors of $\mathbb{R}^d$ by $e_\alpha \in \mathbb{R}^d$, $\alpha = 1, \ldots, d$, and denote by $S_\beta \in \mathbb{R}^{d \times d}$, $\beta = 1, \ldots, \binom{d}{2}$, skew symmetric matrices formed by left and right multiplying the matrix $S = \left[\begin{smallmatrix} 0 & 1 \\ -1 & 0 \end{smallmatrix}\right]$ by distinct two-combinations of the standard basis vectors; i.e.,

$$S_\beta \in \left\{ [e_i \, e_j] S [e_i^\top \, e_j^\top]^\top \,|\, 1 \leq i < d, i < j \leq d \right\}.$$

[4] A similar result appears in [6, Theorem 1]; Thm. 3.1 and its proof connect prior work to the redevelopment of the shape-similarity matrix in Chapter 3.2.

Define the vector space corresponding to infinitesimal translations of x to be

$$V^t = \text{span}\{(\mathbf{1}_n \otimes e_1, \ldots, \mathbf{1}_n \otimes e_d)\};$$

the vector space corresponding to infinitesimal rotations of x to be

$$V^r = \text{span}\{(I_n \otimes S_1)x, \ldots, (I_n \otimes S_{\frac{1}{2}(d^2-d)})x\};$$

and define the vector space corresponding to infinitesimal uniform scaling of x to be

$$V^s = \text{span}\{x\}.$$

Lemma 3.1. *Let x be oriented and $p = \dim(\text{aff}\{x\}) > 1$; the nonzero vectors of $\text{span}\{V^t, V^r, V^s\}$ are linearly independent.*

Proof. Begin by considering the vectors $\mathbf{1}_n \otimes e_\alpha \in V^t$, which are mutually orthogonal because the standard basis vectors are mutually orthogonal; i.e.,

$$(\mathbf{1}_n \otimes e_i)^\top (\mathbf{1}_n \otimes e_j) = e_i^\top (\mathbf{1}_n^\top \otimes I_d)(\mathbf{1}_n \otimes I_d)e_j = 0.$$

Now consider linear independence of the vectors $\mathbf{1}_n \otimes e_\alpha \in V^t$ and $x = V^s$. Suppose that x is linearly dependent of the vectors in $\mathbf{1}_n \otimes e_\alpha$, $\alpha = 1, \ldots, d$, then there exist nontrivial $\zeta_\alpha \in \mathbb{R}$, $\alpha = 1, \ldots, d$, such that

$$x = \sum_{\alpha=1}^{d} \zeta_\alpha (\mathbf{1}_n \otimes e_\alpha). \tag{3.7}$$

Because of the sparse structure of $\mathbf{1}_n \otimes e_\alpha$, which can affect only the α-coordinate of each vertex, (3.7) would require that all $x_1 = x_2 = \ldots = x_n$ and result in $\dim(\text{aff}\{x\}) = 0$, contradicting the assumption that $\dim(\text{aff}\{x\}) > 1$; thus, the vectors of V^t are linearly independent of V^s.

To show linear independence of V^s and the vectors $(I_n \otimes S_\beta)x \in V^r$, note that the matrix $I_n \otimes S_\beta$ is skew symmetric, so $x^\top (I_n \otimes S_\beta)x = 0$, and x is linearly independent of the vectors $(I_n \otimes S_\beta)x \; \forall \beta = 1, \ldots, \binom{d}{2}$.

Linear independence of the vectors $(I_n \otimes S_\beta)x \in V^r$ requires examination of the effect of multiplying x by $I_n \otimes S_\beta$; to do this, multiply x_i by S_β. Such multiplication swaps two of the coordinates of x_i, negates one of them, and sets the rest to zero. For example, consider the following instantiation of x_i and S_β in $\mathbb{R}^3$:

$$S_\beta x_i = \begin{bmatrix} 0 & 1 & 0 \\ -1 & 0 & 0 \\ 0 & 0 & 0 \end{bmatrix} \begin{bmatrix} x_{i,1} \\ x_{i,2} \\ x_{i,3} \end{bmatrix} = \begin{bmatrix} x_{2,i} \\ -x_{1,i} \\ 0 \end{bmatrix}.$$

The Kronecker product repeats this effect for each vertex position in x. Because x is oriented, the last $(d-p)$ coordinates of each vertex position are zero, so there are, generically, exactly $\binom{d}{2} - \binom{d-p}{2}$ nonzero vectors of $(I_n \otimes S_\beta)x$, $\beta = 1, \ldots, \binom{d}{2}$; linear independence of these nonzero vectors is examined.

Suppose that some of the nonzero vectors of $(I_n \otimes S_\beta)x$, $\beta = 1, \ldots, \binom{d}{2}$, are linearly dependent of the rest; let q be the number of linearly independent vectors, and without loss of generality, order them such that the vectors $(I_n \otimes S_\beta)x$, $\beta = 1, \ldots, q$, are linearly independent. There must exist nontrival $\zeta_\beta \in \mathbb{R}$, $\beta = 1, \ldots, q$, such that each linearly dependent vector, e.g., $(I_n \otimes S_{q+1})x$, can be written as

$$(I_n \otimes S_{q+1})x = \sum_{\beta=1}^{q} \zeta_\beta (I_n \otimes S_\beta)x. \tag{3.8}$$

From the sparse structure of $I_n \otimes S_\beta$, no values of ζ_β for $\beta = 1, \ldots, q$ can satisfy (3.8), and the expression in (3.8) holds only for $x_1 = x_2 = \ldots = x_n$, which contradicts the assumption that $\dim(\text{aff}\{x\}) > 1$; thus, the nonzero vectors of $(I_n \otimes S_\beta)x$, $\beta = 1, \ldots, \binom{d}{2}$, are linearly independent.

Finally, consider linear independence of the vectors $\mathbf{1}_n \otimes e_\alpha \in V^t$, and the nonzero vectors of $(I_n \otimes S_\beta)x \in V^r$. Choose an arbitrary $(I_n \otimes S_\beta)x$ and suppose that it is linearly dependent of $\mathbf{1}_n \otimes e_\alpha$, $\alpha = 1, \ldots, d$, then there exists nontrivial ζ_α such that

$$(I_n \otimes S_\beta)x = \sum_{\alpha=1}^{d} \zeta_\alpha (I_n \otimes e_\alpha). \tag{3.9}$$

Because of the sparse structure of $I_n \otimes e_\alpha$, which affects only the α-coordinates of all of the vertices, (3.9) implies that $x_1 = x_2 = \ldots = x_n$, contradicting the assumption that $\dim(\text{aff}\{x\}) > 1$. Thus, $\mathbf{1}_n \otimes e_\alpha$, $\alpha = 1, \ldots, d$, and nonzero $(I_n \otimes S_\beta)x$, $\beta = 1, \ldots, \binom{d}{2}$, are linearly independent. □

The following theorem can now be stated.

Theorem 3.2. *Let $G(x)$ be an oriented framework and $p = \dim(\text{aff}\{x\}) > 1$. $G(x)$ is infinitesimally shape-similar if and only if a basis for $\ker(R_S(x))$ is given by the nonzero vectors of $\text{span}\{V^t, V^r, V^s\}$.*

Proof. To prove Thm. 3.2, it is first shown that $\text{span}\{V^t, V^r, V^s\} \subseteq \ker(R_S(x))$; the proof then follows from Def. 3.2 and Thm. 3.1.

Showing that $\text{span}\{V^t, V^r, V^s\} \subseteq \ker(R_S(x))$ is done by demonstrating that arbitrary vectors of V^t, V^r, and V^s lie in the nullspace of the shape-similarity matrix of $G(x)$, which is done by examining an arbitrary row of $R_S(x)$ as in (3.3).[5] An arbitrary row of $R_S(x)$ as in (3.3) multiplied by an arbitrary vector $(\mathbf{1} \otimes e_\alpha)$, $\alpha = 1, \ldots, d$, yields

$$\left(Q^\top_{z_{ik}}(z_{jk}) + Q^\top_{z_{jk}}(z_{ik}) - Q^\top_{z_{ik}}(z_{jk}) - Q^\top_{z_{jk}}(z_{ik})\right) e_\alpha = 0;$$

thus, $(\mathbf{1} \otimes e_\alpha) \in \ker(R_S(x)) \,\forall\, \alpha = 1, \ldots, d$. Multiplying an arbitrary row of $R_S(x)$ by x

[5] Though without requiring $G(x)$ to be oriented, the basis vectors of Thm. 3.2 were shown in [7] to lie in $\ker(R_S(x))$; this is repeated here for completeness.

yields

$$Q_{z_{ik}}^{\top}(z_{jk})z_{ik} + Q_{z_{jk}}^{\top}(z_{ik})z_{jk} = 0;$$

thus, $x \in \ker(R_S(x))$. Finally, multiplying an arbitrary row of $R_S(x)$ by an arbitrary vector $(I_n \otimes S_\beta)x$, $\beta = 1, \ldots, \binom{d}{2}$,

$$Q_{z_{ik}}^{\top}(z_{jk})S_\beta z_{ik} + Q_{z_{jk}}^{\top}(z_{ik})S_\beta z_{jk} = z_{jk}^{\top}S_\beta z_{ik} + z_{ik}^{\top}S_\beta z_{jk} = 0,$$

which follows from the skew symmetric property of S_β; thus, $(I_n \otimes S_\beta)x \in \ker(R_S(x)) \,\forall\, \beta = 1, \ldots, \binom{d}{2}$.

By Lem. 3.1, the V^t, V^s, and the nonzero vectors of V^r are linearly independent and form the basis for the space of infinitesimal translations, rotations, and uniform scaling of $G(x)$. Dy Def. 3.2, if $G(x)$ is infinitesimally shape-similar, then by Thm. 3.1, the only vectors in $\ker(R_S(x))$ result in infinitesimal translations, rotations, and uniform scalings, so the nonzero vectors of $\operatorname{span}\{V^t, V^r, V^s\}$ form a basis for $\ker(R_S(x))$. The converse follows from Thm. 3.1; vectors in $\ker(R_S(x))$ are angle-consistent motions of the framework. If the nonzero vectors of $\operatorname{span}\{V^t, V^r, V^s\}$ form a basis for $\ker(R_S(x))$, then the only angle-consistent motions of $G(x)$ are infinitesimal translation, rotation, and uniform scaling, so $G(x)$ is infinitesimally shape-similar by Def. 3.2. □

Having found a basis for the nullspace of the shape-similarity matrix of oriented frameworks, the following statements complete the analysis by proving the existence of isometries that orient the positions of the vertices for arbitrary frameworks and proving that the nullspace of the shape-similarity matrix is invariant to such transformations.

Proposition 3.2. *Let $x = [x_1^{\top}, x_2^{\top}, \ldots, x_n^{\top}]^{\top} \in \mathbb{R}^{dn}$ with $p = \dim(\operatorname{aff}\{x\})$. There exists an isometry $T : \mathbb{R}^d \to \mathbb{R}^d$ such that $\bar{x} = [T(x_1)^{\top}, T(x_2)^{\top}, \ldots, T(x_n)^{\top}]^{\top}$ is oriented.*

Proof. By construction, $p = \dim(\operatorname{aff}\{x\}) = \dim(\operatorname{aff}\{\bar{x}\})$. By definition and Lem. A.1,

there exists an isometric transformation T such that $\mathrm{aff}\{\bar{x}\} = T(\mathrm{aff}\{x\})$, which satisfies $\bar{x} = [T(x_1)^\top, T(x_2)^\top, \ldots, T(x_n)^\top]^\top$. □

Lemma 3.2. *The nullspace of the shape-similarity matrix is invariant to isometric transformations.*

Proof. Let $T : \mathbb{R}^d \to \mathbb{R}^d$ be an isometric transformation; thus, for a point $x_i \in \mathbb{R}^d$, $T(x_i) = Mx_i + c$, where $c \in \mathbb{R}^d$ is a translation and $M \in \mathbb{R}^{d\times d}$ is an orthogonal matrix. Consider the cosine of an arbitrary angle in a framework $G(x)$ formed between the transformed vertices $T(x_i)$, $T(x_k)$, and $T(x_j)$ as in (3.1), and verify that it is invariant under the isometry

$$\begin{aligned}\cos(\theta_{ikj}) &= \frac{(T(x_i) - T(x_k))^\top (T(x_j) - T(x_k))}{\|T(x_i) - T(x_k)\|\|T(x_j) - T(x_k)\|} \\ &= \frac{(x_i - x_k)^\top M^\top M (x_j - x_k)}{\|Mx_i - Mx_k\|\|Mx_j - Mx_k\|} \\ &= \frac{(x_i - x_k)^\top (x_j - x_k)}{\|x_i - x_k\|\|x_j - x_k\|}.\end{aligned}$$

Thus, the time derivative $\frac{d}{dt}\cos(\theta_{ikj})$ is invariant under the isometric transformation, so the shape-similarity matrix and its nullspace are invariant to isometric transformations. □

Prop. 3.2 and Lem. 3.2 support the following corollary.

Corollary 3.2.1. *Let $G(x)$ be a framework where $p = \dim(\mathrm{aff}\{x\}) > 1$, and denote the corresponding oriented framework by $G(\bar{x})$. The basis vectors in Thm. 3.2 for $\ker(R_S(\bar{x}))$ are basis vectors for $\ker(R_S(x))$.*

Proof. By Prop. 3.2, there exists an isometric transformation between x and $\bar{x}$, and by Lem. 3.2, $\ker(R_S(x)) = \ker(R_S(\bar{x}))$ and, thus, share the basis vectors of Thm. 3.2. □

Having examined the nullspace of the shape-similarity matrix in Thm. 3.2 and Cor. 3.2.1, a rank condition for evaluating frameworks for infinitesimal shape-similarity is presented.

Theorem 3.3. *The framework $G(x)$, with $p = \dim(\text{aff}\{x\})$, is infinitesimally shape-similar if and only if*

$$\text{rank}(R_S(x)) = dn + \frac{1}{2}p(p+1) - d(p+1) - 1. \tag{3.10}$$

Proof. The necessary and sufficient condition of Thm. 3.3 is proved for three cases of the dimension of the affine hull of the vertices of the framework. First, let $G(x)$ be a framework with $p = 0$. Such a framework is degenerate; it is not infinitesimally shape-similar, and the shape-similarity matrix, and thus the rank of the shape-similarity matrix, is undefined and does not satisfy (3.10). Now, let $G(x)$ be a framework with $p = 1$; the corresponding shape-similarity matrix is a matrix of zeros. By Thm. 3.1, all infinitesimal motions of the framework are angle-consistent, so $G(x)$ is not infinitesimally shape-similar; furthermore, $\text{rank}(R_S(x)) = 0$ and does not satisfy (3.10).

Finally, consider frameworks $G(x)$ with $p > 1$. The nullity of the shape-similarity matrix is the number of basis vectors for $\ker(R_S(x))$. Thm. 3.2 and Cor. 3.2.1 present such a basis, and as a direct result, a framework $G(x)$ is infinitesimally shape-similar if and only if

$$\dim(\ker(R_S(x))) = -\frac{1}{2}p(p+1) + d(p+1) + 1,$$

where from the proof of Thm. 3.2, and the extension to unoriented frameworks in Cor. 3.2.1, there are d basis vectors for translations, one basis vector for uniform scaling, and $\binom{d}{2} - \binom{d-p}{2}$ basis vectors for rotations. The rank condition in (3.10) follows from the necessary and sufficient condition on the nullity of the shape-similarity matrix in Thm. 3.2. □

The following corollary[6] to Thm. 3.3 is presented for frameworks whose affine hull has sufficient dimension.

[6] In contrast with the rank condition of [7, Theorem 3], the dependence of the rank condition in Cor. 3.3.1 on the dimension of the affine hull of the vertices is explicit.

Corollary 3.3.1. *Let $G(x)$ be a framework with*

$$p = \dim(\text{aff}\{x\}) = \max_{x \in \mathbb{R}^{dn}} \left[\dim(\text{aff}\{x\})\right].$$

$G(x)$ is infinitesimally shape-similar if and only if

$$\text{rank}(R_S(x)) = \begin{cases} dn - \frac{1}{2}d(d+1) - 1, & n \geq d \\ \frac{1}{2}(n-2)(n+1), & n < d \end{cases}.$$

Proof. Let $p = \max_{x \in \mathbb{R}^{dn}} \dim(\text{aff}\{x\})$; the rank condition in (3.10) can be conditioned on the relative values of n and d. First, suppose $n > d$; $p = \max_{x \in \mathbb{R}^{dn}}[\dim(\text{aff}\{x\})] = d$ [79, Corollary 1.3.4, pg. 12], for which (3.10) reduces to $\text{rank}(R_S(x)) = dn - \frac{1}{2}d(d+1) - 1$. Similarly, for $n = d$, $p = \max_{x \in \mathbb{R}^{dn}}[\dim(\text{aff}\{x\})] = d-1$, and the rank condition reduces to $\text{rank}(R_S(x)) = dn - \frac{1}{2}d(d+1) - 1$. Finally, for $n < d$, $p = \max_{x \in \mathbb{R}^{dn}}[\dim(\text{aff}\{x\})] = n-1$, in which case, $\text{rank}(R_S(x)) = \frac{1}{2}(n-2)(n+1)$. □

As suggested in Rem. 3.1, the particular embedding of x has a fundamental effect on the infinitesimal shape-similarity of $G(x)$; the following definition characterizes frameworks for which the rank of the shape-similarity matrix does not attain its maximum over all embeddings.

Definition 3.4. *A framework $G(x)$ is* pathological[7] *if*

$$\text{rank}(R_S(x)) < \max_{x \in \mathbb{R}^{dn}} \left[\text{rank}(R_S(x))\right]$$

and non-pathological *otherwise.*

[7] In [7], the term pathological was used to describe frameworks which were degenerate or for which any vertices were collinear; Def. 3.4 better captures those frameworks that do not achieve infinitesimal shape-similarity due to the particular configuration of the vertices.

Theorem 3.4. *If $G(x)$ is a pathological framework, then it is not infinitesimally shape-similar.*

Proof. If $G(x)$ is a pathological framework, then by Def. 3.4,

$$\operatorname{rank}(R_S(x)) < \max_{x \in \mathbb{R}^{dn}} \left[\operatorname{rank}(R_S(x))\right].$$

Let $p = \dim(\operatorname{aff}\{x\})$; for any $G(x)$,

$$\max_{x \in \mathbb{R}^{dn}} \left[\operatorname{rank}(R_S(x))\right] \leq dn + p(p+1)/2 - d(p+1) - 1,$$

with equality if and only if $G(x)$ is infinitesimally shape-similar by Thm. 3.3. Because

$$\operatorname{rank}(R_S(x)) < dn + p(p+1)/2 - d(p+1) - 1,$$

$G(x)$ is not infinitesimally shape-similar. □

Remark 3.2. *Assessing frameworks $G(x)$ for infinitesimal shape-similarity highlights the importance of both the network topology described by $\mathcal{G}$ and the embedding x. Notably, the topology qualifies $G(x)$ for infinitesimal shape-similarity, and the embedding determines whether $G(x)$ is infinitesimally shape-similar. Relating Thm. 3.3 and Thm. 3.4, pathological frameworks with insufficient affine hull dimension do not satisfy the rank condition; for example, a fully connected framework of four vertices in $\mathbb{R}^5$ having $\dim(\operatorname{aff}\{x\}) = 2$ is pathological with $\operatorname{rank}(R_S(x)) = 4$, but is infinitesimally shape-similar with $\operatorname{rank}(R_S(x)) = 5$ when embedded such that $\dim(\operatorname{aff}\{x\}) = 3$. Remarkably, in $\mathbb{R}^2$ and $\mathbb{R}^3$, the spaces of most interest for multi-robot teams, the rank condition of Cor. 3.3.1 always evaluates to the first case, and such frameworks are pathological only if the vertices are collinear.*

3.4 Summary of Conclusions

This chapter has considered formations of robots equipped with bearing-only sensors, which could be used in practice to measure the relative angles formed between neighboring robots in the formation. Within this initialism, the framework property of infinitesimal shape-similarity was developed to characterize the types of formations that can be achieved by, and the available motions to, formations in which these relative angles are maintained. With respect to the primary objective of this thesis, which is the exploration of the interplay between network topology and the interaction modalities of a networked team, the following conclusions from the investigation presented in this chapter can be drawn.

Foremost among these conclusions is the fact that the particular sensing modalities that specify the formation, bearing-only sensors in the case of this chapter, induce a network topology that underlies the formation. From the development of infinitesimal shape-similarity, it is clear that not only is it important to understand the information passed between robots, but also the robots with which this information is shared; furthermore, the embedding of the robots in space fundamentally affects the constitution of the framework. In short, as for the types of formations that can be achieved by maintaining angles, it matters: what information is available, the network induced by the sharing of this information, and where the robots are positioned. This conclusion is substantiated by the tools developed to understand infinitesimal shape-similarity, namely the shape-similarity matrix and its rank condition, which explicitly express the coupling of network topology and the embedding of the robots.

Along with the significance of the network and its embedding are the particular motions available to formations in which the robots maintain the relative angles between themselves and their neighbors. Infinitesimal shape-similarity explicitly characterizes frameworks in which maintaining these angles results in invariance of those angles to translation, rotation, and uniform scaling. As with the previous conclusion, the network topology and the embedding are tightly coupled. For example, pathological frameworks may have the

correct network topology, but still do not achieve infinitesimal shape-similarity. The fact that infinitesimally shape-similar frameworks are invariant to the union of those motions available to infinitesimally rigid and bearing-rigid frameworks is significant, and, as such, is the subject of Chapter 6.

CHAPTER 4
CONTROL OF SHAPE-SIMILAR FORMATIONS

In this chapter, the interplay between network topology and the interaction modalities of networked teams of robots is explored through the design of formation controllers for multi-robot teams described by infinitesimally shape-similar frameworks. In particular, this section explicitly utilizes the tools of infinitesimal shape-similarity developed in Chapter 3, namely the shape-similarity matrix, to achieve control of formations specified by the relative angles between robots. Two approaches to formation control are presented in this section: one exclusively designed to stabilize the formation, and another that uses controller synthesis to incorporate high-level objectives in addition to formation stabilization. Through the design of these formation controllers, the sensing and communication modalities of the multi-robot team are considered, and the design process is used to highlight the need for heterogeneous interaction modalities in formation control. The contents are drawn from [9], but have been adjusted to account for the formulation of shape-similarity presented in Chapter 3.

This chapter is organized in the following way. First, Chapter 4.1 describes the frameworks for which the controllers of this chapter are designed. The approaches to formation control are presented in Chapter 4.2. The formation stabilization controller is presented in Chapter 4.2.1; this controller is used as the foundation for the controller-synthesis approach presented in Chapter 4.2.2. In Chapter 4.3, the implications of the designed formation controllers on the sensing and communication modalities of the multi-robot team are discussed. Chapter 4.4 demonstrates the controller-synthesis approach to formation control on a team of differential-drive robots in the Robotarium. Finally, a summary of the conclusions of this chapter as they pertain to the subject of this thesis is presented in Chapter 4.5.

4.1 Frameworks of Interest

This section characterizes the frameworks for which the formation controllers of this chapter are designed. For the remainder of Chapter 4, the dynamics of the vertices are modelled as single integrators such that $\dot{x} = u$. Frameworks $G(x)$ are assumed to be infinitesimally shape-similar as in Def. 3.2. As such, the shape-similarity matrices $R_S(x)$ of these frameworks satisfy the rank condition of Thm. 3.3, indicating that there are exactly $q_S = \text{rank}(R_S(x)) \leq m$ linearly independent rows of the shape-similarity matrix. Because $G(x)$ is infinitesimally shape-similar, maintaining the q_S *independent angles* which correspond with these linearly independent rows ensures that $\theta(x)$ is invariant for angle-consistent $\dot{x}$. Thus, define the *independent angle set* $\hat{\Theta}$ to be the set of q_S distinct triads of connected vertices corresponding with the linearly independent rows of $R_S(x)$. Similarly, define the *independent angle vector* to be $\hat{\theta} : \mathbb{R}^{nd} \to [0, \pi]^{q_S}$ such that $\hat{\theta}(x)$ is the vector of independent angles; the corresponding *independent angle-constraint function* is $\hat{f}_S : \mathbb{R}^{nd} \to [-1, 1]^{q_S}$, for which $\hat{f}_S(x) = \cos(\hat{\theta}(x))$ is the element-wise cosine of the independent angle vector. The time derivative of the independent angle-constraint function is $\frac{d}{dt}\hat{f}_S(x) = \hat{\Gamma}_S(x)\hat{R}_S(x)u$ following the development of infinitesimal shape-similarity in Chapter 3.

In terms of the cosines of the independent angles, the desired configuration of the vertices is given by $f_S^* \in [-1, 1]^{q_S}$, where this vector is assumed to be geometrically viable (e.g., a triangular framework should not have f_S^* corresponding with three angles whose sum exceeds π). With this construction, the error between the current and desired angles is

$$e_S(x) = [e_{S,1}(x), \ldots, e_{S,q_S}(x)]^\top = f_S^* - \hat{f}_S(x);$$

the ordering of the errors $e_{S,a}(x)$ is arbitrary, and it will occasionally be convenient to

reference the error corresponding to θ_{ikj} by $e_{S,(i,k,j)}(x)$. The *angle-error system* is given by:

$$\dot{e}_S(x) = -\frac{d}{dt}\hat{f}_S(x) = -\hat{\Gamma}_S(x)\hat{R}_S(x)u. \tag{4.1}$$

The remainder of this chapter designs stabilizing controllers for this angle-error system.

4.2 Formation Stabilization for Infinitesimally Shape-Similar Frameworks

This section presents a method of formation stabilization for formations described by infinitesimally shape-similar frameworks. Beginning in Chapter 4.2.1, a controller that achieves formation stabilization of infinitesimally shape-similar frameworks by stabilizing the origin of the angle-error system is described; this formation controller is used to introduce the theoretical underpinnings of the controller-synthesis approach in Chapter 4.2.2.

4.2.1 Asymptotic Formation Stabilization

As previously mentioned, the purpose of the controller presented in this subsection is to asymptotically stabilize the origin of the angle-error system in (4.1). With this regard, consider the controller presented in the following theorem.

Theorem 4.1. *Let $G(x)$ be an infinitesimally shape-similar framework for which $e_S(x) \in D = \{(-2,2)^{q_S}\}$; under*

$$u = \hat{R}_S^\top(x)\hat{\Gamma}_S^\top(x)e_S(x), \tag{4.2}$$

the origin of the angle-error system in (4.1)*, $e_s(x) = 0$, is locally asymptotically stable.*

Proof. Consider the candidate Lyapunov function

$$V_S(e_S(x)) = \frac{1}{2}\|e_S(x)\|^2, \tag{4.3}$$

which satisfies $V_S(e_S(x)) > 0$ for $e_S(x) \in D - \{0\}$ and has the time derivative $\dot{V}_S(e_S(x)) =$

$e_S^\top(x)\dot{e}_S(t)$; substituting the error system in (4.1) into this expression yields

$$\dot{V}_S(e_S(x)) = \frac{\partial V_S(e_S(x))}{\partial x} u = -e_S^\top(x)\hat{\Gamma}(x)\hat{R}_S(x)u. \tag{4.4}$$

Further substituting the controller in (4.2) into (4.4), yields

$$\dot{V}_S(e_S(x)) = -e_S^\top(x)\hat{\Gamma}_S(x)\hat{R}_S(x)\hat{R}_S^\top(x)\hat{\Gamma}_S^\top(x)e_S(x).$$

For $e_S(x) \in D$, $\hat{\Gamma}_S(x)$ is positive definite; furthermore, for $e_S(x) \in D$, $\hat{R}_S(x)$ is full rank, so $\hat{R}_S(x)\hat{R}_S^\top(x) \succ 0$. Thus, $\dot{V}_S(e_S(x)) = -\|\hat{R}_S^\top(x)\hat{\Gamma}_S^\top(x)e_S(x)\| < 0$ for $e_S(x) \in D - \{0\}$, so $e_S(x) = 0$ is locally asymptotically stable. □

As it is presented in Thm. 4.1, the controller in (4.2) can be separated into the individual controllers for each robot in the formation, enabling examination of the sensing and communication requirements of this method. To do this, consider the term $\frac{\partial \hat{f}_S^\top(x)}{\partial x} = \hat{R}_S^\top(x)\hat{\Gamma}_S^\top(x)$ of (4.2), which can be written as

$$\frac{\partial \hat{f}_S^\top(x)}{\partial x} = \begin{bmatrix} \frac{\partial \hat{f}_{S,1}}{\partial x_1} & \cdots & \frac{\partial \hat{f}_{S,q_S}}{\partial x_1} \\ \vdots & \ddots & \vdots \\ \frac{\partial \hat{f}_{S,1}}{\partial x_n} & \cdots & \frac{\partial \hat{f}_{S,q_S}}{\partial x_n} \end{bmatrix}. \tag{4.5}$$

Thus, the control input for each robot can be expressed as

$$u_i = \sum_{a=1}^{q_S} \frac{\partial \hat{f}_{S,a}(x)}{\partial x_i} e_{S,a}(x). \tag{4.6}$$

To elucidate the sensing and communication requirements of the controller in (4.2), the following notation is introduced. Let $\hat{\Theta}_i \subset \hat{\Theta}$ be the elements of the independent angle-set which include i. By $\hat{\Theta}_i^C \subset \hat{\Theta}_i$, denote the elements of the independent angle-set for which i is vertex about which the angles θ_{kij} are formed, and denote by $\hat{\Theta}_i^{\neg C} \subset \hat{\Theta}_i$ the elements of the independent angle-set containing i, but for which the corresponding angles θ_{ikj} are not

centered on i. Note that $\hat{\Theta}_i = \hat{\Theta}_i^C \cup \hat{\Theta}_i^{\neg C}$. With this notation, and from the derivation of the shape-similarity matrix in Chapter 3.1, partial derivatives of (4.5) in (4.6) take the following forms:

$$\frac{\partial \hat{f}_{S,a}^{\top}(x)}{\partial x_i} = \begin{cases} -\gamma_{kij}\left(Q_{z_{ki}}(z_{ji}) + Q_{z_{ji}}(z_{ki})\right) & a \in \hat{\Theta}_i^C \\ \gamma_{ikj} Q_{z_{ik}}(z_{jk}) & a \in \hat{\Theta}_i^{\neg C} \\ \mathbf{0} & \text{otherwise,} \end{cases} \tag{4.7}$$

so for each robot, (4.6) can be expressed as

$$u_i = \sum_{a=(k,i,j)\in\hat{\Theta}_i^C} -e_{S,a}(x)\gamma_{kij}\left(Q_{z_{ki}}(z_{ji}) + Q_{z_{ji}}(z_{ki})\right) + \sum_{a=(i,k,j)\in\hat{\Theta}_i^{\neg C}} e_{S,a}(x)\gamma_{kij}Q_{z_{ik}}(z_{jk}). \tag{4.8}$$

A discussion of the implication of this controller on the sensing and communication modalities of the networked multi-robot team is given in Chapter 4.3. A simulation of five vertices executing the controller in (4.8) is shown in left image of Figure 4.1; the corresponding value of the Lyapunov function in (4.3) is shown in the right image.

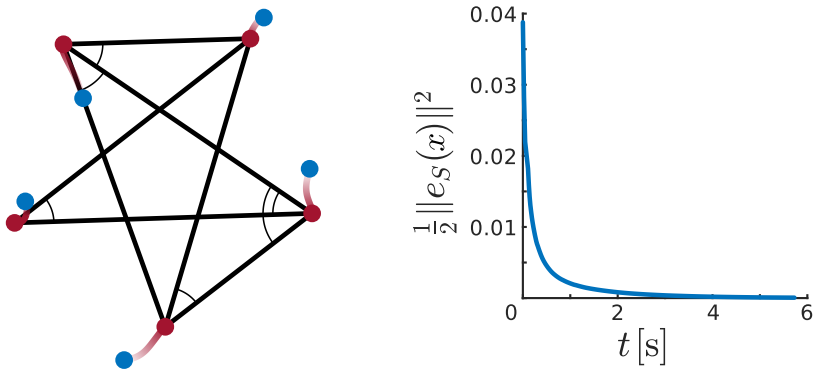

Figure 4.1: The controller in (4.8) was executed by five vertices. (Left) From the initial positions (blue dots), the vertices move along the red trajectories to their final positions (red dots); the black lines indicate the network topology, and the angles corresponding to the error system are denoted by the black arcs. (Right) The Lyapunov function in (4.3) decreases asymptotically to zero.

4.2.2 Controller-Synthesis Formation-Control Strategy

As with the stabilizing controller presented in (4.2), the controller-synthesis approach to formation control stabilizes the origin of the angle-error system in (4.1); the controller-synthesis approach also supports a mechanism for incorporating high-level, user-designated objectives, which is a feature that is explored in simulation and implementation on a team of differential-drive robots in Chapter 4.4. To begin, a validating controller is presented to exponentially stabilize $e_S(x) = 0$ with a particular convergence rate.

Theorem 4.2. *Let $G(x)$ be an infinitesimally shape-similar framework for which $e_S(x) \in D = \{(-2, 2)^{q_S}\}$; under*

$$u = \hat{R}_S^\top(x)\hat{\Gamma}_S^\top(x)\left(\hat{\Gamma}_S(x)\hat{R}_S(x)\hat{R}_S^\top(x)\hat{\Gamma}_S^\top(x)\right)^{-1} e_S(x) \tag{4.9}$$

the origin of the angle-error system in (4.1)*, $e_s(x) = 0$, is locally exponentially stable.*

Proof. Consider the Lyapunov function in (4.3), the time derivative of which is given in (4.4). For $e_S(x) \in D$, $\hat{R}_S(x)$ is full row-rank, and $\hat{\Gamma}_S(x)$ is positive definite, so the matrix $\hat{\Gamma}_S(x)\hat{R}_S(x)\hat{R}_S^\top(x)\hat{\Gamma}_S^\top(x)$ is invertible; substitution of the expression in (4.9) yields $\dot{V}_S(x) = -\|e_S(x)\|^2 \leq -2V_S(x)$, so $e_S(x) = 0$ is locally exponentially stable. □

The controller in (4.9) provides an immediate means of provably exponentially stabilizing the origin of the angle-error system with a fixed convergence rate, which is a modest improvement over the statement in Thm. 4.1. More importantly, however, (4.9) is a validating controller for the synthesized controller given by solving the following optimization problem:

$$\begin{aligned} u^* = &\underset{u\in\mathbb{R}^{dn}}{\arg\min}\frac{1}{2}\|u - u^{\text{nom}}\|^2 \\ &\text{s.t.} \quad -e_S^\top(x)\hat{\Gamma}_S(x)\hat{R}_S(x)u \leq -\frac{\rho_S}{2}\|e_S(x)\|^2, \end{aligned} \tag{4.10}$$

where u_{nom} is a nominal controller for the formation, and $\rho_S \in \mathbb{R}_+$ is a parameter that can be chosen to affect convergence of the angle-error to the origin. The synthesized controller

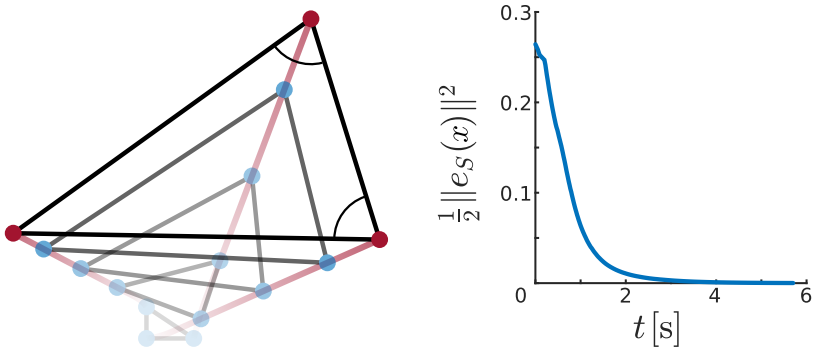

Figure 4.2: (Left) Along the red trajectories as opacity increases, three vertices executing the synthesized controller in (4.10) translate, rotate, and scale until reaching their final positions (red dots); the black lines indicate the network topology, and the angles corresponding to the error system are denoted by the black arcs. (Right) The Lyapunov function in (4.3) converges to zero.

in (4.10) has the following attractive features.

Foremost, because of the inequality constraint of (4.10), which utilizes the Lyapunov function in (4.3) as a CLF, solutions to this optimization problem ensure that the origin of the angle-error is locally exponentially stable; the existence of the validating controller in (4.9) suggests that the set of solutions to (4.10) is nonempty.

A secondary feature of the controller-synthesis formulation in (4.10) is the ease with which the method admits a variety of nominal controllers. Choosing the nominal controller is a straightforward mechanism for addressing high-level objectives, such as moving the formation along planned trajectories or executing the desired motion of a human pilot; this versatility is an advantage over controllers similar to those in (4.2) and (4.9), which cannot be used to simultaneously address the low-level objective of stabilizing the origin of the angle-error system while also addressing high-level objectives of the team. To showcase the utility of the nominal controller, consider the MATLAB simulation presented in Figure 4.2; the image shows a framework translating, rotating, and scaling uniformly by solving the QP in (4.10), using the function `quadprog`, for a nominal controller that is the difference of the current and desired positions of the vertices.

Finally, the structure of the CLF constraint of (4.10) and the shape-similarity matrix can be exploited to formulate individual controller-synthesis problems for each robot that ensure

satisfaction of the original inequality in (4.10).

The principle behind the decentralized formulation of the controller-synthesis strategy is that by decoupling the inequality constraint of (4.10), an optimization problem for each robot in the formation can be written such that the inequality constraint of the original problem is satisfied. With regards to this decentralized formulation, consider the CLF in (4.3), which recognizing that each angle is formed between three vertices, can be expressed as the sum

$$V_S(e_S(x)) = \frac{\rho_S}{6} \sum_{i=1}^{n} \sum_{a \in \hat{\Theta}_i} (e_{S,a}(x))^2. \tag{4.11}$$

Now, examine the derivative as in (4.4), which, similar to that of (4.6), can be written as:

$$\dot{V}_S(e_S(x)) = -\sum_{i=1}^{n} \sum_{a \in \hat{\Theta}_i} e_{S,a} \frac{\partial \hat{f}_{S,a}}{\partial x_i} u_i. \tag{4.12}$$

For each robot, the synthesized controller is given by

$$\begin{aligned} u_i^* = \underset{u_i \in \mathbb{R}^d}{\arg\min} & \frac{1}{2} \|u - u_i^{\text{nom}}\|^2 \\ \text{s.t. } & -\sum_{a \in \hat{\Theta}_i} e_{S,a} \frac{\partial \hat{f}_{S,a}(x)}{\partial x_i} u_i \leq -\frac{\rho_S}{6} \sum_{a \in \hat{\Theta}_i} (e_{S,a}(x))^2. \end{aligned} \tag{4.13}$$

By the following lemma, if the inequality constraint of (4.13) is satisfied for each robot in the formation, then the original inequality constraint of (4.10) is satisfied.

Lemma 4.1. *For $i = 1, \ldots, n$, if each u_i satisfies the inequality constraint of* (4.13)*, then the original inequality constraint of* (4.10) *is satisfied.*

Proof. The inequality

$$-\sum_{a \in \hat{\Theta}_i} e_{S,a} \frac{\partial \hat{f}_{S,a}(x)}{\partial x_i} u_i \leq -\frac{\rho_S}{6} \sum_{a \in \hat{\Theta}_i} (e_{S,a}(x))^2$$

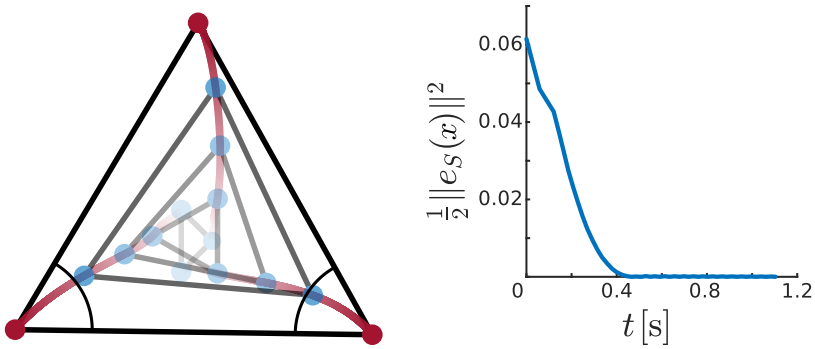

Figure 4.3: (Left) Along the red trajectories as opacity increases, three vertices executing the synthesized controller in (4.13) rotate and scale until reaching their final positions (red dots); the black lines indicate the network topology, and the angles corresponding to the error system are denoted by the black arcs. (Right) The Lyapunov function in (4.3) converges to zero as expected.

implies that

$$-\sum_{i=1}^{n}\sum_{a\in\hat{\Theta}_i} e_{S,a}\frac{\partial \hat{f}_{S,a}(x)}{\partial x_i}u_i \leq -\frac{\rho_S}{6}\sum_{i=1}^{n}\sum_{a\in\hat{\Theta}_i}(e_{S,a}(x))^2,$$

which by equality to (4.11) and (4.12), implies $-e_S^\top(x)\hat{\Gamma}_S(x)\hat{R}_S(x)u \leq -\frac{\rho_S}{2}\|e_S(x)\|^2$. □

Having shown that satisfying the inequality constraints of (4.13) amount to satisfying the inequality constraint of (4.10), the following can be stated as a direct result of Lem. 4.1.

Theorem 4.3. *Suppose the synthesized controllers u_i^* of* (4.13) *exist for each $i = 1, \ldots, n$. Under $u^* = [u_1^{*\top}, \ldots, u_n^{*\top}]^\top$, the origin of the angle-error system in* (4.1)*, $e_S(x) = 0$, is locally exponentially stable.*

Demonstrating the synthesized controller in (4.13), the MATLAB simulation in Figure 4.3 shows the trajectory of three vertices executing the synthesized controller for a nominal control input which is the difference between the desired and current positions of the vertices.

4.3 Sensing and Communication Requirements

Here, the inequality constraint of the decentralized formulation of the controller-synthesis formation-control strategy in (4.13) is examined to understand the trade-offs between assumptions on the underlying network topology of the formation and the sensing and

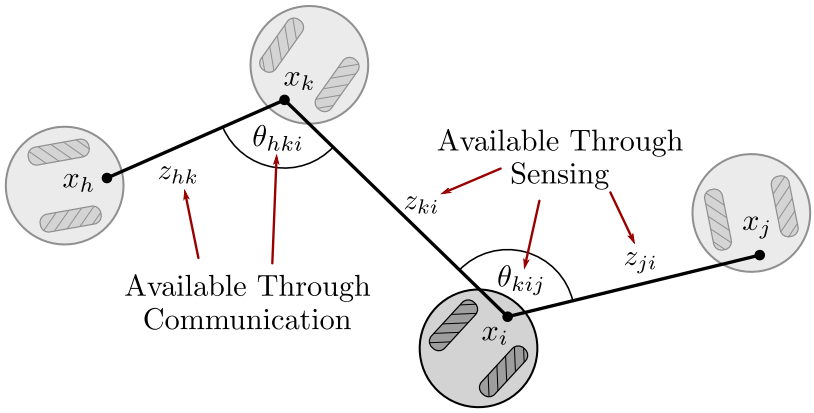

Figure 4.4: Without assuming a particular network topology, robot i must use sensors capable of measuring distances and bearings as well as communication with its neighbors in order to calculate the controllers in (4.8) and (4.13).

communication requirements of the robots. As presented in the development of the controller in (4.8), the only assumption on the network topology is that the framework is infinitesimally shape-similar. Without further restrictions on the structure of the network, term-by-term examination of the partial derivatives in (4.7), which constitute the inequality in (4.13), reveals the sensing and communication requirements of the robots; Figure 4.4 depicts the information available to an arbitrary robot.

To begin, consider the sensing requirements of the controller in (4.13). From the perspective of an arbitrary robot i in the formation, begin by examining the first case in (4.7), in which i is the vertex about which the angles are formed. To evaluate the partial derivates in this case, robot i must have sufficient information to determine the vectors z_{ki} and z_{ji}; this implies that the robot should be equipped with sensors capable of measuring the distances and bearings to its neighbors. With such a sensor suite, robot i is able to calculate: the orthogonal projections $Q_{z_{ji}}(z_{ki})$ and $Q_{z_{ki}}(z_{ji})$; the angles θ_{kij} formed about itself, as well as the corresponding angle error $e_{S,(k,i,j)}(x)$; and the scaling term γ_{kij}.

Now, examine the communication requirements of (4.13). Consider the second case in (4.7), for which the angle is not formed about robot i. Without assuming a particular network topology, robot i cannot locally determine: the scaling term γ_{ikj}, the orthogonal projection $Q_{z_{ik}}(z_{jk})$, or the angle θ_{ikj} with corresponding angle error $e_{S,(ikj)}$; however, because robot

k can calculate these terms using its own sensors, communication between robot i and its neighbors can be used to recover this information. The communicated information includes a vector that must be represented in the reference frame of robot i, which for arbitrary graph topologies, requires a common reference frame between robots i and k.

Highlighting the trade-offs between the structure of the network and the interaction modalities of the team, relaxations of the communication requirements are possible when assumptions on the topology of the formation can be made. For example, a common reference as described in the previous paragraph is unnecessary for planar formations because there is a single plane of rotation. For adjacent robots i and k, if robot k communicates the vector z_{ik} in its own reference frame to robot i, robot i has sufficient information to rotate into its own reference frame any communicated vectors, such as the vector z_{jk}, given in the reference frame of robot k. Extending this to frameworks in higher dimensions, the rotation between reference frames can be determined if robots i and k have a common neighbor in the plane defined by robots i, k, and j; this corresponds with the existence of a triangular subframework, an idea that will be developed in Chapter 5. Furthermore, if robots i, k, and j are all neighbors, and robot i is equipped with distance and bearing sensors, then communication is unnecessary to recover the requisite information.

4.4 Robotarium Demonstration

In this section, the controller-synthesis formation-control strategy presented in Chapter 4.2.2 is demonstrated on a team of differential-drive robots in the Robotarium, which is described in Chapter 2.4.

Six differential-drive robots are used to demonstrate the utility of the controller-synthesis formation-control strategy. As discussed in Chapter 4.2.2, controllers synthesized according to (4.10) admit a nominal controller that can be used to address a high-level, user-designated objective. In the demonstration scenario, the nominal controller enables a human pilot to navigate the formation of robots through an environment. The pilot interfaces with the

formation via a keyboard and is able to direct the motion of the robots through choices of translations, rotation, and uniform scaling, which are the available angle-consistent motions of infinitesimally shape-similar frameworks. Encoding the pilot's commands through the nominal controller as indicated in the bottom right image of Figure 4.5, the robots execute the synthesized controller in (4.10) to maintain the inter-robot angles of the formation.

Stills from the demonstration are shown in Figure 4.5. The dark regions projected onto the testbed surface represent obstacles that the pilot would like the robots to avoid, and the red circle designates the desired final position of the formation. At the direction of the pilot, the robots maintain the formation by executing the synthesized controller in (4.10). Along the numbered images, the robots first translate before contracting to pass through a narrow passage; finally, the robots expand and rotate about the location designated by the red dot.

4.5 Summary of Conclusions

In this chapter, two approaches to formation control of infinitesimally shape-similar frameworks were presented to explore the coupling between network topology and the interaction modalities of a multi-robot team through controller design. The first of these approaches was a gradient descent controller that explicitly used the results of Chapter 3, namely the

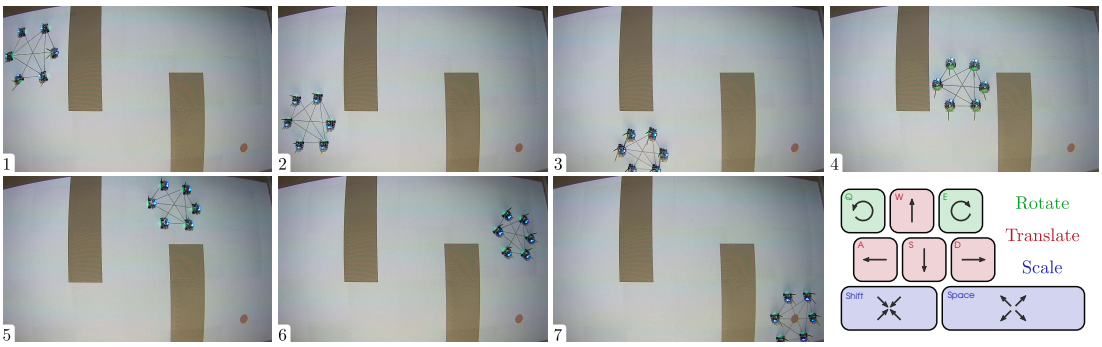

Figure 4.5: In the demonstration shown above, a human pilot directs the motion of a team of six differential-drive robots, which execute the synthesized controller in (4.10) to maintain the formation. The proposed controller-synthesis approach to formation control enables the pilot to instruct the robots to translate, rotate, and scale in order to navigate the formation through the environment projected onto the testbed surface. (Bottom Right) The pilot directs the motion of the formation using a keyboard; the nominal controller is the sum of vectors corresponding to each pressed key.

shape-similarity matrix, to locally asymptotically stabilize the origin of the angle-error system, which captures the difference between the current and desired angles of the formation. The second approach to formation control presented in this section relies on the solution of an optimization problem in which the Lyapunov function of the previous approach is used as a CLF inequality constraint on the solution. The synthesized controller made explicit use of the shape-similarity matrix to achieve formation stabilization with the additional benefit of minimizing, in a least-squares sense, the difference of the solution from a nominal control input, which allows higher-level objectives to be incorporated; this approach was demonstrated on a team of differential-drive robots in the Robotarium.

In Chapter 4.3, the implications of the designed formation controllers on the required sensing and communication modalities of the multi-robot team were discussed. In particular, in order to calculate the errors and partial derivatives necessary to execute the controllers, each robot needs access to distance and bearing information as well as communication with its neighbors; this discussion lays the foundation for subsequent chapters of this thesis in the following ways. First, despite the initialism of infinitesimal shape-similarity, which is founded on the maintenance of the relative angles between robots, the bearing-only sensors necessary to measure these angles are not sufficient to achieve and maintain them, suggesting that heterogeneous interaction modalities can play an important role even for frameworks specified by homogeneous quantities. Second, the discussion in Chapter 4.3 suggests that a fundamental trade-off between these sensing requirements and the network topology can be made in the case of triangular subframeworks; these trade-offs are explored explicitly in Chapter 5.

CHAPTER 5

ASSEMBLY AND CONTROL OF A CLASS OF TRIANGULATIONS

In this chapter, triangulations, a class of frameworks which will be shown to be infinitesimally shape-similar, are used in the threefold task of characterization, assembly, and control design to explore the interplay between network topology and the interaction modalities of a multi-robot team. In particular, this chapter serves as a case-study in the significance of heterogeneous interaction modalities, which will be used to effectively control a formation of robots equipped with bearing-only sensors, described by a class of triangulations. The contents of this chapter are drawn from a number of works: originally, characterization and assembly of triangulations was presented in [7]; an approach to control of these assembled triangulations was proposed in [10]; and, finally, [8] consolidated these results and identified the class of assembled triangulations to be maximally outer plane graphs.

This section is structured in the following manner. First, Chapter 5.1 characterizes triangulations by defining them and proving that they are infinitesimally shape-similar using the rank condition on the shape-similarity matrix presented in Chapter 3. Following in Chapter 5.2, a class of triangulations, maximally outerplane graphs, is identified, and a method of self-assembly of this class of frameworks by robots equipped with bearing-only sensors is presented alongside a demonstration on a team of differential-drive robots. In Chapter 5.3, the limitations of the controller used in self-assembly are discussed, suggesting the significance of access to heterogeneous interaction modalities by the networked team; a strategy for formation control of maximally outerplane graphs is designed to leverage the incorporation of a single robot capable of measuring distances in addition to bearings. In Chapter 5.4, this formation-control strategy is demonstrated on a team of differential-drive robots in the Robotarium. In Chapter 5.5, the conclusions of this section as they pertain to the investigation of network topology and the interaction modalities of a team are summarized.

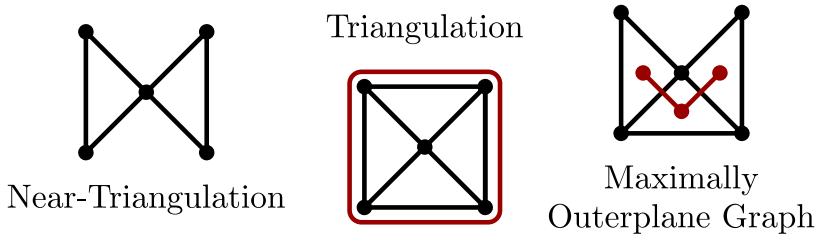

Figure 5.1: This image highlights the relationship between near-triangulations, triangulations, and maximally outerplane graphs. Triangulations are near-triangulations whose outer face is a cycle; maximally outerplane graphs are triangulations for which the weak dual graph is a tree.

5.1 Characterizing Triangulations

Previously in Chapter 3, infinitesimal shape-similarity was introduced to characterize the motions available to teams of robots in which angles in the formation are maintained. To further demonstrate the significance of these developments in the context of multi-robot formations, this section characterizes triangulations, a structured class of frameworks. First, triangulations are precisely defined; then, triangulations are shown to be infinitesimally shape-similar.

To introduce the definition of triangulations, a broader-class of frameworks, to which triangulations belong, is first defined.

Definition 5.1 ([34, pg. 405])**.** *A* near-triangulation *is a plane graph all of whose inner faces have degree three.*

From the picture of the near-triangulation in Figure 5.1, it is trivial to prove that near-triangulations are not necessarily infinitesimally shape-similar. For example, using the pictured near-triangulation, it is possible to scale one half of the framework differently than the other; such a motion preserves the angles but is not a translation, rotation, or uniform scaling, so the framework is not infinitesimally shape-similar. While the broader class of frameworks is not necessarily infinitesimally shape-similar, certain classes of near-triangulations are. For this reason, the following class of frameworks is defined.

Definition 5.2. *A* triangulation *is a near-triangulation whose outer face is a cycle.*[1]

Def. 5.2, which captures the features of the class of frameworks of interest, differs from other definitions of the term triangulation. For example, in [34], triangulations refer to maximal planar graphs, which are plane graphs whose faces have degree three. The choice to define triangulations as in Def. 5.2 was adopted in [8] to improve clarity in the terminology of this work when compared to that of [7].

Relating Def. 5.2 to the results presented in Chapter 3, triangulations are planar objects; these frameworks are embedded in the plane with $x \in \mathbb{R}^{2n}$. Furthermore, as a consequence of Def. 5.2, triangulations are non-degenerate and non-pathological.

Having established the definition and some properties of triangulations, interest in this class of frameworks is justified by showing that triangulations are infinitesimally shape-similar. To begin, consider the following theorem pertaining to the complete framework $G^{\kappa}(x)$.

Theorem 5.1. *If the complete framework $G^{\kappa}(x)$ with $n \geq 3$ vertices is non-pathological and non-degenerate, then it is infinitesimally shape-similar.*[2]

Proof. If the complete framework $G^{\kappa}(x)$ with $n \geq 3$ vertices is non-pathological and non-degenerate, then the corresponding shape-similarity matrix $R_S(x)$ satisfies

$$\operatorname{rank}(R_S(x)) = \max_{x \in \mathbb{R}^{dn}} \left[\operatorname{rank}(R_S(x))\right].$$

Because the complete graph contains all edges, and thus all angles, the rank of the shape-similarity matrix of the complete framework satisfies

$$\operatorname{rank}(R_S(x)) = \max_{\mathcal{E}} \left[\max_{x \in \mathbb{R}^{dn}} \left[\operatorname{rank}(R_S(x))\right] \right]$$

[1] The same definition is used by [80] to define triangulated disks.

[2] A similar result was stated in [7, Lemma 1]; Thm. 5.1 and its proof reflect changes to the definition of pathological frameworks in Def. 3.4.

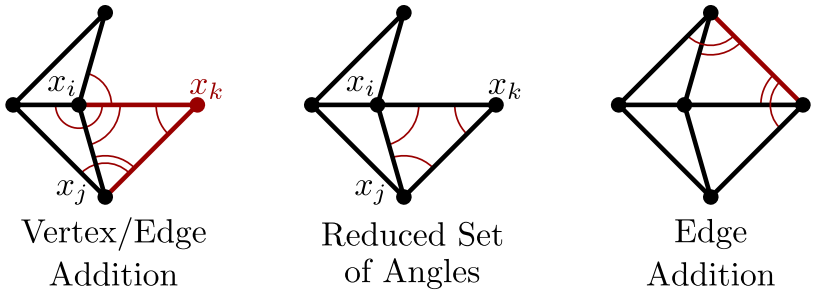

Figure 5.2: This image depicts the angles produced by vertex/edge-addition to aid in visualization of the proof of Thm. 5.2. The left image shows the angles produced by the addition of x_k, the center image shows the reduced set of angles, and the right image shows the angles resulting from edge-addition.

and equals the rank condition in (3.10), so by Thm. 3.3, $G^\kappa(x)$ is infinitesimally shape-similar. □

Having proved Thm. 5.1, the main result of this section can now be proved.

Theorem 5.2. *Triangulations are infinitesimally shape-similar.*[3]

Proof. The theorem is proved by induction, and for the purpose of this proof, $G(x^k)$ refers to a triangulation of k vertices; the corresponding shape-similarity matrix is $R_S(x^k)$.

Consider the triangulation $G(x^3)$, which by Thm. 5.1, is infinitesimally shape-similar with $\text{rank}(R_S(x^3)) = 2$. Suppose $G(x^{k-1})$ is an infinitesimally shape-similar triangulation with m angles. Connect x_k to adjacent vertices x_i and x_j on the outer face by two edges (Left, Figure 5.2). The triangulation is $G(x^k)$, whose shape-similarity matrix can be written as:

$$R_S(x^k) = \begin{bmatrix} R_S(x^{k-1}) & \mathbf{0} \\ A(x^k) & B(x^k) \end{bmatrix},$$

where $R_S(x^{k-1}) \in \mathbb{R}^{m \times 2(k-1)}$, $A(x^k) \in \mathbb{R}^{q \times 2(k-1)}$, $B(x^k) \in \mathbb{R}^{q \times 2}$, and q is the number of new angles formed by the vertex/edge-addition. The matrix $A(x^k)$ is composed of orthogonal projections of vectors including x_k onto vectors not including x_k, and $B(x^k)$ is formed of orthogonal projections onto vectors including x_k.

[3] [7, Theorem 4] proved that triangulated frameworks are infinitesimally shape-similar. Thm. 5.2 and its proof reflect clarifications to the definitions of triangulations and pathology; the proof is restructured to emphasize the edge additions that do not increase the rank of the shape-similarity matrix.

Consider the reduced shape-similarity matrix $\bar{R}_S(x^k)$ of $G(x^k)$ formed by considering only the three angles of the new triangle created by the vertex/edge-addition rather than the q new angles (Center, Figure 5.2), which can be written as

$$\bar{R}_S(x^k) = \begin{bmatrix} R_S(x^{k-1}) & \mathbf{0} \\ \bar{A}(x_i, x_j, x_k) & \bar{B}(x_i, x_j, x_k) \end{bmatrix},$$

where $\bar{A}(x_i, x_j, x_k)$ and $\bar{B}(x_i, x_j, x_k)$ are the rows of $A(x^k)$ and $B(x^k)$ corresponding with the three angles of the new triangle. Because $\bar{R}_S(x^k)$ has $q-3$ fewer rows than $R_S(x^k)$, $\operatorname{rank}(\bar{R}_S(x^k)) \leq \operatorname{rank}(R_S(x^k)) \leq 2k-4$.

Replacing $\bar{A}(x_i, x_j, x_k)$ with zeros yields the block diagonal matrix $\hat{R}_S(x^k)$, which is related to $\bar{R}_S(x^k)$ through the rank relationship: $\operatorname{rank}(\hat{R}_S(x^k)) \leq \operatorname{rank}(\bar{R}_S(x^k))$.

From the construction of the shape-similarity matrix,

$$\bar{B}(x_i, x_j, x_k) = \begin{bmatrix} -Q^\top_{z_{ik}}(z_{jk}) - Q^\top_{z_{jk}}(z_{ik}) \\ Q^\top_{z_{kj}}(z_{ji}) \\ Q^\top_{z_{ki}}(z_{ij}) \end{bmatrix}.$$

The rank of $\bar{B}(x_i, x_j, x_k)$ is at most 2. If the last two rows of $\bar{B}(x_i, x_j, x_k)$ were linearly dependent then there would exist a nonzero $\alpha \in \mathbb{R}$ such that $\alpha Q_{z_{kj}}(z_{ji}) = Q_{z_{ki}}(z_{ij})$, which re-written as $-\alpha Q_{z_{kj}}(z_{ij}) = Q_{z_{ki}}(z_{ij})$, can be expanded to

$$-\alpha\left(I_2 - \frac{z_{kj}z_{kj}^\top}{\|z_{kj}\|^2}\right) z_{ij} = \left(I_2 - \frac{z_{ki}z_{ki}^\top}{\|z_{ki}\|^2}\right) z_{ij}.$$

Such an α would require that z_{ki} be parallel with z_{kj}, contradicting the fact that $G(x^k)$ is a triangulation. Thus $\operatorname{rank}(\bar{B}(x_i, x_j, x_k)) = 2$, and because $\hat{R}_S(x^k)$ is block diagonal,

$$\operatorname{rank}(\hat{R}_S(x^k)) = \operatorname{rank}(R_S(x^{k-1})) + \operatorname{rank}(\bar{B}(x_i, x_j, x_k)) = 2k-4.$$

Because $\mathrm{rank}(\hat{R}_S(x^k)) \leq \mathrm{rank}(R_S(x^k))$, $R_S(x^k)$ satisfies the rank condition in (3.10) for infinitesimal shape-similarity.

To complete the proof, consider additional edges that could be added to $G(x^k)$ such that the resulting framework is still a triangulation (Right, Figure 5.2). Denote the shape-similarity matrix resulting from these edge-additions by $\tilde{R}_S(x^k)$. The edge-additions produce angles, so $\tilde{R}_S(x^k)$ has more rows than $R_S(x^k)$. Accordingly,

$$2k - 4 = \mathrm{rank}(R_S(x^k)) \leq \mathrm{rank}(\tilde{R}_S(x^k)) \leq 2k - 4,$$

so any edge-additions between vertices in the triangulation do not affect the rank, which was already at its maximum. By induction, triangulations are infinitesimally shape-similar. □

Remark 5.1. *The proof of Thm. 5.2 highlights the importance of the underlying repeated structure of triangulations. In the proof, each additional triangle created through vertex/edge addition increases the rank of the shape-similarity matrix of the triangulation by exactly two; this observation can be leveraged when controlling formations of mobile robots described by triangulations by requiring that one robot for each triangular face maintain two angles of that triangle.*

5.2 Assembly of a Class of Triangulations

Having established that all triangulations are infinitesimally shape-similar, this section introduces maximally outerplane graphs, a class of triangulations amenable to assembly by teams of bearing-only robots. Chapter 5.2.1 defines maximally outerplane graphs and comments on their properties. Then, Chapter 5.2.2 addresses the task of self-assembly of maximally outerplane graphs by teams of robots equipped with bearing-only sensors; a graph grammar is introduced to determine the desired network topology, and a controller that respects the interaction modalities available in the team is designed to realize the formation. In Chapter 5.2.3, the self-assembly mechanism is demonstrated on the Robotarium.

5.2.1 Defining Maximally Outerplane Graphs

Evident in the proof of Thm. 5.2, which iteratively examined the rank of the shape-similarity matrix of the triangulation to prove its infinitesimal shape-similarity, triangulations that are assembled by subsequent addition of triangular faces on the outer face of the framework exhibit an underlying structure that can be exploited. In fact, such triangulations are maximally outerplane graphs, defined as follows.

Definition 5.3 ([34, pg. 293])**.** *A* maximally outerplane graph *is a simple plane graph (a plane graph for which there are no parallel edges or loops) for which any edge addition results in a graph which is not an outerplane graph.*

Figure 5.1 distinguishes maximally outerplane graphs[4] from the broader class of triangulations. Maximally outerplane graphs with at least three vertices are triangulations as in Def. 5.2, so they are infinitesimally shape-similar. Furthermore, the weak dual graph of a maximally outerplane graph is a tree [81]; this is related to the observation of Rem. 5.1. The following subsection exploits the tree-structure of the weak dual graph in the design of a self-assembly mechanism for maximally outerplane graphs.

5.2.2 Self-Assembly of Maximally Outerplane Graphs

Here, a mechanism for self-assembly of maximally outerplane graphs by teams of robots equipped with bearing-only sensors is presented. The mechanism is composed of two parts, representing the duality of network topology and the interaction modalities available in a multi-robot team: a graph grammar to set the underlying graph structure, and a realizing bearing-only controller executed by all but two robots such that each triangular face becomes equilateral. These two parts of the self-assembly mechanism are described in turn.

[4]The assembled triangulations of [10] are maximally outerplane graphs.

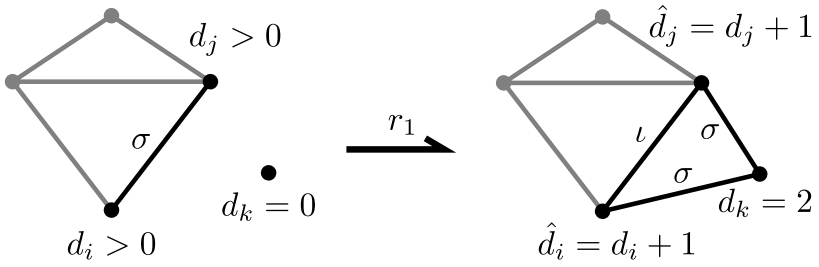

Figure 5.3: The rule r_1 connects disconnected vertices across adjacent vertices on the outer face of of a maximally outerplane graph.

A Graph Grammar to Set the Network Topology

To construct maximally outerplane graphs, define the graph grammar $\Phi = \{r_1\}$ consisting of the rule defined in Figure 5.3. Vertices are labeled by their degrees, denoted d_i for $i = 1, \ldots, n$. Edges are labeled as σ when they are on the outer face of the plane graph, or ι when it is not; r_1 connects a disconnected vertex to two vertices across a σ edge.

Theorem 5.3. *Let $\mathcal{G}_0$ be an initial plane graph consisting of n vertices in which three vertices form a triangle and the rest are disconnected. Let $g_0 = (\mathcal{G}_0, \nu)$ be an initial labeled graph where vertex i is labeled d_i, the degree of vertex i, and the three edges are labeled σ. Let $\Phi = \{r_1\}$ be the graph grammar, where r_1 is defined [5] as in Figure 5.3. For the system (g_0, Φ), the graphs $\mathcal{G}_k \in \{g_k\}_{k=0}^n$ have a single connected component, which is a maximally outerplane graph.*

Proof. The theorem will be proved by induction. The connected component of the initial plane graph $\mathcal{G}_0$ is a maximally outerplane graph. Consider $\mathcal{G}_k \in \{g_k\}_{k=0}^n$ for arbitrary $k < n$. By assumption, the single connected component of $\mathcal{G}_k$ is a maximally outerplane graph.

Apply r_1 to $\mathcal{G}_k$. The graph grammar $\Phi = \{r_1\}$ connects a zero degree vertex to two adjacent vertices connected by a σ edge on the outer face. Applying r_1 results in the maximally outer plane graph $\mathcal{G}_{k+1}$ because the new vertex can always be placed in the outer face of $\mathcal{G}_k$ such that: the new vertex is on the boundary of the outer face, no vertex

[5] In support of a self-assembly mechanism, the graph grammar of [7, Theorem 5] applied only to vertices with degree less than six; here, r_1 does not restrict the degree of the vertices.

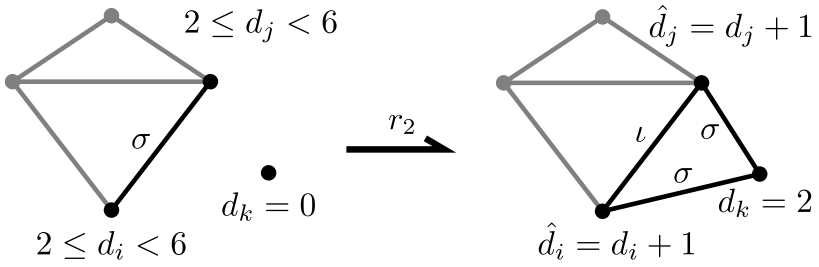

Figure 5.4: The rule r_2 connects disconnected vertices across adjacent vertices of degree less than six on the outer face of a maximally outerplane graph.

is removed from the boundary of the outer face, the two new edges intersect other edges only at the vertices, and $\mathcal{G}_k$ is edge maximal. By induction, the connected component of $\mathcal{G}_k \in \{g_k\}_{k=0}^n$ is a maximally outerplane graph. □

The graph grammar in Thm. 5.3 generates the network topology of the maximally outerplane graph. In the context of self-assembly of maximally outerplane graphs, it will be advantageous from a design perspective to restrict the degree of the vertices in the framework to between two and six; this will facilitate the assembly of isometric grid formations of regular triangles. With this regard, the following corollary, whose proof is nearly identical to that of Thm. 5.3, is presented for use in the self-assembly mechanism for maximally outerplane graphs.

Corollary 5.3.1. *Let $\mathcal{G}_0$ be an initial plane graph consisting of n vertices in which three vertices form a triangle and the rest are disconnected. Let $g_0 = (\mathcal{G}_0, \nu)$ be an initial labeled graph where vertex i is labeled d_i, the degree of vertex i, and the three edges are labeled σ. Let $\Phi = \{r_2\}$ be the graph grammar, where r_2 is defined as in Figure 5.4. For the system (g_0, Φ), the graphs $\mathcal{G}_k \in \{g_k\}_{k=0}^n$ have a single connected component, which is a maximally outerplane graph.*

Remark 5.2. *Numerous methods can be employed to produce triangulations: using embedded graph grammars [82]; Delaunay triangulation of a set of points; etc.. Similarly, there are various procedures for generating maximally outerplane graphs; e.g., ear clipping of certain polygons produces maximally outerplane graphs. The graph grammars in $\Phi = \{r_1\}$*

and $\Phi = \{r_2\}$ are notable because of the implicit role of the weak dual of the maximally outerplane graph and its relationship to the proof of Thm. 5.2, in which triangular faces are incorporated along the weak dual; this structure is exploited in self-assembly as well as in Chapter 4.2 when controlling mobile robot formations described by maximally outerplane graphs.

A Realizing Bearing-Only Controller

Here, the realizing bearing-only controller, henceforth referred to as the triangulation-maintenance controller for reasons that will be made apparent in due order, is developed to achieve self-assembly. In words, the purpose of this controller is to drive the robots to form equilateral triangles with neighbors in the maximally outerplane graph, as determined by the graph grammar in Cor. 5.3.1, while respecting the bearing-only sensing capabilities of the robots.

To begin, the capabilities of the robots are precisely stated. The frameworks $G(x)$ are assumed to be maximally outerplane graphs as generated according to the graph grammar in Cor. 5.3.1. The positions of the vertices of $G(x)$, $x = [x_1^\top, x_2^\top, \ldots, x_n^\top]^\top \in \mathbb{R}^{2n}$, represent the positions of mobile robots in the team; as such, the terms framework and vertex are analogous to formation and robot. The robots are assumed to have single-integrator dynamics of the form $\dot{x}_i = u_i$ for $i = 1, \ldots, n$. The velocities of the robots $\dot{x} = [\dot{x}_1^\top, \dot{x}_2^\top, \ldots, \dot{x}_n^\top]^\top$ are the infinitesimal motions of $G(x)$. By default, the robots are equipped with bearing-only sensors, which yield unit vectors relative to a local reference frame, and can only communicate with neighboring robots; i.e. if $(i, j) \in \mathcal{E}$, the robots i and j, henceforth referenced by their positions x_i and x_j, can communicate.

Proposition 5.1. *Because robots are positioned in the plane, communication of a common bearing between neighboring robots allows each robot to convert the bearing measurements of its neighbors into its own reference frame.*

Proof. Let $z_{ij}/\|z_{ij}\|$ be the bearing in the reference frame of x_j pointing from x_j to x_i, and

$\xi_{ij}/\|\xi_{ij}\| = -\xi_{ji}/\|\xi_{ji}\|$ be the same bearing in the reference frame of x_i. Because the robots are positioned in the plane, the reference frames of x_j and x_i differ by a single rotation. If x_i sends $\xi_{ij}/\|\xi_{ij}\|$ to x_j, x_j can determine the angle $\psi_{ij} = \cos^{-1}(z_{ij}^\top \xi_{ij}/\|z_{ij}\|\|\xi_{ij}\|)$ between their local reference frames. Using a rotation matrix $r(\psi_{ij}) \in \mathbb{R}^{2\times 2}$ satisfying $z_{ij}/\|z_{ij}\| = r(\psi_{ij})\xi_{ij}/\|\xi_{ij}\|$, bearings in the reference frame of x_i, such as $\xi_{ki}/\|\xi_{ki}\|$, can be expressed in the reference frame of x_j by $r(\psi_{ij})\xi_{ik}/\|\xi_{ik}\|$. □

Designed for robots equipped with bearing-only sensors, the triangulation-maintenance control strategy for maximally outerplane graphs is the realizing controller for the self-assembly mechanism. To develop this controller, control of a single face of the maximally outerplane graph is first considered; then, along the weak dual graph of the framework, the same controller is applied for each face to realize the assembled framework in which the inner faces are equilateral.

Consider the triangular subframework[6] $G(x_{ijk})$ formed by $x_{ijk} = [x_i^\top, x_j^\top, x_k^\top]^\top$ (Left, Figure 5.5). From the derivation of the shape-similarity matrix in (3.4),

$$\begin{bmatrix} \frac{d}{dt}\cos(\theta_{kji}) & \frac{d}{dt}\cos(\theta_{kij}) & \frac{d}{dt}\cos(\theta_{ikj}) \end{bmatrix}^\top = \Gamma(x_{ijk}) R_S(x_{ijk}) \dot{x}_{ijk},$$

where $R_S(x_{ijk}) \in \mathbb{R}^{3\times 6}$ is the shape-similarity matrix given explicitly in (3.5), $\Gamma(x_{ijk}) = \text{diag}(\gamma_{kji}, \gamma_{kij}, \gamma_{ikj}) \in \mathbb{R}^{3\times 3}$ is a diagonal matrix of positive scalars, and $\dot{x}_{ijk}$ are the velocities of the robots. Denote the first two rows of $R_S(x_{ijk})$ by

$$\begin{aligned} \bar{R}_S(x_{ijk}) &= \left[\begin{array}{cc|c} Q_{z_{ij}}^\top(z_{kj}) & -Q_{z_{ij}}^\top(z_{kj}) - Q_{z_{kj}}^\top(z_{ij}) & Q_{z_{kj}}^\top(z_{ij}) \\ -Q_{z_{ji}}^\top(z_{ki}) - Q_{z_{ki}}^\top(z_{ji}) & Q_{z_{ji}}^\top(z_{ki}) & Q_{z_{ki}}^\top(z_{ji}) \end{array}\right] \\ &= \left[\begin{array}{c|c} A_{ijk} & B_{ijk} \end{array}\right], \end{aligned}$$

[6]The notation x_{ijk} distinguishes the subframework $G(x_{ijk})$ from $G(x)$.

where $A_{ijk} \in \mathbb{R}^{2\times 4}$ and $B_{ijk} \in \mathbb{R}^{2\times 2}$ are partitions of $\bar{R}_S(x_{ijk})$, and define

$$b_{ijk} = A_{ijk} \begin{bmatrix} \dot{x}_i \\ \dot{x}_j \end{bmatrix}.$$

Associated with $\bar{R}_S(x_{ijk})$, $\bar{\Gamma}(x_{ijk}) = \text{diag}(\gamma_{kji}, \gamma_{kij})$ where

$$\gamma_{kji} = (\|z_{kj}\|\|z_{ij}\|)^{-1} \qquad \gamma_{kij} = (\|z_{ji}\|\|z_{ki}\|)^{-1}.$$

Finally, define the matrix

$$C_{ijk} = \text{diag}(\|z_{kj}\|, \|z_{ki}\|)B_{ijk} = \begin{bmatrix} \|z_{kj}\| Q_{z_{kj}}^\top(z_{ij}) \\ \|z_{ki}\| Q_{z_{ki}}^\top(z_{ji}) \end{bmatrix}$$

such that the matrix $\hat{R}_S(x_{ijk}) = \begin{bmatrix} \mathbf{0} & \mathbf{0} & C_{ijk} \end{bmatrix}$.

The purpose of the triangulation-maintenance controller is to stabilize the origin of the angle error

$$e^a_{ijk} = e^a(x_i, x_j, x_k) = \begin{bmatrix} \cos(\theta_{kji}) - \cos\left(\frac{\pi}{3}\right) \\ \cos(\theta_{kij}) - \cos\left(\frac{\pi}{3}\right) \end{bmatrix}.$$

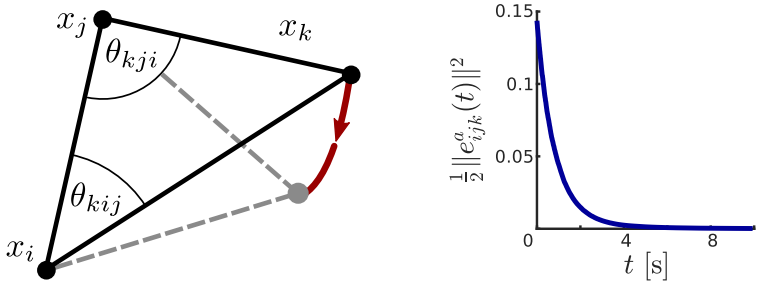

Figure 5.5: (Left) In a simulation of the triangulation-maintenance controller in Thm. 5.4, x_k moves along the red trajectory in order to drive the angles θ_{kij} and θ_{kji} to $\pi/3$. (Right) As stated in Thm. 5.4, under the triangulation-maintenance controller, the angle error converges asymptotically to zero.

The angle-error system has dynamics

$$\dot{e}^a_{ijk} = \begin{bmatrix} \frac{d}{dt}\cos(\theta_{kji}) \\ \frac{d}{dt}\cos(\theta_{kij}) \end{bmatrix} = \bar{\Gamma}(x_{ijk})\bar{R}_S(x_{ijk})\dot{x}_{ijk}.$$

Theorem 5.4. *If robot x_k executes*

$$\dot{x}_k = -C^\top_{ijk}\bar{\Gamma}(x_{ijk})e^a_{ijk} - B^\top_{ijk}(B_{ijk}B^\top_{ijk})^{-1}b_{ijk},$$

then $e^a_{ijk} = 0$ is locally asymptotically stable on the domain $D = \{e^a_{ijk} \in (-3/2, 1/2)^2\}$.[7]

Proof. Consider the Lyapunov function candidate $V(e^a_{ijk}) = \frac{1}{2}\|e^a_{ijk}\|^2$, for which $V(0) = 0$ and $V(e^a_{ijk}) > 0$ for $e^a_{ijk} \in D - \{0\}$. Define

$$\begin{aligned} \dot{x}^1_k &= -C^\top_{ijk}(x_{ijk})\bar{\Gamma}(x_{ijk})e^a_{ijk} \\ \dot{x}^2_k &= -B^\top_{ijk}(B_{ijk}B^\top_{ijk})^{-1}b_{ijk}; \end{aligned}$$

$B_{ijk}B^\top_{ijk}$ is invertible because because B_{ijk} is full rank. Writing the dynamics of x_k as $\dot{x}_k = \dot{x}^1_k + \dot{x}^2_k$ gives

$$\dot{x}_{ijk} = \begin{bmatrix} \mathbf{0} \\ \mathbf{0} \\ \dot{x}^1_k \end{bmatrix} + \begin{bmatrix} \dot{x}_i \\ \dot{x}_j \\ \dot{x}^2_k \end{bmatrix} = -\hat{R}^\top_S(x_{ijk})\bar{\Gamma}(x_{ijk})e^a_{ijk} + \begin{bmatrix} \dot{x}_i \\ \dot{x}_j \\ \dot{x}^2_k \end{bmatrix}.$$

Substituting these dynamics into the error dynamics yields

$$\dot{e}^a_{ijk} = -\bar{\Gamma}(x_{ijk})\bar{R}_S(x_{ijk})\hat{R}^\top_S(x_{ijk})\bar{\Gamma}(x_{ijk})e^a_{ijk} + \bar{\Gamma}(x_{ijk})\bar{R}_S(x_{ijk}) \begin{bmatrix} \dot{x}_i^\top & \dot{x}_j^\top & \dot{x}_k^{2\top} \end{bmatrix}^\top;$$

[7] A similar controller is presented in [10, Theorem 2]; the controller in Thm. 5.4 reflects the reformulation of the shape-similarity matrix in Chapter 3.2.

The vector $\dot{x}_k^2$ is chosen such that $[\dot{x}_i^\top,\, \dot{x}_j^\top,\, \dot{x}_k^{2\top}]^\top \in \ker(\bar{R}_S(x_{ijk}))$, so

$$\dot{e}_{ijk}^a = -\bar{\Gamma}(x_{ijk})\bar{R}_S(x_{ijk})\hat{R}_S^\top(x_{ijk})\bar{\Gamma}(x_{ijk})e_{ijk}^a,$$

and the time derivative of the Lyapunov function is

$$\dot{V}(e_{ijk}^a) = -e_{ijk}^{a\top}\bar{\Gamma}(x_{ijk})\bar{R}_S(x_{ijk})\hat{R}_S^\top(x_{ijk})\bar{\Gamma}(x_{ijk})e_{ijk}^a.$$

Recognizing that

$$\bar{R}_S(x_{ijk})\hat{R}_S^\top(x_{ijk}) = B_{ijk}B_{ijk}^\top \operatorname{diag}(\|z_{kj}\|, \|z_{ki}\|) \succ 0,$$

$\dot{V}(e_{ijk}^a) < 0 \in D - \{0\}$; thus, the origin $e_{ijk}^a = 0$ is locally asymptotically stable. □

A simulation of the triangulation-maintenance controller is shown in Figure 5.5: the left image shows the trajectory of x_k as it executes the triangulation-maintenance controller, and the right image confirms that the squared norm of the angle error converges to zero. To calculate this controller, x_k must communicate with x_i and x_j to determine the bearing $z_{ij}/\|z_{ij}\|$ and the velocities $\dot{x}_i$ and $\dot{x}_j$ (Prop. 5.1). From its own bearing measurements and the bearing $z_{ij}/\|z_{ij}\|$, robot x_k can construct $\dot{x}_k^1$ because the quantities $Q_{z_{kj}}^\top(z_{ij}/\|z_{ij}\|)$ and $Q_{z_{ki}}^\top(z_{ji}/\|z_{ji}\|)$ are composed of bearings; similarly, $\dot{x}_k^2$ can be constructed from information available through communication. To show this, examine B_{ijk} and b_{ijk} :

$$B_{ijk} = \begin{bmatrix} Q_{z_{kj}}^\top(z_{ij}) \\ Q_{z_{ki}}^\top(z_{ji}) \end{bmatrix},$$

$$b_{ijk} = \begin{bmatrix} Q_{z_{ij}}^\top(z_{kj})\,(\dot{x}_i - \dot{x}_j) - Q_{z_{kj}}^\top(z_{ij})\dot{x}_j \\ Q_{z_{ji}}^\top(z_{ki})\,(\dot{x}_j - \dot{x}_i) - Q_{z_{ki}}^\top(z_{ji})\dot{x}_i \end{bmatrix}.$$

When the vectors z_{ij}, z_{kj}, and z_{ki} are replaced with bearings,

$$\hat{B}_{ijk} = \begin{bmatrix} Q_{z_{kj}}^{\top} \left(\frac{z_{ij}}{\|z_{ij}\|} \right) \\ Q_{z_{ki}}^{\top} \left(\frac{z_{ji}}{\|z_{ij}\|} \right) \end{bmatrix} = \frac{1}{\|z_{ij}\|} B_{ijk}.$$

Because x_k can communicate with x_i and x_j, it can determine θ_{kij}, θ_{kji}, and θ_{ikj}. By the Law of Sines,

$$\nu_1 = \frac{\|z_{kj}\|}{\|z_{ij}\|} = \frac{\sin(\theta_{kij})}{\sin(\theta_{ikj})} \qquad \nu_2 = \frac{\|z_{ki}\|}{\|z_{ij}\|} = \frac{\sin(\theta_{kji})}{\sin(\theta_{ikj})},$$

so the distances $\|z_{ki}\|$ and $\|z_{kj}\|$ can be determined relative to $\|z_{ij}\|$ with bearing-only sensing; using ν_1 and ν_2, define

$$\hat{b}_{ijk} = \begin{bmatrix} Q_{z_{ij}}^{\top} \left(\frac{\nu_1 z_{kj}}{\|z_{kj}\|} \right) (\dot{x}_i - \dot{x}_j) - Q_{z_{kj}}^{\top} \left(\frac{z_{ij}}{\|z_{ij}\|} \right) \dot{x}_j \\ Q_{z_{ji}}^{\top} \left(\frac{\nu_2 z_{ki}}{\|z_{ki}\|} \right) (\dot{x}_j - \dot{x}_i) - Q_{z_{ki}}^{\top} \left(\frac{z_{ji}}{\|z_{ij}\|} \right) \dot{x}_i \end{bmatrix}.$$

Because $\hat{B}_{ijk}^{\top}(\hat{B}_{ijk}\hat{B}_{ijk}^{\top})^{-1}\hat{b}_{ijk}$ can be determined using bearing-only sensors and communication, and because

$$\hat{B}_{ijk}^{\top}(\hat{B}_{ijk}\hat{B}_{ijk}^{\top})^{-1}\hat{b}_{ijk} = B_{ijk}^{\top}(B_{ijk}B_{ijk}^{\top})^{-1}b_{ijk},$$

$\dot{x}_k^2$ can be calculated by x_k.

The Complete Self-Assembly Mechanism

Having introduced the graph grammar in Cor. 5.3.1 for generating the maximally outerplane graph and the realizing bearing-only controller in Thm. 5.4 for the maintenance of equilateral triangles, the complete self-assembly mechanism for maximally outerplane graphs is presented. As suggested in the development, self-assembly is executed in two repeating steps: first, the network topology is determined using the graph grammar; then,

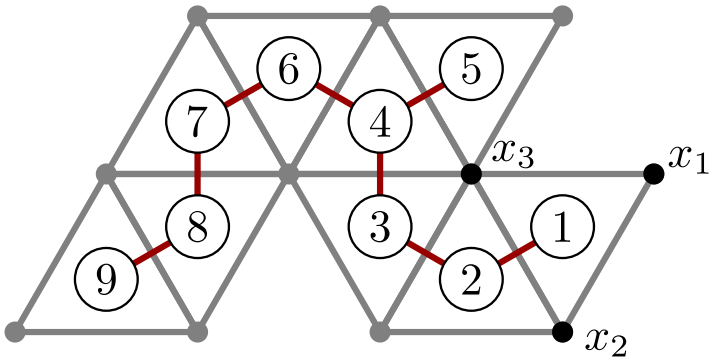

Figure 5.6: To control maximally outerplane graphs, a direction is assigned to the weak dual graph; starting with the first triangular face, which has x_1 and x_2 on its boundary, the triangulation-maintenance controller of Thm. 5.4 is applied for each face along the tree.

the triangulation-maintenance controller is executed. The two-step process described here is repeated until all robots are incorporated into the maximally outerplane graph.

In detail, this self-assembly process executes the triangulation-maintenance controller of Thm. 5.4 to each triangular face along the weak dual graph of the maximally outerplane graph $G(x)$, locally asymptotically stabilizing the origins of the angle-error systems of each face. Implicit in the graph-grammar, a direction is assigned to the weak dual graph of the framework, as in Figure 5.6, such that it forms a directed tree whose root corresponds with a triangular face which has x_1 and x_2 on its boundary. For convenience, robots x_i, for $i = 3, \ldots, n$, are ordered according to the directed tree such that x_i corresponds to the triangular face $i - 2$. Applied in this way, the self-assembly mechanism results in a maximally outerplane graph for which each triangular face asymptotically approaches an equilateral triangle; to prove this, the following quantities are introduced.

The total angle error is defined to be the vector of the angle errors of each of the $n - 2$ triangular faces, $e^a = [e_1^{a\top}, \ldots, e_{n-2}^{a\top}]^\top$. It is occasionally convenient to refer to each angle error by the corresponding vertices of the triangular face; e.g., $e_1^a = e_{123}^a$. The self-assembly mechanism described above yields the following theorem.

Theorem 5.5. *Let $G(x)$ be a maximally outerplane graph, and suppose $\dot{x}_1 = \dot{x}_2 = 0$. If each x_i for $i = 3, ..., n$ executes the triangulation-maintenance controller in Thm. 5.4 for a*

triangular face along the directed weak dual graph of $G(x)$, then the origin of the total angle error, $e^a = 0$, is locally asymptotically stable on the domain $D = \{e^a \in (-3/2, 1/2)^{2(n-2)}\}$.

Proof. For each triangular face, define the Lyapunov functions $V_\ell(e^a_\ell) = \frac{1}{2}\|e^a_\ell\|^2 > 0 \; \forall e^a \in D - \{0\}$; under the controller in Thm. 5.4, $\dot{V}_\ell(e^a_\ell) < 0 \quad \forall e^a \in D - \{0\}$. Consider the Lyapunov function $V(e^a) = \sum_{\ell=1}^{n-2} V_\ell(e^a_\ell) > 0 \; \forall e^a \in D - \{0\}$, which has the time derivative, $\dot{V}(e^a) = \sum_{\ell=1}^{n-2} \dot{V}_\ell(e^a_\ell)$.

First, note that $\dot{x}_1 = \dot{x}_2 = 0$ and do not depend on any x_i for $i = 3, ..., n$. Now, consider an arbitrary triangular face $G(x_{ijk})$ and corresponding angle-error system $e^a_\ell(x_i, x_j, x_k)$. Because there is exactly one vertex executing the controller in Thm 5.4 for each triangular face, $\dot{x}_i$ and $\dot{x}_j$ do not depend on x_k, and $\dot{x}_k$ depends only on the positions and velocities of robots x_i and x_j. Thus,

$$\dot{V}_\ell(e^a_\ell) = \frac{\partial V_\ell(e^a_\ell)}{\partial e^a} \frac{\partial e^a}{\partial x} \dot{x} = \frac{\partial V_\ell(e^a_\ell)}{\partial e^a_\ell} \frac{\partial e^a_\ell}{\partial x_{ijk}} \dot{x}_{ijk},$$

so the angle errors are decoupled, $\dot{V}(e^a) < 0 \; \forall e^a \in D - \{0\}$, and $e^a = 0$ is locally asymptotically stable. □

When used in exclusion of self-assembly, or to maintain a maximally outerplane graph which has already been assembled, the control strategy described in Thm. 5.5 is referred to as the triangulation-maintenance control strategy, so named because this strategy can only be used to maintain the formation as explained in the following remark.

Remark 5.3. *While the control strategy described in Thm. 5.5 locally asymptotically stabilizes the total-angle-error system, the triangulation-maintenance-control strategy does not control the position, heading, or scale of the formation, which are determined by $x_1(0)$ and $x_2(0)$. Because angles are invariant to scale, robots equipped with bearing-only sensors cannot directly recover the distance information needed to control these quantities, which motivates the incorporation of a single robot that can measure both distances and bearings.*

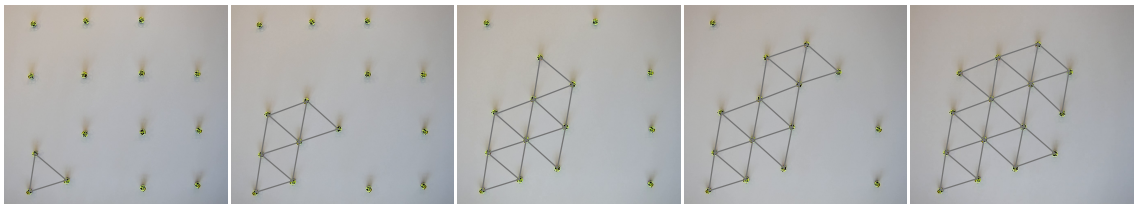

Figure 5.7: The graph grammar in Cor. 5.3.1 and the realizing bearing-only controller Thm. 5.4 were used to self-assemble a maximally outerplane graph of 15 differential-drive robots. Starting with the initial triangle, the self-assembly mechanism is iteratively applied until all are in formation; the black lines indicate the underlying graph topology of the maximally outerplane graph.

5.2.3 Self-Assembly Demonstration

In order to demonstrate the efficacy of the self-assembly mechanism for formations of robots equipped with bearing-only sensors described by maximally outerplane graphs as described in Chapter 5.2.2, self-assembly was performed by a team of differential-drive robots on the Robotarium. Figure 5.7 shows the self-assembly of a maximally outerplane graph of 15 differential-drive robots. With respect to the initial conditions of the first two robots, the first triangular face is formed by the third robot, which executes the triangulation-maintenance controller in Thm. 5.4. Having established the initial triangular framework $G_0(x)$ required by the graph grammar in Cor. 5.3.1, the self-assembly mechanism is applied successively by each robot until the final realization of the maximally outerplane graph is achieved. As stated in Thm. 5.5, the faces of the maximally outerplane graph all asymptotically become regular.

5.3 Leveraging Heterogeneous Interactions for Control

In this section, the previously developed self-assembly mechanism, and in particular, the triangulation-maintenance control strategy, are revisited to examine the importance of the incorporation of heterogeneous interaction modalities in a multi-robot team for the purpose of achieving effective formation control. Previously, a team of robots equipped with bearing-only sensors was considered, and the triangulation-maintenance controller was designed to respect this sensing constraint; however, it was noted in Rem. 5.3 that with this restriction,

controlling the formation to achieve objectives other than formation stabilization, such as navigation through an environment, was not feasible. Thus, to demonstrate the significance of heterogeneity and to explore methods of leveraging heterogeneous interaction modalities in a multi-robot team, this section builds on the triangulation-maintenance control strategy, addressing formation control of a team of bearing-only robots in which a single robot is additionally capable of measuring distances.

To begin, the following notation is introduced to complement that of Chapter 5.2.2. In particular, the capabilities of the robots are precisely stated, and the position, heading, and scale of formations of robots are defined. Again, the frameworks $G(x)$ are assumed to be maximally outerplane graphs, and as previously assumed, the robots are equipped with bearing-only sensors, which yield unit vectors relative to a local reference frame, and can only communicate with neighboring robots.

Now, designate the first robot as the leader, $x_1 = x_l$, and the second robot as the first follower, $x_2 = x_f$. Define the position of $G(x)$ to be x_l, the scale to be $\|x_l(t) - x_f(t)\|/\|x_l(0) - x_f(0)\| = \|z_{lf}(t)\|/\|z_{lf}(0)\|$, and the heading to be $z_{lf}/\|z_{lf}\|$. Unlike every other robot in the team, with exception, perhaps, to the leader as will be discussed later in this section, the first follower is assumed to be able to measure distances in addition to bearings. Leveraging this incorporation of distance information, this section develops a decentralized, heterogeneous, leader-follower control strategy for multi-robot formations described by maximally outerplane graphs.

5.3.1 Position, Scale, and Heading Control of Maximally Outerplane Graphs

To leverage the capability of the first follower to measure distances in addition to bearings, a heterogeneous formation-control strategy is developed here to control the position, heading, and scale of the team of robots described by a maximally outerplane graph as assembled in Chapter 5.2.2. The development of this control strategy relies on assigning controllers to the leader and first follower, which for triangulation maintenance, as previously stated in

Thm. 5.5, were otherwise assumed to be equivalently zero. To begin, the role of the leader will be discussed.

As detailed in the introduction of the heterogeneous formation-control strategy in Chapter 5.3, the position of the leader is the position of the formation; thus, position control is achieved through control of the leader. Because the desired position of the formation depends on the specific objectives of the team, the particular choice of $\dot{x}_l$ is unspecified. For example, if the objective of the team is simply to drive to a particular location $\zeta \in \mathbb{R}^2$, a proportional controller of the form $\dot{x}_l = \zeta - x_l$, suffices. The choice of $\dot{x}_l$ has implications on the required sensing capabilities of the leader. Continuing the example, to calculate $\zeta - x_l$, the leader must know its position relative to ζ, which could be given to x_l by: a supervisory planner responsible for determining the desired position of the formation; a human pilot, which is directing the motion of the formation; or the robot itself, which would at least require distance and bearing sensors. Due to the coupling with the objective of the team, and because $\dot{x}_l$ can be chosen independently of the positions of the other robots, the sensing capabilities of x_l are not explicitly considered.

Using the leader to control the position of the formation, the first follower is used to set its scale and heading as defined in the introduction of Chapter 5.3. Let Δ be the desired distance between x_l and x_f, and define the scale error

$$e^s_{lf} = e^s(x_l, x_f) = \Delta - \|x_l - x_f\| = \Delta - \|z_{lf}\|;$$

the scale-error system is

$$\dot{e}^s_{lf} = -\frac{d}{dt}\left(\|z_{lf}\|\right) = -\frac{z_{lf}^\top}{\|z_{lf}\|}\left(\dot{x}_l - \dot{x}_f\right).$$

To describe the desired heading of the formation, use

$$\frac{z_{pl}}{\|z_{pl}\|} = \frac{p - x_l}{\|p - x_l\|},$$

where p is a virtual point determined by the first follower that moves according to $\dot{p} = \dot{x}_l$; the vector $z_{pl} = z_{pf} + z_{fl}$ can be determined by x_f because it has bearing and distance sensors. The error between the cosine of the desired and current heading can be written as

$$e^h_{lf} = \cos(0) - \cos(\theta_{plf}) = 1 - \frac{z_{pl}^\top z_{fl}}{\|z_{pl}\|\|z_{fl}\|};$$

the heading-error system is

$$\begin{aligned}
\dot{e}^h &= -\frac{d}{dt}\cos(\theta_{plf}) \\
&= -\gamma_{plf}\left(Q^\top_{z_{pl}}(z_{fl})\dot{p} - Q^\top_{z_{fl}}(z_{pl}) - Q^\top_{z_{pl}}(z_{fl}) + Q^\top_{z_{fl}}(z_{pl})\dot{x}_f\right) \\
&= -\gamma_{plf} Q^\top_{z_{fl}}(z_{pl})\left(\dot{x}_f - \dot{x}_l\right),
\end{aligned}$$

where $\gamma_{plf} = (\|z_{pl}\|\|z_{fl}\|)^{-1}$.

Theorem 5.6. *Suppose $x_f(0) \neq x_l(0)$, and suppose the velocity of the first follower is given by*[8]

$$\dot{x}_f = \gamma^{-1}_{plf} Q_{z_{fl}}(z_{pf}) + \frac{z_{lf}}{\|z_{lf}\|}\left(\|z_{lf}\| - \Delta\right) + \dot{x}_l;$$

then $e^s_{lf} = 0$ is globally exponentially stable, and $e^h_{lf} = 0$ is locally asymptotically stable on $D = \{e^h_{lf} \in (0, 2)\}$.

[8] Thm. 5.6 updates the controller of [10, Theorem 3] to reflect necessary changes in the development of the shape-similarity matrix in Chapter 3.

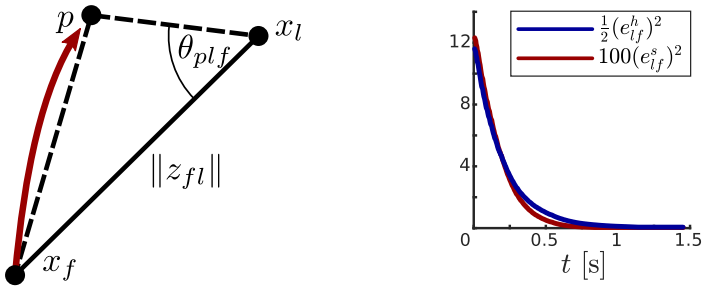

Figure 5.8: (Left) In a simulation of the scale-heading controller in Thm. 5.6, x_f moves along the red trajectory in order to drive $\|z_{lf}\| \to \Delta$ and $\theta_{plf} \to 0$. (Right) As stated in Thm. 5.6, the squared norms of the scale and heading errors, scaled to appear on the same axes, converge asymptotically to zero.

Proof. Notice that $Q_{z_{fl}}(z_{pf})$ is orthogonal to z_{lf}. Substituting $\dot{x}_f$ into the scale-error system yields

$$\dot{e}^s_{lf} = -\frac{z_{lf}^\top}{\|z_{lf}\|}\left(\frac{z_{lf}}{\|z_{lf}\|}e^s_{lf}\right) = -e^s_{lf},$$

so $e^s_{lf} = 0$ is globally exponentially stable.

For stability of $e^h_{lf} = 0$, consider the Lyapunov function $V(e^h_{lf}) = \frac{1}{2}(e^h_{lf})^2$, where $V(e^h_{lf}) > 0\ \forall e^h_{lf} \in D - \{0\}$ and $V(0) = 0$. The time derivative is

$$\begin{aligned}\dot{V}(e^h_{lf}) &= -e^h_{lf}\frac{d}{dt}\cos(\theta_{plf}) \\ &= -e^h_{lf}\gamma_{plf}Q^\top_{z_{fl}}(z_{pl})\left(\gamma^{-1}_{plf}Q_{z_{fl}}(z_{pf})\right) \\ &= -e^h_{lf}z^\top_{pl}Q_{z_{fl}}(z_{pf}) < 0\ \forall e^h_{lf} \in D - \{0\}\end{aligned}$$

because $z^\top_{pl}Q_{z_{fl}}(z_{pf}) > 0$ in $D - \{0\}$. Thus, $e^h_{lf} = 0$ is locally asymptotically stable. □

A simulation of the scale-heading controller of Thm. 5.6 is shown in Figure 5.8: the left image depicts the trajectory of x_f as it executes the controller, and the right image confirms that the scale and heading errors converge asymptotically to zero. To determine the scale-heading controller in Thm. 5.6, the dynamics $\dot{x}_l$ must be communicated to x_f as in Prop. 5.1.

Finally, with controllers for x_l and x_f to set the position, scale, and heading of the formation, the complete heterogeneous formation-control strategy for teams of robots

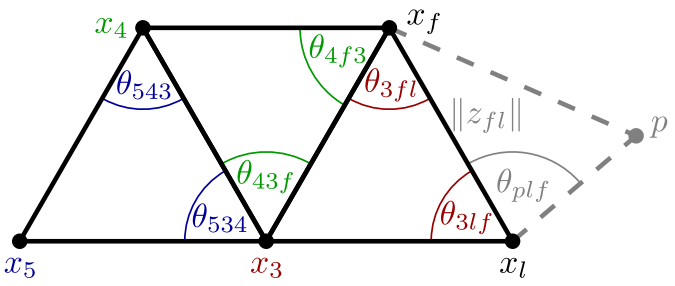

Figure 5.9: The leader x_l sets position of the formation, and the first follower x_f executes the scale-heading controller in Thm. 5.6 to control the scale and heading by driving $\|z_{lf}\| \to \Delta$ and $\theta_{plf} \to 0$. The remaining robots execute the triangulation-maintenance controller in Thm. 5.4 (colored labels indicate the robots responsible for the angles).

described by maximally outerplane graphs is presented. As in the previous section, the triangulation-maintenance controller is applied for each triangular face along the weak dual graph of the framework with the additional controllers for x_l and x_f in the first triangular face as depicted in Figure 5.9.

Theorem 5.7. *Let $G(x)$ be a maximally outerplane graph; suppose that $\dot{x}_l = u_l$ is independent of x_i for $i = 2, \ldots, n$ and that $\dot{x}_f$ is the scale-heading controller of Thm. 5.6. If each x_i for $i = 3, ..., n$ executes the triangulation-maintenance controller in Thm. 5.4 for a triangular face along the directed weak dual graph of $G(x)$, then $e^a = 0$ is locally asymptotically stable on the domain $D = \{e^a \in (-3/2, 1/2)^{2(n-2)}\}$.*

Proof. Substituting $\dot{x}_l$ and $\dot{x}_f$, which are independent of x_i for $i = 3, \ldots, n$, the proof follows from that of Thm. 5.5. □

Note the following of the formation-control strategy in Thm. 5.7. First, the formation-control strategy is heterogeneous in the controllers executed by the robots and their sensing capabilities; only one robot explicitly requires distance information. Second, the formation-control strategy is decentralized because each robot needs only communicate with its neighbors. Third, the formation-control strategy offers a clear method of directing the motion of the formation through control of the leader and choices of the desired heading and scale. Lastly, the asymptotic stability of the various error systems ensures robustness for execution by multi-robot teams, showcased in the demonstration of the following section.

5.4 Robotarium Demonstration

In this section, the formation-control strategy for maximally outerplane graphs in Thm. 5.7 is executed by a team of differential-drive robots in the Robotarium [5].

Stills from the demonstration are shown in Figure 5.10. Projected onto the testbed surface, the black lines denote adjacency relationships in the formation, and the dark regions represent obstacles; the leader and first follower are indicated by the green and red LEDs

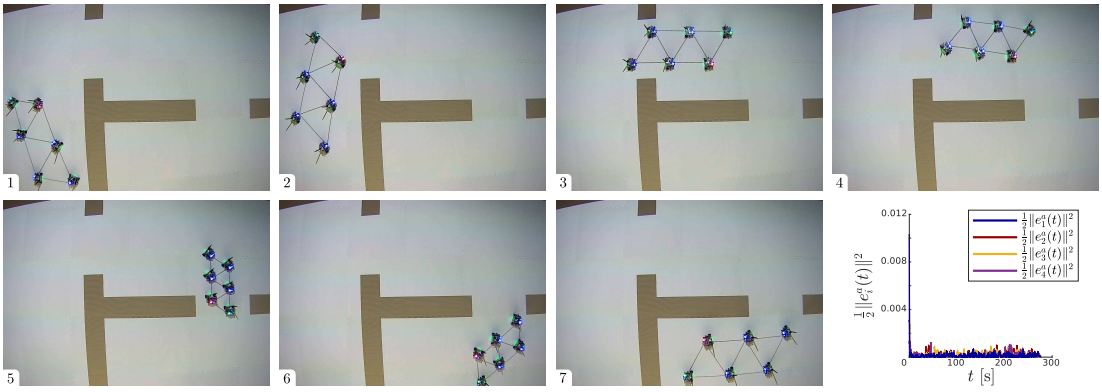

Figure 5.10: The heterogeneous formation-control strategy in Thm. 5.7 is executed by a team of six differential-drive robots on the Robotarium [5]. Projected onto the testbed surface, the dark regions represent obstacles, and the black lines denote the underlying network topology of the team. Using the formation-control strategy, the robots maintain the maximally outerplane graph as they translate, rotate, and scale uniformly to navigate through two narrow passages in the environment. In the bottom right image, the squared norm of the angle error of each triangular face along the weak dual graph is shown.

respectively. Beginning with the initial positions in the first image, the six differential-drive robots form the maximally outerplane graph. In the demonstration, the leader executes a controller to visit a sequence of points along a planned path through the environment; as the leader moves, the first follower executes the scale-heading controller in Thm. 5.6 for a corresponding sequence of desired scales and headings. The remaining robots execute the triangulation-maintenance controller in Thm. 5.4 to maintain the formation as the team translates, rotates, and scales to navigate the narrow passages in the environment; shown in the bottom right image of Figure 5.10, the efficacy of triangulation maintenance is quantified by the squared norm of the angle errors of the triangular faces, which decreases from the initial conditions and remains near zero throughout the demonstration.

5.5 Summary of Conclusions

In this chapter, formation control of a class of triangulations of robots was used to illustrate the importance of heterogeneity in the interaction modalities of a multi-robot team. First, using the theoretical tools of Chapter 3, triangulations were first shown to be infinitesimally shape-similar, a process that not only made explicit use of the shape-similarity matrix and its rank condition, but revealed the structure of a class of triangulations, maximally

outerplane graphs, which were amenable to formation control. From there, a self-assembly mechanism for teams of robots equipped with bearing-only sensors was developed to realize formations described by maximally outerplane graphs. The self-assembly mechanism, and the triangulation-maintenance control strategy that resulted from it, highlighted the extent of the capabilities of a team of robots equipped with bearing-only sensors; in particular, formation stabilization of the maximally outerplane graph was possible with bearing-only sensors, but achieving higher-level objectives demonstrated the need for some additional sensing modality in the network. With this regard, a single robot was additionally equipped with a distance sensor; with this additional capability, the triangulation-maintenance control strategy was modified to include controllers for the previously unused robots in the first triangular face of the maximally outerplane graph. With the lead robot to set the position of the framework, and the first follower to set the heading and scale of the formation, the leader-follower, heterogeneous formation-control strategy for teams of robots described by maximally outerplane graphs was designed and demonstrated on a team of differential-drive robots.

From the developments of this section, the following conclusions can be drawn with respect to the overarching objective of this thesis to investigate the interplay between network topology and the sensing and communication modalities of a multi-robot team. First, regarding the structure of the maximally outerplane graphs and the triangulation-maintenance controller designed for them, and in contrast with the sensing and communication requirements of the controllers in Chapter 4, bearing-only information, as opposed to bearing and distance information, was sufficient stabilize the formation due to the underlying network structure of the maximally outerplane graphs; this substantiates the claim in Chapter 4.3 that there are potential trade-offs between network structure and the required interaction modalities of a team. The demonstration of the existence of this trade-off between network topology and the required interaction modalities is a major conclusion of this chapter.

Following this first conclusion and with regard to the overall objective of this thesis,

the development of the heterogeneous formation-control strategy for maximally outerplane graphs yields another important revelation. As shown in the development of the triangulation-maintenance controller, limitation of the sensing modalities available in the networked team effectively restricted the capabilities of the formation. Interestingly, the incorporation of a single robot capable of measuring distances, exploited by a controller designed to drive the length and bearing of a single edge in the framework to desired values, was sufficient to enable control of the position, heading, and scale of the formation as an extension of the self-assembly mechanism for maximally outerplane graphs. The fact that control of the scale and heading of the formation required the control of the length and bearing of a single edge in the framework is fundamentally coupled with the fact that maximally outerplane graphs are infinitesimally shape-similar, and thus, angle maintenance results in invariance to translation, rotation, and uniform scaling. In order to achieve a particular rotation, control of a bearing, which is not invariant to rotation, was necessary, and in order to achieve a particular scale, control of a distance was required; this observation suggests that the need for heterogeneous interaction modalities is necessary when invariance to certain motions is not desirable. As such, Chapter 6 explicitly compares the framework properties of infinitesimal rigidity, bearing-rigidity, and shape-similarity to further expose the significance of heterogeneous interaction modalities in a networked multi-robot team.

CHAPTER 6
COMPARING FRAMEWORK PROPERTIES

To expand the exploration of the interplay between network topology and the interaction modalities available in a multi-robot team, this chapter exposes the relationships between the framework properties of infinitesimal rigidity, bearing-rigidity, and shape-similarity. In order to understand the underlying relationships between these framework properties, algebraic relationships between the rigidity, bearing-rigidity, and shape-similarity matrices are examined. Significantly, these relationships are sensitive to dimension; as such this section is divided into two parts: Chapter 6.1 presents established results in the literature to prove the equivalence of these properties in the plane, and Chapter 6.2 explores the implications of these properties, providing counterexamples to explain that equivalence does not hold in higher dimensions. Finally, Chapter 6.3 summarizes the conclusions that are drawn from this investigation as they pertain to the coupling of network topology and available interaction modalities.

6.1 Framework Properties in the Plane

In this section, the framework properties of infinitesimal rigidity, bearing-rigidity, and shape-similarity are related for frameworks in the plane, i.e., for $G(x)$ in $\mathbb{R}^2$ for which $x \in \mathbb{R}^{2n}$. To relate these properties, results established in [78] and [57] are first presented as lemmas using the parlance of this thesis.

The following lemma relating infinitesimal shape-similarity and infinitesimal bearing-rigidity in the plane can be found in [78]; to express this result in the language of this thesis, the following substitution has been made. As mentioned in Chapter 3, infinitesimal angle-rigidity as defined in [78, Definition 3.4] is equivalent to that infinitesimal shape-similarity when restricting frameworks to the plane. As such, in the following lemma, infinitesimal

shape-similarity replaces infinitesimal angle-rigidity, and explicit reference to the dimension of the framework is made.

Lemma 6.1 ([78, Theorem 3])**.** *In $\mathbb{R}^2$, a framework is infinitesimally shape-similar if and only if it is infinitesimally bearing-rigid.*

Next, the following lemma relates infinitesimal bearing-rigidity and infinitesimal rigidity in the plane; note that the authors of [57] refer to rigidity by the phrase "distance rigidity."

Lemma 6.2 ([57, Theorem 8])**.** *In $\mathbb{R}^2$, a framework is infinitesimally bearing-rigid if and only it is infinitesimally rigid.*

Having introduced these two supporting lemmas, the following theorem relates infinitesimal shape-similarity and infinitesimal rigidity in the plane.

Theorem 6.1. *In $\mathbb{R}^2$, a framework is infinitesimally shape-similar if and only if it is infinitesimally rigid.*

Proof. The statement holds as an immediate consequence of the equivalences presented in Lem. 6.1 and Lem. 6.2. □

The following observations discuss the unique nature of the plane as it pertains to these results, and highlights the significance of these results to this thesis.

The equivalence between infinitesimal rigidity, bearing-rigidity, and shape-similarity is derived from the unique nature of the plane as compared to higher dimensional spaces. In particular, in the plane, rotation of a set of points, and any subset of those points, occurs in the same plane. As such, vectors that are orthogonal in the plane, such as those pointing between vertices in a framework, can be easily represented as a rotation of the vector by $\pi/2$ in the only available plane of rotation; this fact is used explicitly in both the proof of Lem. 6.1 and Lem. 6.2, and the breakdown of these equivalences in higher dimension is a result of the $\binom{d}{2}$ available planes of rotation.

Taken together, these three results are significant for a number of reasons. For formation control of mobile ground robots, these results are significant because they pertain to the plane, in which such robots are usually assumed to operate. From the perspective of generating infinitesimally shape-similar frameworks in the plane, the result in Thm. 6.1 suggests that any method of generating infinitesimally rigid frameworks in the plane, such as the Henneberg construction or other methods as in [47], immediately produce frameworks that are infinitesimally shape-similar. For examining the interplay between network topology and the interaction modalities of a multi-robot team, the results in Lem. 6.1, Lem. 6.2, and Thm. 6.1 indicate that for the same underlying graph topology, it is the particular constraints themselves, be they distance, bearing, or angle constraints, that determine the available motions of the framework.

6.2 Framework Properties in Higher Dimensions

In this section, the relationships between infinitesimal rigidity, bearing-rigidity, and shape-similarity are explored in dimensions higher than two. The presentation of these relationships first involves the development of algebraic relationships that are used to support the implications between them. As will be demonstrated through counterexamples, the equivalence between the three framework properties seen in two dimensions does not extend to higher dimensions due to the increased available planes of rotation.

This section is organized as follows. First, Chapter 6.2.1 relates infinitesimal rigidity and bearing-rigidity. In Chapter 6.2.2, the implication between infinitesimal shape-similarity and bearing-rigidity is established. Finally, Chapter 6.2.3 considers the relationship between infinitesimal rigidity and infinitesimal shape-similarity.

6.2.1 Infinitesimal Rigidity and Bearing-Rigidity

Here, infinitesimal rigidity and infinitesimal bearing-rigidity are compared for frameworks in $\mathbb{R}^d$. In particular, an algebraic relationship is established that allows the bearing-rigidity

matrix to be expressed in terms of the rigidity matrix. The algebraic expression between the two matrices yields insight into the corresponding framework properties, and this insight is then used to understand the implication between infinitesimal rigidity and infinitesimal bearing-rigidity.

To begin, the algebraic relationship between the bearing-rigidity and rigidity matrices is developed.

Theorem 6.2. *The bearing-rigidity matrix $R_B(x)$ can be expressed in terms of the rigidity matrix $R_D(x)$ as*

$$R_B(x) = \operatorname{diag}\left(\frac{1}{\|z_b\|} I_d\right)\left(H_d - \operatorname{diag}\left(\frac{z_b}{\|z_b\|^2}\right) R_D(x)\right). \tag{6.1}$$

Proof. Begin by examining the expression for $R_B(x)$ in (2.4); the diagonal matrix of scaled orthogonal projection matrices can be expressed as

$$\operatorname{diag}\left(\frac{Q_{z_b}}{\|z_b\|}\right) = \operatorname{diag}\left(\frac{1}{\|z_b\|} I_d\right) \operatorname{diag}\left(Q_{z_b}\right),$$

and the diagonal matrix of orthogonal projection matrices can be written as

$$\begin{aligned} \operatorname{diag}(Q_{z_b}) &= \operatorname{diag}\left(I_d - \frac{z_b z_b^\top}{\|z_b\|^2}\right) \\ &= I_{\epsilon d} - \operatorname{diag}\left(\frac{z_b}{\|z_b\|^2}\right) \operatorname{diag}(z_b^\top). \end{aligned}$$

Distributing H_d and substituting the expression for $R_D(x)$ in (2.3) yields the expression for $R_B(x)$ in (6.1). □

The algebraic relationship presented in Thm. 6.2 merits discussion with respect to the framework properties of infinitesimal bearing-rigidity and infinitesimal rigidity. As described in the background information on these two properties in Chapter 2, frameworks which are infinitesimally rigid render the framework invariant to infinitesimal translations

and rotations by maintenance of the squared distances between vertices corresponding with edges in the underlying graph. For infinitesimally bearing-rigid frameworks, the framework is rendered invariant to infinitesimal translations and uniform scaling provided the bearings associated with each edge in the graph are maintained.

Because of the nature of the constraints represented by each edge, the bearing-rigid motions of translation and uniform scaling and the rigid motions of translation and rotation are achieved in different ways; moreover, for frameworks that are not infinitesimally bearing-rigid or not infinitesimally rigid, the available bearing preserving motions and distance preserving motions are fundamentally different due to the differences in the time derivatives of the bearings and squared distances respectively. Of all of the bearing preserving and distance preserving motions, infinitesimal translations are the only motion shared; this is a result of the incidence matrix, which appears on the right for both the rigidity and bearing-rigidity matrices. From the algebraic relationship in (6.1), it is clear that infinitesimal rotations are not in the nullspace of the bearing-rigidity matrix; infinitesimal uniform scalings are not in the nullspace of the rigidity matrix, but are in the nullspace of the bearing-rigidity matrix because $H_d x = \mathrm{vec}(z_b) \in \ker(\mathrm{diag}(Q_{z_b}))$. Acknowledging the singular shared class of infinitesimal motions between infinitesimally rigid and bearing-rigid frameworks, and noting the stark differences in all other motions that may be in the nullspace of the corresponding matrices, the following lemmas are developed to support the exploration of the comparison of these to framework properties.

The following lemma establishes the important skew-symmetric property of a particular matrix that appears in central comparison of infinitesimal rigidity and infinitesimal bearing-rigidity in this section.

Lemma 6.3. *For $\beta = 1, \ldots, \binom{d}{2}$, $L \otimes S_\beta$ is skew symmetric.*

Proof. Because L is symmetric and S_β is skew symmetric,

$$(L \otimes S_\beta)^\top = (L^\top \otimes S_\beta^\top) = -(L \otimes S_\beta),$$

so $L \otimes S_\beta$ is skew symmetric. $\square$

Now, it is established that the element-wise rotation of a vector of the infinitesimal motions of vertices in a framework, which does not correspond with infinitesimal translation, rotation, or uniform scaling, does not correspond with infinitesimal translation or rotation.

Lemma 6.4. *Let* $v = [v_1^\top, \ldots, v_d^\top]^\top \in \mathbb{R}^{dn}$. *If* $v \notin \text{span}\{V^t, V^r, V^s\}$, *then* $w = (I_n \otimes S_\beta)v \notin \text{span}\{V^t, V^r\}$, *for some* $\beta = 1, \ldots, \binom{d}{2}$.

Proof. Consider the contrapositive, and suppose that $w = (I_n \otimes S_\beta) \in \text{span}\{V^t, V^r\}$ for all $\beta = 1, \ldots, \binom{d}{2}$; there are two cases.

First, suppose that $w = (\mathbf{1}_n \otimes S_\beta)v \in \text{span}\{V^r\}$, which indicates that w can be written as a linear combination of the vectors of V^r for all $\beta = 1, \ldots, \binom{d}{2}$; i.e., for all $\beta = 1, \ldots, \binom{d}{2}$, there exist $p_i \in \mathbb{R}$, $i = 1, \ldots, \binom{d}{2}$, not all zero, such that

$$\begin{aligned}(I_n \otimes S_\beta)v &= \sum_{i=1}^{\binom{d}{2}} p_i (I_n \otimes S_\beta)x \\ &= p_\beta (I_n \otimes S_\beta)x \end{aligned} \tag{6.2}$$

Because each S_β is sparse, and because (6.2) must hold for all $\beta = 1, \ldots, \binom{d}{2}$, $v \in V^s$.

Second, suppose that $w = [w_1^\top, \ldots, w_n^\top]^\top \in \text{span}\{V^t\}$, indicating that w can be written as a linear combination of the vectors of V^t; i.e., there exist some $p_i \in \mathbb{R}$, $i = 1, \ldots, d$, not all equal to zero, such that for all $\beta = 1, \ldots, d$,

$$w = (I_n \otimes S_\beta)v = \sum_{i=1}^{d} p_i (\mathbf{1}_n \otimes e_i). \tag{6.3}$$

From the sparse structure of $(\mathbf{1}_n \otimes e_i)$, (6.3) implies that $w_1 = \ldots = w_n$. In order to hold for all $\beta = 1, \ldots, \binom{d}{d}$, (6.3) implies that $v_1 = \ldots = v_d$, so $v \in V^t$.

Thus, $w = (I_n \otimes S_\beta) \in \text{span}\{V^t, V^r\}$ for all $\beta = 1, \ldots, \binom{d}{2}$ implies that $v \in \text{span}\{V^t, V^r, V^s\}$, completing the contrapositive. $\square$

Having presented the algebraic relationship in Thm. 6.2 and the supporting results in Lem. 6.3 and Lem. 6.4, the main result of this section can now be stated.

Theorem 6.3. *For frameworks $G(x)$ for which $x \in \mathbb{R}^{dn}$, if $G(x)$ is infinitesimally rigid, then $G(x)$ is infinitesimally bearing-rigid.*

Proof. Consider the contrapositive. If $G(x)$ is not infinitesimally bearing-rigid, then there exists infinitesimal motion $v = [v_1^\top, \ldots, v_n^\top]^\top \in \mathbb{R}^{nd}$ other than translation or uniform scaling (i.e., $v \notin \operatorname{span}\{V^t, V^s\}$) such that $R_B(x)v = \mathbf{0}_{\epsilon d}$, or, equivalently, such that $\operatorname{diag}(Q_{z_b})H_d v = \mathbf{0}_{\epsilon d}$. Because $\ker(H_d) = V^t$, and because v does not correspond with a translation, $v \notin \ker(H_d)$, so $H_d v \in \ker(\operatorname{diag}(Q_{z_b}))$. Writing $H_d v = [h_1^\top, \ldots, h_\epsilon^\top]^\top \in \mathbb{R}^{\epsilon d}$, for each h_b, for $b = 1, \ldots, \epsilon$, $H_d v \in \ker(\operatorname{diag}(Q_{z_b}))$ implies that $h_b \in \ker(Q_{z_b})$; i.e., no component h_b of $H_d v$ is orthogonal to the corresponding vector z_b of $\operatorname{vec}(z_b)$. Thus, by assumption, v is not a uniform scaling, so it must be a non-uniform scaling.

Now, consider the non-trivial vector w formed by rotating each component v_i, for $i = 1, \ldots, n$, of v in one of the available planes of rotation, written as $w = (I_n \otimes S_\beta)v$, for some $\beta = 1, \ldots, \binom{d}{2}$. Because $v \notin \operatorname{span}\{V^t, V^s\}$ and $v \in \ker(R_B(x))$, $v \notin \operatorname{span}\{V^t, V^r, V^s\}$, which, by Lem. 6.4, implies that $w \notin \operatorname{span}\{V^t, V^r\}$; w corresponds with an infinitesimal rotation of a subframework of $G(x)$. By Lem. 6.3,

$$v^\top H_d^\top H_d w = v^\top L_d(I_n \otimes S_\beta)v = v^\top (L \otimes S_\beta)v = 0.$$

Because $H_d w = [g_1^\top, \ldots, g_\epsilon^\top]^\top$ is orthogonal to $H_d v$, which has no component orthogonal to corresponding components of $\operatorname{vec}(z_b)$, each component vector g_b, for $b = 1, \ldots, \epsilon$, is orthogonal to the corresponding vector z_b, yielding

$$R_D(x)w = \operatorname{diag}(z_b^\top)H_d w = \mathbf{0}_m,$$

which indicates that w preserves distances, but is not a translation or rotation of $G(x)$. Thus,

$G(x)$ is not infinitesimally rigid, completing the contrapositive. □

From Thm. 6.3, frameworks that are infinitesimally rigid are infinitesimally bearing-rigid in any dimension greater than two. Interestingly, the converse does not hold for greater than two dimensions, a fact that is shown in the following theorem.

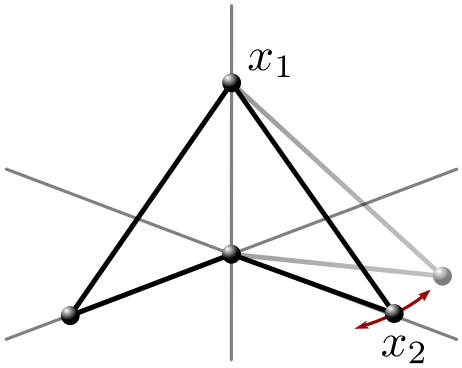

Figure 6.1: As stated in Thm. 6.4, infinitesimal bearing-rigidity does not imply infinitesimal rigidity. The framework pictured here is infinitesimally bearing-rigid, but is not infinitesimally rigid because motion of x_2 along the red vectors preserves distances but is not a translation or rotation of the framework.

Theorem 6.4. *For frameworks $G(x)$ for which $x \in \mathbb{R}^{dn}$ where $d > 2$, infinitesimal bearing-rigidity does not imply infinitesimal rigidity.*

Proof. The statement will be proved by counter-example to the following statement: for frameworks $G(x)$ for which $x \in \mathbb{R}^{dn}$ where $d > 2$, infinitesimal bearing-rigidity implies infinitesimal rigidity. The counter-example makes use of a cyclical framework of four vertices in three dimensions, the dimension of the affine hull of which is three, i.e., the four vertices are not in a plane. Such a framework is depicted in Figure 6.1, where for the purpose of illustration, the vertices take the following values:

$$x_1 = \begin{bmatrix} 0 \\ 0 \\ 1 \end{bmatrix} \quad x_2 = \begin{bmatrix} 1 \\ 0 \\ 0 \end{bmatrix} \quad x_3 = \begin{bmatrix} 0 \\ 0 \\ 1 \end{bmatrix} \quad x_4 = \begin{bmatrix} 0 \\ 0 \\ 0 \end{bmatrix}.$$

The framework is infinitesimally bearing-rigid, satisfying the rank condition on the bearing-rigidity matrix in Thm. 2.2:

$$\text{rank}(R_B(x)) = dn - d - 1 = 8.$$

In contrast, the rank condition on the rigidity matrix in Thm. 2.1 indicates that the rigidity matrix must have rank equal to six, but in fact, for the framework depicted in Figure 6.1,

$$\text{rank}(R_D(x)) = 4 < 6.$$

Thus, the framework is infinitesimally bearing-rigid, but not infinitesimally rigid, completing the proof. □

Having established the algebraic relationship between the bearing-rigidity and rigidity matrices in Thm. 6.2, the fact that infinitesimal rigidity implies infinitesimal bearing-rigidity in Thm. 6.3, and the fact that infinitesimal bearing-rigidity does not imply infinitesimal rigidity in dimensions greater than two in Thm. 6.4, the comparison of infinitesimal bearing-rigidity and infinitesimal rigidity is complete.

6.2.2 Infinitesimal Shape-Similarity and Bearing-Rigidity

Here, infinitesimal shape-similarity and infinitesimal bearing-rigidity are examined to understand the underlying relationship between these two framework properties in greater than two dimensions. To begin, an algebraic relationship between the shape-similarity matrix and the bearing-rigidity matrix is examined; this expression allows the shape-similarity matrix to be expressed in terms of the bearing-rigidity matrix, which is useful for relating the types of angle preserving and bearing preserving infinitesimal motions of the framework. After developing this algebraic relationship and commenting on the types of motions shared between angle and bearing constrained frameworks, the underlying implication between the two properties is stated.

The following expression relates the shape-similarity and bearing-rigidity matrices.

Theorem 6.5. *The shape-similarity matrix $R_S(x)$ can be expressed in terms of the bearing-rigidity matrix $R_B(x)$ as*

$$R_S(x) = \Gamma^{-1}(x)\frac{\partial f_S(x)}{\partial \operatorname{vec}(\hat{z}_b)}R_B(x). \tag{6.4}$$

Proof. The expression in Thm. 6.5 follows from the development of the shape-similarity matrix in Chapter 3 and the development of the bearing-rigidity matrix, described in Chapter 2. To derive the shape-similarity matrix, the angle-constraint function was originally differentiated with respect to the vertex positions; instead, differentiating with respect to the bearings in the framework yields:

$$\Gamma_S(x)R_S(x) = \frac{\partial f_S(x)}{\partial \operatorname{vec}(\hat{z}_b)}\frac{d}{dt}\operatorname{vec}(\hat{z}_b).$$

Because $f_B = \operatorname{vec}\hat{z}_b$, and because $\frac{d}{dt}\operatorname{vec}(\hat{z}_b) = R_B(x)\dot{x}$, the expression in (6.4) immediately follows, where $\Gamma_S(x)$ is invertible because the framework is non-degenerate by assumption. □

Having developed the algebraic expression in (6.4) to relate the shape-similarity and bearing-rigidity matrices, the similarity and differences in the available angle and bearing preserving motions can be discussed. Recall that for frameworks which are infinitesimally shape-similar, the framework is rendered invariant to infinitesimal translations, rotations, and uniform scalings while preserving the angles of the framework; for infinitesimally bearing-rigid frameworks, bearing maintenance renders the framework invariant to infinitesimal translations and uniform scaling. Notably, both properties exhibit invariance to translation and uniform scaling, so a relationship between the two seems likely. In fact, the algebraic relationship proposed in Thm. 6.5 can be used to reveal the underlying implication between them.

Theorem 6.6. *For all frameworks $G(x)$ in $\mathbb{R}^d$, i.e. frameworks for which $x \in \mathbb{R}^{dn}$, if $G(x)$ is infinitesimally shape-similar, then $G(x)$ is infinitesimally bearing-rigid.*

Proof. Consider the contrapositive. Suppose $G(x)$ is not infinitesimally bearing-rigid; then, there exists some vector $v \in \mathbb{R}^{nd}$ such that $v \notin \text{span}\{V^t, V^s\}$ and $v \in \ker(R_B(x))$; such vectors correspond with non-uniform scaling. Because $v \in \ker(R_B(x))$, $v \notin V^r$. Furthermore, by the algebraic relationship in Thm. 6.5, $v \in \ker(R_B(x))$ implies that $v \in \ker(R_S(x))$, so $G(x)$ is not infinitesimally shape-similar, completing the contrapositive. □

Together with Thm. 6.3, Thm. 6.6 suggests that infinitesimal bearing-rigidity is the weakest of the three framework properties. Of significance to the exploration of the interplay between network topology and interaction modalities in a multi-robot team, a consequence of Thm. 6.3 and Thm. 6.6 is that in dimensions greater than two, fewer edges, and, therefore, fewer bearings, are required to ensure that a framework is infinitesimally bearing-rigid than the number of distances and angles as required by infinitesimal rigidity and shape-similarity respectively.

Interestingly, as with infinitesimal bearing-rigidity and rigidity, the converse of Thm. 6.6 does not hold, a fact which is captured by the following statement.

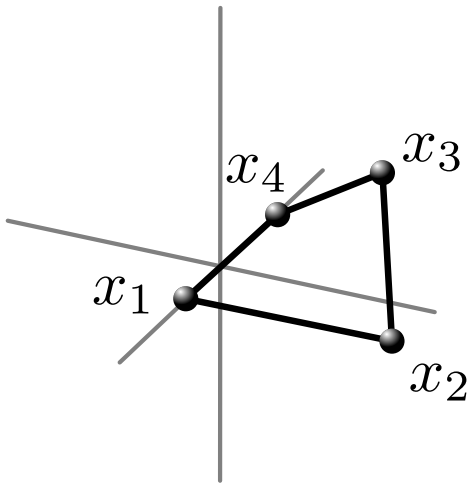

Figure 6.2: As stated in Thm. 6.7, infinitesimal bearing-rigidity does not imply infinitesimal shape-similarity. The framework pictured here is infinitesimally bearing-rigid, but is not infinitesimally shape-similar.

Theorem 6.7. *For frameworks $G(x)$ for which $x \in \mathbb{R}^{dn}$ where $d > 2$, infinitesimal bearing-rigidity does not imply infinitesimal shape-similarity.*

Proof. The statement will be proved by counter-example to the following statement: for frameworks $G(x)$ for which $x \in \mathbb{R}^{dn}$ where $d > 2$, infinitesimal bearing-rigidity implies infinitesimal shape-similarity. The counter-example makes use of a cyclical framework of four vertices in three dimensions, the dimension of the affine hull of which is three, i.e., the four vertices are not in a plane. Such a framework is depicted in Figure 6.2, where for the purpose of illustration, the vertices take the following values:

$$x_1 = \begin{bmatrix} 0 \\ 1 \\ 0 \end{bmatrix} \quad x_2 = \begin{bmatrix} 1 \\ 1 \\ 0 \end{bmatrix} \quad x_3 = \begin{bmatrix} -1 \\ 1 \\ 1 \end{bmatrix} \quad x_4 = \begin{bmatrix} 0 \\ -1 \\ 0 \end{bmatrix}.$$

The framework is infinitesimally bearing-rigid, satisfying the rank condition on the bearing-rigidity matrix in Thm. 2.2:

$$\operatorname{rank}(R_B(x)) = dn - d - 1 = 8.$$

In contrast, the rank condition on the shape-similarity matrix in Thm. 3.3 indicates that the shape-similarity matrix must have rank equal to five, but in fact, for the framework depicted in Figure 6.2,

$$\operatorname{rank}(R_D(x)) = 4 < 5.$$

Thus, the framework is infinitesimally bearing-rigid, but not infinitesimally shape-similar, completing the proof. □

With Thm. 6.6 and Thm. 6.7, it can be concluded that in dimensions greater than two, infinitesimal shape-similarity implies that the framework is infinitesimally bearing-rigid, and not the converse. Connecting this relationship to the algebraic relationship presented in

Thm. 6.5 yields the following observation. From (6.4), the nullspace of the shape-similarity matrix can be characterized in terms of the range and nullspace of the bearing-rigidity matrix according to:

$$\ker(R_S(x) = \left(\ker\left(\frac{\partial f_S(x)}{\partial \operatorname{vec}(\hat{z}_b)}\right) \cap \operatorname{range}(R_B(x))\right) \cup \ker(R_B(x)). \tag{6.5}$$

When the framework is not infinitesimally bearing-rigid, it is clear from (6.5) and from the proof of Thm. 6.6 that the framework is not infinitesimally shape-similar. However, when the framework is infinitesimally bearing-rigid, it is not clear whether the framework is infinitesimally shape-similar; in order for such a framework to be infinitesimally shape-similar it must be that the intersection between $\ker\left(\frac{\partial f_S(x)}{\partial \operatorname{vec}(\hat{z}_b)}\right)$ and $\operatorname{range}(R_B(x))$ is spanned by the vectors of V^r corresponding with infinitesimal rotations of the framework.

6.2.3 Infinitesimal Rigidity and Shape-Similarity

Here, the relationship between the frameworks properties of infinitesimal shape-similarity and infinitesimal rigidity are considered. First, an algebraic relationship between the shape-similarity and rigidity matrices is developed by exploiting the expressions in Thm. 6.1, for writing the bearing-rigidity matrix in terms of the rigidity matrix, and Thm. 6.5, for writing the shape-similarity matrix in terms of the bearing-rigidity matrix. After developing this algebraic relationship, the implication between infinitesimal rigidity and infinitesimal shape-similarity is considered.

To begin, the algebraic relationship between the shape-similarity matrix and the rigidity matrix is first developed.

Theorem 6.8. *The shape-similarity matrix $R_S(x)$ can be expressed in terms of the rigidity matrix $R_B(x)$ as*

$$R_S(x) = \Gamma^{-1}(x)\frac{\partial f_S(x)}{\partial \operatorname{vec}(\hat{z}_b)} \operatorname{diag}\left(\frac{1}{\|z_b\|} I_d\right)\left(H_d - \operatorname{diag}\left(\frac{z_b}{\|z_b\|^2}\right) R_D(x)\right). \tag{6.6}$$

Proof. The expression in (6.6) follows by substituting the expression for the bearing-rigidity matrix in terms of the rigidity matrix in (6.1) into the expression in (6.4) for the shape-similarity matrix in terms of the bearing-rigidity matrix. □

Having developed the algebraic expression that allows the shape-similarity matrix to be written in terms of the rigidity matrix, the relationship between these two framework properties can be explored. In particular, unlike the two-dimensional case, the following statement indicates that infinitesimal shape-similarity does not imply infinitesimal rigidity in dimensions greater than two.

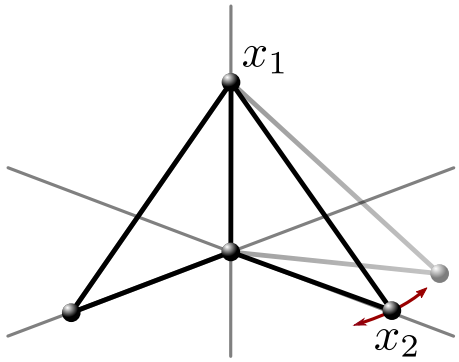

Figure 6.3: As stated in Thm. 6.9, infinitesimal shape-similarity does not imply infinitesimal rigidity. The framework pictured here is infinitesimally shape-similar, but is not infinitesimally rigid because motion of x_2 along the red vectors preserves distances but is not a translation or rotation of the framework.

Theorem 6.9. *For frameworks $G(x)$ for which $x \in \mathbb{R}^{dn}$ where $d > 2$, infinitesimal shape-similarity does not imply infinitesimal rigidity.*

Proof. The statement will be proved by counter-example to the following statement: for frameworks $G(x)$ for which $x \in \mathbb{R}^{dn}$ where $d > 2$, infinitesimal shape-similarity implies infinitesimal rigidity. The counter-example makes use of a framework of four vertices in three dimensions, the dimension of the affine hull of which is three, i.e., the four vertices are not in a plane. The edge-set is given as follows:

$$\mathcal{E} = \{(1,2),(2,3),(3,4),(1,4),(1,3)\}.$$

Such a framework is depicted in Figure 6.1, where for the purpose of illustration, the vertices take the following values:

$$x_1 = \begin{bmatrix} 0 \\ 0 \\ 1 \end{bmatrix} \quad x_2 = \begin{bmatrix} 1 \\ 0 \\ 0 \end{bmatrix} \quad x_3 = \begin{bmatrix} 0 \\ 0 \\ 1 \end{bmatrix} \quad x_4 = \begin{bmatrix} 0 \\ 0 \\ 0 \end{bmatrix}.$$

The framework is infinitesimally shape-similar, satisfying the rank condition on the shape-similarity matrix Thm. 3.3, and in particular, the rank condition in Cor. 3.3.1 for frameworks with sufficient affine hull dimension:

$$\operatorname{rank}(R_B(x)) = dn - \frac{1}{2}(d(d+1)) - 1 = 5.$$

In contrast, the rank condition on the rigidity matrix in Thm. 2.1 indicates that the rigidity matrix must have rank equal to six, but in fact, for the framework depicted in Figure 6.1,

$$\operatorname{rank}(R_D(x)) = 5 < 6.$$

Thus, the framework is infinitesimally shape-similar, but not infinitesimally rigid, completing the proof. □

The statement in Thm. 6.9 demonstrably shows that infinitesimal shape-similarity does not imply that a framework is infinitesimally rigid in higher than two dimensions. It is conjectured that infinitesimal rigidity implies infinitesimal shape-similarity.

6.3 Summary of Conclusions

The purpose of this chapter was to explore the role of network topology and the interaction modalities used to specify and constrain a multi-robot formation. In particular, this chapter served to expose the underlying relationships between the framework properties of infinites-

imal rigidity, bearing-rigidity, and shape-similarity, which are relevant to the central thesis topic when considering, respectively, interaction modalities based on distance, bearing, and angle maintenance in formation.

The results of this chapter began by revealing an important property of the plane, to which the relationships between the framework properties were sensitive. In particular, it was found that infinitesimal rigidity, bearing-rigidity, and shape-similarity are equivalent in the plane, and it was argued that the fact that there is a single plane in which vectors can rotate is central in this relationship; this finding is significant to teams of mobile ground robots, which are assumed in this thesis to operate in the plane. Notably, when seeking frameworks in the plane with a particular property, such as infinitesimal shape-similarity or infinitesimal bearing-rigidity, existing methods of finding infinitesimally rigid frameworks equivalently yield frameworks that are infinitesimally bearing-rigid and infinitesimally shape-similar.

In higher than two dimensions, the relationships between these three framework properties were explored. Algebraic relationships were found which allowed the bearing-rigidity and shape-similarity matrices to be expressed in terms of the rigidity matrix. Furthermore, it was shown that infinitesimal rigidity implies infinitesimal bearing-rigidity, and that infinitesimal shape-similarity implies infinitesimal bearing-rigidity. It was also shown that the three framework properties are not equivalent in higher dimensions. Thus, the relationship between these framework properties has been explored for three and higher dimensions.

The understanding of the relationships between the three framework properties presented by this chapter is significant in the exploration of the interplay between network topology and the interaction modalities of a multi-robot formation. In particular, each of these framework properties concerns the role of the underlying graph topology induced by maintaining a particular set of inter-vertex constraints, which requires a particular interaction modality. When considering formations composed of heterogeneous constraints, the relationships between these framework properties bear significance in determining the types of formations that can be achieved under these heterogeneous constraints, the available motions to such

formations, and the efficacy of particular control strategies that can be employed to leverage this heterogeneity. Extending the discussion in this regard, the results of this chapter are composed with the case-study in the importance of heterogeneous interaction modalities in Chapter 5 and the controller-synthesis approach to formation control of Chapter 4 in the consideration of formations with heterogeneous constraints following in Chapter 7.

CHAPTER 7
FORMATIONS WITH HETEROGENEOUS CONSTRAINTS

In this chapter, formation control of frameworks specified by heterogeneous constraints is considered as a mechanism to drive the discussion on the interplay between network topology and the interaction modalities available in a multi-robot team. As such, this chapter is a culmination of the results presented in the previous chapters of this thesis: the controller-synthesis approach to formation control in Chapter 4 is revisited for infinitesimally rigid and bearing-rigid formations; the utility of heterogeneity described in Chapter 5 motivates the characterization of formations specified by heterogeneous constraints; and the relationship between the framework properties of infinitesimal rigidity, bearing-rigidity, and shape-similarity in Chapter 6 support the design of formation-control strategies for frameworks leveraging this source of heterogeneity. In addition to these topics, the issue of constraint violation is addressed to consider situations when the constraints defining the formation should be violated and to suggest a mechanism for balancing the objective of maintaining the formation against other objectives of the team.

This chapter is structured as follows. Beginning in Chapter 7.1, the controller synthesis technique posed in Chapter 4 is formulated for control of infinitesimally rigid and bearing-rigid frameworks. In particular, the focus of this section is not the development of novel methods of formation control of infinitesimally rigid or bearing-rigid frameworks; rather, the developments of Chapter 4 are mirrored to explicitly investigate differences in formation control that arise due to distance and bearing constraints as compared to angle constraints. In Chapter 7.2, formations which are specified by heterogeneous constraints are characterized using the background information on infinitesimal rigidity and bearing-rigidity provided in Chapter 2 and the development of infinitesimal shape-similarity in Chapter 3. With this characterization, a controller-synthesis approach to control of formations of robots

specified by heterogeneous constraints is detailed in Chapter 7.3, and a demonstration of this approach on a team of differential-drive robots is provided in Chapter 7.3.1. Based on this controller-synthesis approach, the issue of constraint violation is posed in Chapter 7.4, and a demonstration of the proposed constraint violation mechanism is demonstrated on a team of differential-drive robots in Chapter 7.4.1. Finally, Chapter 7.5 summarizes the conclusions of this chapter.

7.1 Synthesized Controllers for Rigid and Bearing-Rigid Frameworks

In this section, the process of developing the controller-synthesis approach to formation control of infinitesimally shape-similar frameworks is repeated for infinitesimally rigid and bearing-rigid frameworks to examine the differences in formation control and the induced interaction modalities that arise due to the maintenance of distances and bearings as opposed to angles. As mentioned in the introduction of this chapter, because the purpose of this section is to investigate the significance of particular constraints on formation control rather than the development of formation controllers themselves, the structure of this section mirrors that of Chapter 4. With this regard, supporting formation controllers for formation stabilization of infinitesimally rigid and bearing-rigid frameworks are first presented to highlight the differences induced by the maintenance of distances and bearings respectively. Then, the controller-synthesis approach to formation control of infinitesimally shape-similar frameworks presented in Chapter 4 is formulated for control of infinitesimally rigid and bearing-rigid frameworks to support subsequent efforts in control of frameworks with heterogeneous distance, bearing, and angle constraints. In summary, the controllers presented in this section mirror the structure and developments presented in Chapter 4, and the emphasis of this section is completeness in the presentation of the controllers for frameworks with homogeneous constraints and demonstration of the extensibility and applicability of the controller-synthesis approach.

This section is organized as follows. Chapter 7.1.1 considers control of infinitesimally

rigid frameworks while Chapter 7.1.2 considers control of infinitesimally bearing-rigid frameworks. In each subsection, an error system corresponding with the relevant constraints is first defined. Then, formation controllers that asymptotically stabilize these error systems are designed. Finally, the controller-synthesis approach is introduced, and simulations demonstrate the method.

7.1.1 Control of Infinitesimally Rigid Frameworks

Here, control of infinitesimally rigid frameworks is considered. Corresponding with the approach taken to control of infinitesimally shape-similar frameworks in Chapter 4, an error system for frameworks specified by distances is first introduced. Asymptotic controllers for formation stabilization are presented before introducing the controller-synthesis approach, which is first demonstrated in simulation before commenting on the induced sensing and communication requirements. A demonstration of the synthesized controller by a team of differential-drive robots described by an infinitesimally rigid framework concludes the consideration of control of frameworks specified by distances.

The Distance-Error System

For the purpose of this subsection, the following assumptions are made. The dynamics of the vertices are modelled as single integrators such that $\dot{x} = u$. Frameworks $G(x)$ are assumed to be infinitesimally rigid as in Def. 2.5. As such, the rigidity matrices $R_D(x)$ of these frameworks satisfy the rank condition of Thm. 2.1, indicating that each has exactly $q_D = \text{rank}(R_D(x)) \leq \epsilon$ linearly independent rows. Because $G(x)$ is infinitesimally rigid, maintaining the q_D *independent distances*, which correspond with these linearly independent rows, ensures that $f_D(x)$ is invariant for distance preserving $\dot{x}$. Thus, define the *independent distance set* $\hat{\mathcal{E}}_D$ to be the set of q_D edges of $\mathcal{G}$ corresponding with the linearly independent rows of $R_D(x)$; corresponding with this edge set, let $\hat{\mathcal{N}}_i$ be the *independent neighbors* of vertex i, which are those vertices which share an edge in $\hat{\mathcal{E}}_D$ with vertex i. Similarly,

define the *independent distance function* to be $\hat{f}_D : \mathbb{R}^{nd} \to \mathbb{R}^{q_D}$ such that $\hat{f}_D(x)$ is the vector of independent distances. The time derivative of the independent distance function is $\frac{d}{dt}\hat{f}_D(x) = \hat{R}_D(x)u$ following the development of infinitesimal rigidity in Chapter 2.

In terms of the independent distances, the desired configuration of the vertices is given by $f_D^* \in \mathbb{R}^{q_D}$, where this vector is assumed to be geometrically viable. With this construction, the error between the current and desired distances is

$$e_D(x) = [e_{D,1}(x), \ldots, e_{D,q_D}(x)]^\top = f_D^* - \hat{f}_D(x);$$

the ordering of the errors $e_{D,b}(x)$ is arbitrary, and it will occasionally be convenient to reference the error corresponding to the edge (i, j) by $e_{D,(i,j)}(x)$. The *distance-error system* is given by:

$$\dot{e}_D(x) = -\frac{d}{dt}\hat{f}_D(x) = -\hat{R}_D(x)u. \tag{7.1}$$

The stabilizing controllers for this distance-error system are now introduced.

Formation Stabilization

Here, a controller that asymptotically stabilizes the origin of the distance-error system is presented.

Theorem 7.1. *Let $G(x)$ be an infinitesimally rigid framework for which $e_D(x) \in D = \mathbb{R}^{q_D}$; under*

$$u = \hat{R}_D^\top(x)e_D(x), \tag{7.2}$$

the origin of the distance-error system in (7.1)*, $e_D(x) = 0$, is locally asymptotically stable.*

Proof. Consider the candidate Lyapunov function

$$V_D(e_D(x)) = \frac{1}{2}\|e_D(x)\|^2, \tag{7.3}$$

which satisfies $V_D(e_D(x)) > 0$ for $e_D(x) \in D - \{0\}$ and has the time derivative $\dot{V}_D(e_D(x)) = e_D^\top(x)\dot{e}_D(t)$; substituting the error system in (7.1) into this expression yields

$$\dot{V}_D(e_D(x)) = \frac{\partial V_D(e_D(x))}{\partial x} u = -e_D^\top(x)\hat{R}_D(x)u. \tag{7.4}$$

Further substituting the controller in (7.2) into (7.4), yields

$$\dot{V}_D(e_D(x)) = -e_D^\top(x)\hat{R}_D(x)\hat{R}_D^\top(x)e_D(x).$$

For $e_D(x) \in D$, $\hat{R}_D(x)$ is full rank, so $\hat{R}_D(x)\hat{R}_D^\top(x) \succ 0$. Thus,

$$\dot{V}_D(e_D(x)) = -\|\hat{R}_D^\top(x)e_D(x)\| < 0$$

for $e_D(x) \in D - \{0\}$, so $e_D(x) = 0$ is locally asymptotically stable. □

As it is presented in Thm. 7.1, the controller in (7.2) can be separated into the individual controllers for each robot in the formation as

$$u_i = \sum_{b=1}^{q_D} \frac{\partial \hat{f}_{D,b}^\top(x)}{\partial x_i} e_{D,b}(x) = \sum_{\substack{b=(i,j)\in\hat{\mathcal{E}}_D \\ j\in\hat{\mathcal{N}}_i}} e_{D,b}(x) z_{ij}, \tag{7.5}$$

which, compared to the expression for the formation stabilizing controller for infinitesimally shape-similar frameworks in (4.8), is decidedly simpler. Interestingly, and relevant to the exploration of the interplay between network topology and the interaction modalities in a multi-robot team, the simplicity of this expression as compared to the formation-stabilization controller for infinitesimally shape-similar frameworks in (4.8) is derived from a fundamental difference between distances and angles—distance constraints are pair-wise, while angle constraints are triple-wise, a fact that influences formation controllers designed around these quantities.

Controller Synthesis

Here, the controller-synthesis approach to formation control of infinitesimally rigid frameworks is presented. As in Chapter 4, a validating controller, which exponentially stabilizes the origin of the distance-error system with a fixed convergence rate is first presented.

Theorem 7.2. *Let $G(x)$ be an infinitesimally rigid framework for which $e_D(x) \in D = \mathbb{R}^{q_D}$; under*

$$u = \hat{R}_D^\top(x) \left(\hat{R}_D(x) \hat{R}_D^\top(x) \right)^{-1} e_D(x) \tag{7.6}$$

the origin of the distance-error system in (7.1)*, $e_D(x) = 0$, is locally exponentially stable.*

Proof. Consider the Lyapunov function in (7.3), the time derivative of which is given in (7.4). For $e_D(x) \in D$, $\hat{R}_D(x)$ is full row-rank, so the matrix $\hat{R}_D(x)\hat{R}_D^\top(x)$ is invertible; substitution of the expression in (7.6) yields $\dot{V}_D(x) = -\|e_D(x)\|^2 \leq -2V_D(x)$, so $e_D(x) = 0$ is locally exponentially stable. □

The controller in (7.6) is a validating controller to the following QP, the solution to which is the synthesized formation controller for infinitesimally rigid frameworks:

$$\begin{aligned} u^* = & \underset{u \in \mathbb{R}^{dn}}{\arg\min} \frac{1}{2} \|u - u^{\text{nom}}\|^2 \\ & \text{s.t.} \quad -e_D^\top(x) \hat{R}_D(x) u \leq -\frac{\rho_D}{2} \|e_D(x)\|^2, \end{aligned} \tag{7.7}$$

where u_{nom} is a nominal controller for the formation, and $\rho_D \in \mathbb{R}_+$ is a parameter that can be chosen to affect convergence of the distance-error to the origin. The solution to (7.7) ensures exponential stability of the origin of the distance-error system, thereby ensuring that the desired distances are achieved, while admitting higher-level objectives encoded through the nominal controller.

The structure of the CLF constraint of (7.7) and the rigidity matrix can be exploited to formulate individual controller-synthesis problems for each robot that ensure satisfaction of

the original inequality in (7.7). Towards this formulation, consider the CLF in (7.3), which can be expressed as the sum

$$V_D(e_D(x)) = \frac{\rho_D}{4} \sum_{i=1}^{n} \sum_{\substack{b=(i,j)\in\hat{\mathcal{E}}_D \\ j\in\hat{\mathcal{N}}_i}} (e_{D,b}(x))^2. \tag{7.8}$$

Now, examine the derivative as in (7.4), which can be written as:

$$\dot{V}_D(e_D(x)) = -\sum_{i=1}^{n} \sum_{\substack{b=(i,j)\in\hat{\mathcal{E}}_D \\ j\in\hat{\mathcal{N}}_i}} e_{D,b}(x) \frac{\partial \hat{f}_{D,b}}{\partial x_i} u_i. \tag{7.9}$$

For each robot, the synthesized controller is given by

$$\begin{aligned} u_i^* = \arg\min_{u_i\in\mathbb{R}^d} & \frac{1}{2}\|u - u_i^{\text{nom}}\|^2 \\ \text{s.t. } - & \sum_{\substack{b=(i,j)\in\hat{\mathcal{E}}_D \\ j\in\hat{\mathcal{N}}_i}} e_{D,b}(x) \frac{\partial \hat{f}_{D,b}(x)}{\partial x_i} u_i \leq -\frac{\rho_D}{4} \sum_{\substack{b=(i,j)\in\hat{\mathcal{E}}_D \\ j\in\hat{\mathcal{N}}_i}} (e_{D,b}(x))^2. \end{aligned} \tag{7.10}$$

By the following lemma, if the inequality constraint of (7.10) is satisfied for each robot in the formation, then the original inequality constraint of (7.7) is satisfied.

Lemma 7.1. *For $i = 1, \ldots, n$, if each u_i satisfies the inequality constraint of* (7.10)*, then the original inequality constraint of* (7.7) *is satisfied.*

Proof. The inequality

$$- \sum_{\substack{b=(i,j)\in\hat{\mathcal{E}}_D \\ j\in\hat{\mathcal{N}}_i}} e_{D,b}(x) \frac{\partial \hat{f}_{D,b}(x)}{\partial x_i} u_i \leq -\frac{\rho_D}{4} \sum_{\substack{b=(i,j)\in\hat{\mathcal{E}}_D \\ j\in\hat{\mathcal{N}}_i}} (e_{D,b}(x))^2$$

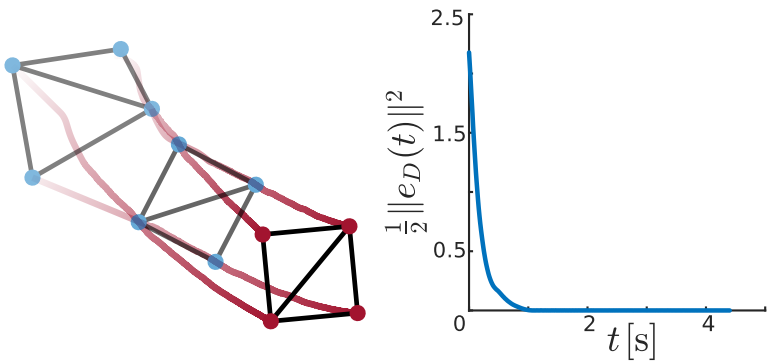

Figure 7.1: (Left) Along the red trajectories as opacity increases, four vertices in an infinitesimally rigid framework execute the synthesized controller in (7.10), translating and rotating until reaching their final positions (red dots); the black lines indicate the network topology. (Right) The Lyapunov function in (7.3) converges to zero as expected.

implies that

$$-\sum_{i=1}^{n}\sum_{\substack{b=(i,j)\in\hat{\mathcal{E}}_D\\ j\in\hat{\mathcal{N}}_i}} e_{D,b}(x)\frac{\partial \hat{f}_{D,b}(x)}{\partial x_i}u_i \leq -\frac{\rho_D}{4}\sum_{i=1}^{n}\sum_{\substack{b=(i,j)\in\hat{\mathcal{E}}_D\\ j\in\hat{\mathcal{N}}_i}} (e_{D,b}(x))^2$$

which by equality to (7.8) and (7.9), implies that $-e_D^\top(x)\hat{R}_D(x)u \leq -\frac{\rho_D}{4}\|e_D(x)\|^2$. □

Having shown that satisfying the inequality constraints of (7.10) amount to satisfying the inequality constraint of (7.7), the following can be stated as a direct result of Lem. 7.1.

Theorem 7.3. *Suppose the synthesized controllers u_i^* of* (7.10) *exist for each $i = 1, \ldots, n$. Under $u^* = [u_1^{*\top}, \ldots, u_n^{*\top}]^\top$, the origin of the distance-error system in* (7.1)*, $e_D(x) = 0$, is locally exponentially stable.*

Demonstrating the synthesized controller in (7.10), the MATLAB simulation in Figure 7.1 shows the trajectory of four vertices executing the synthesized controller for a nominal control input which is the difference between the desired and current positions of the vertices.

Sensing and Communication Requirements

To conclude the introduction of the controller-synthesis approach to formation control of infinitesimally rigid frameworks considered in this chapter, the implications of the designed formation controllers on the sensing and communication requirements are presented. In particular, the asymptotic controller in (7.5) and the controller-synthesis approach in (7.10) are examined. In each controller, the partial derivative of the distance-constraint function with respect to each robot position plays a central role in determining the interaction modalities required of the robots. From the partial derivative $\frac{\partial \hat{f}_D(x)}{\partial x_i}$, it can be concluded from the structure of the rigidity matrix that each robot must be capable of measuring the distance and bearing to each of its neighbors, but communication is not necessary. As commented previously, relative to the induced interaction modalities of the controller-synthesis approach to formation control of infinitesimally shape-similar frameworks, formation control of distance constrained formations as described here does not require communication to achieve formation stabilization because distance constraints are pair-wise, while angle constraints are triple-wise.

Robotarium Demonstration

To demonstrate the controller-synthesis approach to formation control of teams of robots described by infinitesimally rigid frameworks, the controller synthesized by solving (7.7) was deployed on a team of five differential-drive robots in the Robotarium. Beginning from the top left, where the robots are initialized, and proceeding in the numbered sequence, Figure 7.2 contains stills taken from a demonstration in which the robots execute the synthesized controller to exponentially stabilize the origin of the distance-error system. The synthesized controller is a minimal modification of the nominal controller subject to the CLF inequality constraint. In the demonstration shown in Figure 7.2, the nominal controller is a proportional controller taken to be the difference from the centroid of the robot positions and a desired location; this controller, were it applied to each robot, would not stabilize

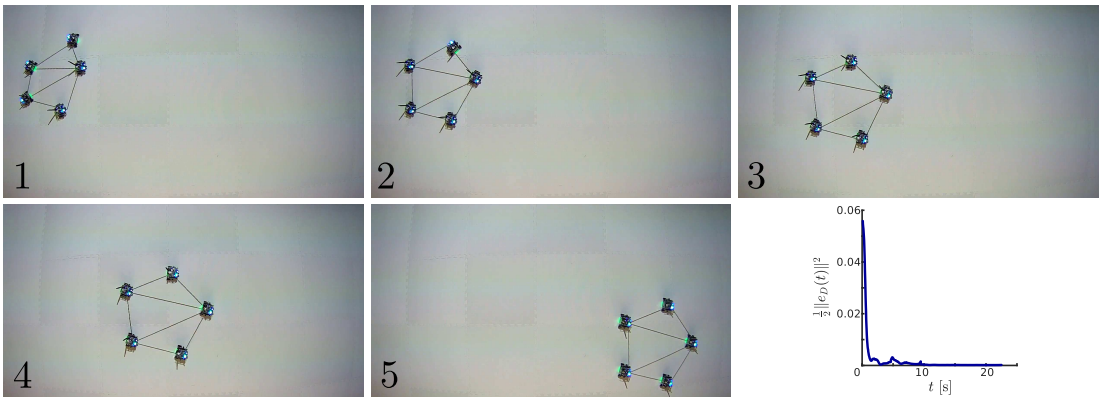

Figure 7.2: The formation controller synthesized by solving (7.7) to exponentially stabilize the origin of the distance-error system was executed by a team of five differential-drive robots described by an infinitesimally rigid framework in the Robotarium. Along the numbered sequence, the robots are initialized and execute the synthesized controller under a nominal controller that directs the high-level motion of the team. In the bottom right, the squared norm of the distance error is shown, quantifying the success of the controller-synthesis formation-control strategy.

the origin of the distance-error system, but because of the CLF constraint, as shown in the bottom right image of the figure, the squared norm of the distance error converges to zero as intended despite measurement error in the overhead motion-tracking system and the non-holonomic nature and low-level motor controllers of the differential-drive robots, mitigated in part by the use of the near-identity diffeomorphism given in (2.6).

7.1.2 Control of Infinitesimally Bearing-Rigid Frameworks

Here, control of infinitesimally bearing-rigid frameworks is considered. As in the previous subsection, the development mirrors that of the approach taken to control of infinitesimally shape-similar frameworks in Chapter 4 for completeness in the presentation of the heterogeneous approach to formation control presented later in this chapter. As such, this subsection begins with the introduction of an error system for frameworks specified by bearings. Asymptotic controllers for formation stabilization are presented before introducing the controller-synthesis approach, which is demonstrated in simulation. Comments on the sensing and communication requirements of this approach conclude the consideration of control of frameworks specified by bearings.

The Bearing-Error System

As in the previous presentations, the following assumptions are made. The dynamics of the vertices are modelled as single integrators such that $\dot{x} = u$. Here, frameworks $G(x)$ are assumed to be infinitesimally bearing-rigid as in Def. 2.7. As such, the bearing-rigidity matrices $R_B(x)$ of these frameworks satisfy the rank condition of Thm. 2.2. Because $G(x)$ is infinitesimally bearing-rigid, maintaining the q_B *independent bearings*, which correspond with those bearings whose removal decreases the rank of the bearing-rigidity matrix, ensures that $f_B(x)$ is invariant for bearing preserving $\dot{x}$. Thus, define the *independent bearing set* $\hat{\mathcal{E}}_B$ to be the set of q_B edges of $\mathcal{G}$ corresponding with the independent bearings; associated with this edge set, let $\hat{\mathcal{N}}_i$ be the *independent neighbors* of vertex i, which are those vertices which share an edge in $\hat{\mathcal{E}}_B$ with vertex i. Similarly, define the *independent bearing function* to be $\hat{f}_B : \mathbb{R}^{nd} \to \mathbb{R}^{dq_B}$ such that $\hat{f}_B(x)$ is the vector of independent bearings. The time derivative of the independent bearing function is $\frac{d}{dt}\hat{f}_B(x) = \hat{R}_B(x)u$ following the development of infinitesimal bearing-rigidity in Chapter 2.

In terms of the independent bearings, the desired configuration of the vertices is given by $f_B^* \in \mathbb{R}^{dq_B}$, where this vector is assumed to be geometrically viable. With this construction, the error between the current and desired bearings is

$$e_B(x) = [e_{B,1}^\top(x), \ldots, e_{B,q_B}^\top(x)]^\top = f_B^* - \hat{f}_B(x);$$

the ordering of the errors $e_{B,b}(x)$ is arbitrary, and it will occasionally be convenient to reference the error corresponding to the edge (i, j) by $e_{B,(i,j)}(x)$, where $e_{B,(i,j)}(x) = -e_{B,(j,i)}(x)$ because it is signed. Note that unlike the angle-error and distance-error, $e_B(x)$ is a vector of vectors, which impacts the controllers presented in this section. The *bearing-error system* is given by:

$$\dot{e}_B(x) = -\frac{d}{dt}\hat{f}_B(x) = -\hat{R}_B(x)u. \tag{7.11}$$

The stabilizing controllers for this bearing-error system are now introduced.

Formation Stabilization

Here, a controller that stabilizes the origin of the bearing-error system is presented. In this presentation, the same formulation used to develop the formation-stabilization controllers for distance and angle-constrained frameworks is used.

Theorem 7.4. *Let $G(x)$ be an infinitesimally bearing-rigid framework for which $e_B(x) \in D = \{e_B(x) \in \mathbb{R}^{dq_B} | \hat{z}_b^\top \hat{e}_{B,b}(x) > -1 \, \forall b = 1, \ldots, q_B\}$; under*

$$u = \hat{R}_B^\top(x) e_B(x), \tag{7.12}$$

the origin of the bearing-error system in (7.11)*, $e_B(x) = 0$, is locally asymptotically stable.*

Proof. Consider the candidate Lyapunov function

$$V_B(e_B(x)) = \frac{1}{2}\|e_B(x)\|^2, \tag{7.13}$$

which satisfies $V_B(e_B(x)) > 0$ for $e_B(x) \in D - \{0\}$ and has the time derivative $\dot{V}_B(e_B(x)) = e_B^\top(x)\dot{e}_B(t)$; substituting the error system in (7.11) into this expression yields

$$\dot{V}_B(e_B(x)) = \frac{\partial V_B(e_B(x))}{\partial x} u = -e_B^\top(x)\hat{R}_B(x)u. \tag{7.14}$$

Further substituting the controller in (7.12) into (7.14), yields

$$\dot{V}_B(e_B(x)) = -e_B^\top(x)\hat{R}_B(x)\hat{R}_B^\top(x)e_B(x).$$

Because $\hat{R}_B(x)$ is not full rank, $\hat{R}_B(x)\hat{R}_B^\top(x) \succeq 0$; however, for $e_B(x) \in D$, $R_B^\top(x)e_B(x)$

is equal to zero only when $e_B(x)$ is trivial. Thus,

$$\dot{V}_B(e_B(x)) = -\|\hat{R}_B^\top(x)e_B(x)\| < 0$$

for $e_B(x) \in D - \{0\}$, so $e_B(x) = 0$ is locally asymptotically stable. □

The asymptotically stabilizing controller for bearing-constrained frameworks is presented for the following reasons. Foremost, the purpose of this presentation is to compare directly with the controllers for angle-constrained frameworks in Chapter 4 rather than to simply develop controllers for infinitesimally bearing-rigid frameworks, effective examples of which can be found in works such as [57]. In mirroring the structure of these developments, fundamental differences between angle-maintenance and bearing-maintenance can be explored. As it is presented in Thm. 7.4, the controller in (7.12) can be separated into the individual controllers for each robot in the formation as

$$u_i = \sum_{b=1}^{q_B} \frac{\partial \hat{f}_{B,b}^\top(x)}{\partial x_i} e_{B,b}(x) = \sum_{\substack{b=(i,j)\in\hat{\mathcal{E}}_B \\ j\in\hat{\mathcal{N}}_i}} \frac{1}{\|z_{ij}\|} Q_{\hat{z}_{ij}}(e_{B,b}(x)). \tag{7.15}$$

Like the asymptotic controller for formation control of infinitesimally rigid frameworks in (7.5), compared to the expression for the formation stabilizing controller for infinitesimally shape-similar frameworks in (4.8), the controller in (7.15) is decidedly simpler because bearing constraints, like distance constraints, are pair-wise rather than triple-wise in the case of angle constraints. However, unlike the asymptotic controller for formation stabilization of infinitesimally rigid frameworks in (7.5), the error terms $e_{B,(i,j)}(x)$ in (7.15) are vectors that must be represented in local coordinate frame.

Controller Synthesis

Here, the controller-synthesis approach to formation control of infinitesimally bearing-rigid frameworks is presented. Consider the following QP, the solution to which is the synthesized

formation controller for infinitesimally bearing-rigid frameworks:

$$\begin{aligned} u^* =& \arg\min_{u\in\mathbb{R}^{dn}} \frac{1}{2}\|u-u^{\text{nom}}\|^2 \\ &\text{s.t.} \quad -e_B^\top(x)\hat{R}_B(x)u \leq -\frac{\rho_B}{2}\|e_B(x)\|^2, \end{aligned} \tag{7.16}$$

where u_{nom} is a nominal controller for the formation, and $\rho_B \in \mathbb{R}_+$ is a parameter that can be chosen to affect convergence of the bearing-error to the origin. Solutions to (7.16), if they exist, ensure exponential stability of the origin of the bearing-error system, thereby ensuring that the desired bearings are achieved while admitting higher-level objectives, which are encoded through the nominal controller.

The structure of the CLF constraint of (7.16) and the bearing-rigidity matrix can be exploited to formulate individual controller-synthesis problems for each robot that ensure satisfaction of the original inequality in (7.16). Towards this formulation, consider the CLF in (7.13), which can be expressed as the sum

$$V_B(e_B(x)) = \frac{\rho_B}{4}\sum_{i=1}^{n}\sum_{\substack{b=(i,j)\in\hat{\mathcal{E}}_B \\ j\in\hat{\mathcal{N}}_i}} \|e_{B,b}(x)\|^2. \tag{7.17}$$

Now, examine the derivative as in (7.14), which can be written as:

$$\dot{V}_B(e_B(x)) = -\sum_{i=1}^{n}\sum_{\substack{b=(i,j)\in\hat{\mathcal{E}}_B \\ j\in\hat{\mathcal{N}}_i}} e_{B,b}^\top(x)\frac{\partial \hat{f}_{B,b}}{\partial x_i}u_i. \tag{7.18}$$

For each robot, the synthesized controller is given by

$$\begin{aligned} u_i^* =& \arg\min_{u_i\in\mathbb{R}^d} \frac{1}{2}\|u-u_i^{\text{nom}}\|^2 \\ &\text{s.t.} \; -\sum_{\substack{b=(i,j)\in\hat{\mathcal{E}}_B \\ j\in\hat{\mathcal{N}}_i}} e_{B,b}^\top(x)\frac{\partial \hat{f}_{B,b}(x)}{\partial x_i}u_i \leq -\frac{\rho_B}{4}\sum_{\substack{b=(i,j)\in\hat{\mathcal{E}}_B \\ j\in\hat{\mathcal{N}}_i}} \|e_{B,b}(x)\|^2. \end{aligned} \tag{7.19}$$

By the following lemma, if the inequality constraint of (7.19) is satisfied for each robot in the formation, then the original inequality constraint of (7.16) is satisfied.

Lemma 7.2. *For $i = 1, \ldots, n$, if each u_i satisfies the inequality constraint of* (7.19)*, then the original inequality constraint of* (7.16) *is satisfied.*

Proof. The inequality

$$-\sum_{\substack{b=(i,j)\in\hat{\mathcal{E}}_B \\ j\in\hat{\mathcal{N}}_i}} e_{B,b}^{\top}(x)\frac{\partial \hat{f}_{B,b}(x)}{\partial x_i}u_i \leq -\frac{\rho_B}{4}\sum_{\substack{b=(i,j)\in\hat{\mathcal{E}}_B \\ j\in\hat{\mathcal{N}}_i}} \|e_{B,b}(x)\|^2$$

implies that

$$-\sum_{i=1}^{n}\sum_{\substack{b=(i,j)\in\hat{\mathcal{E}}_B \\ j\in\hat{\mathcal{N}}_i}} e_{B,b}^{\top}(x)\frac{\partial \hat{f}_{B,b}(x)}{\partial x_i}u_i \leq -\frac{\rho_B}{4}\sum_{i=1}^{n}\sum_{\substack{b=(i,j)\in\hat{\mathcal{E}}_B \\ j\in\hat{\mathcal{N}}_i}} \|e_{B,b}(x)\|^2$$

which by equality to (7.17) and (7.18), implies $-e_B^{\top}(x)\hat{R}_B(x)u \leq -\frac{\rho_B}{4}\|e_B(x)\|^2$. □

Having shown that satisfying the inequality constraints of (7.19) amount to satisfying the inequality constraint of (7.16), the following can be stated as a direct result of Lem. 7.2.

Theorem 7.5. *Suppose the synthesized controllers u_i^* of* (7.19) *exist for each $i = 1, \ldots, n$. Under $u^* = [u_1^{*\top}, \ldots, u_n^{*\top}]^{\top}$, the origin of the bearing-error system in* (7.11)*, $e_B(x) = 0$, is locally exponentially stable.*

Demonstrating the synthesized controller in (7.19), the MATLAB simulation in Figure 7.3 shows the trajectory of four vertices executing the synthesized controller for a nominal control input which is the difference between the desired and current positions of the vertices.

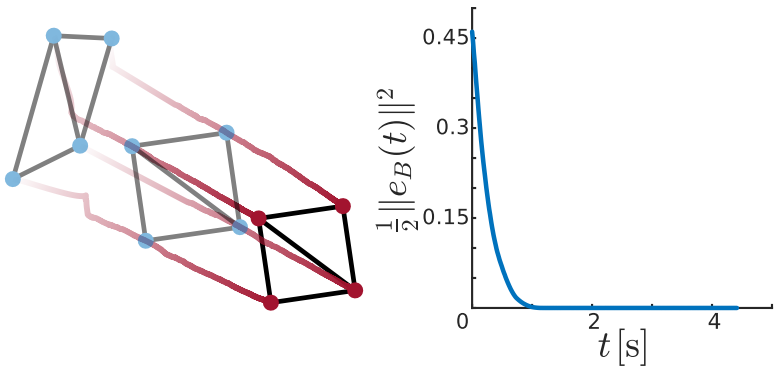

Figure 7.3: (Left) Along the red trajectories as opacity increases, four vertices in an infinitesimally bearing-rigid framework execute the synthesized controller in (7.19), translating and scaling until reaching their final positions (red dots); the black lines indicate the network topology. (Right) The Lyapunov function in (7.13) converges to zero as expected.

Sensing and Communication Requirements

To conclude the introduction of the controller-synthesis approach to formation control of infinitesimally bearing-rigid frameworks considered in this chapter, the implications of the designed formation controllers on the sensing and communication requirements are presented. In particular, the asymptotic controller in (7.15) and the controller-synthesis approach in (7.19) are examined. In each controller, the partial derivative of the bearing-constraint function with respect to each robot position plays a central role in determining the interaction modalities required of the robots. From the partial derivative $\frac{\partial \hat{f}_B(x)}{\partial x_i}$, it can be concluded from the structure of the bearing-rigidity matrix that each robot must be capable of measuring the distances and bearings to its neighbors. It is worth noting that the formation-stabilization controller in (7.15) can be made to be bearing-only by removing the distance term as done in [57]; however, it is unclear whether such a modification can be made to the CLF in (7.19) while preserving exponential stability. As commented previously, relative to the induced interaction modalities of the controller-synthesis approach to formation control of infinitesimally shape-similar frameworks, formation control of bearing constrained formations as described here does not require communication to achieve formation stabilization because bearing constraints are pair-wise, while angle constraints are triple-wise. However, unlike the error systems of distance and angle constrained frameworks,

bearing-errors are vectors that must be written in the local coordinate frames of each vertex when executing the controllers in (7.15) and (7.19).

7.2 Formations Characterized by Heterogeneous Constraints

In this section, the background information on infinitesimal rigidity and infinitesimal bearing-rigidity in Chapter 2, the developments of infinitesimal shape-similarity in Chapter 3, and the relationships between these three framework properties described in Chapter 6 are used to understand formations characterized by heterogeneous constraints. As suggested by the reference to prior chapters, the subject of heterogeneous constraints in multi-robot formations is relevant in the exploration of network topology and the interaction modalities available in a multi-robot team.

To begin, the characterization of formations with heterogeneous constraints is first presented. Then, using the tools afforded in Chapter 2, Chapter 3, and Chapter 6, the central research question posed in Chapter 3 regarding the available motions of frameworks constrained by angle maintenance is posed for frameworks in which distances, bearings, and angles are maintained. After determining the available motions of formations characterized by heterogeneous constraints, Chapter 7.3 adapts the controller-synthesis approach described in Chapter 4 and Chapter 7.1 to formation control of such frameworks, and suggests methods of applying this technique to leverage the available motions of infinitesimally rigid, bearing-rigid, and shape-similar frameworks.

In this work, heterogeneous constraints refer to the desired quantities of the formation to be maintained. Here, consideration of such constraints is limited to inter-robot distances, bearings, and angles, but generally, the approach described here could apply to functions of the relative robot states at large. These distances, bearings, and angles serve in two ways: first, they specify the desired embedding of the formation in terms of the relative positions of the robots; second, when these quantities are maintained, they constrain the motion of the formation. For these reasons, the inter-robot distances, bearings, and angles considered here

are referred to as heterogeneous constraints.

Consideration of formations specified by heterogeneous constraints has been considered in the literature. In particular, the initialism described in [83] suggests a structured method of accounting for heterogeneous distance and bearing constraints. In [84], [85], and [86], the approach of [83] is adopted, and asymptotic formation-stabilization controllers for frameworks with heterogeneous constraints are described. In the remainder of this subsection, the approach presented by [83] is modified to include consideration of frameworks constrained by distances, bearings, and angles. In addition to consideration of angle constraints, the focus of the presentation of this thesis differs from that of [83] in that characterization of the available motions of heterogeneously constrained frameworks, and exploitation of these motions through controller synthesis, are the principle subject of this chapter.

To characterize formations of robots through these heterogeneous constraints, the distance-constraint, bearing-constraint, and angle-constraint functions are used. Because these functions can be applied over certain sub-frameworks of $G(x)$, rather than the entire framework as considered previously in the characterization of formations by homogeneous constraints, care must be taken to precisely indicate to which sub-frameworks these constraints apply. Thus, the following notation is introduced. Let $G_D(x)$ be the sub-framework of $G(x)$ constrained by distances; let $G_B(x)$ be the sub-framework of $G(x)$ constrained by bearings, and let $G_S(x)$ be the sub-framework of $G(x)$ constrained by angles. The framework $G(x)$ is assumed to be given by union of these sub-frameworks; i.e.,

$$G(x) = G_D(x) \cup G_B(x) \cup G_S(x).$$

Using this subscript convention, the constraint functions f_D, f_B, and f_S, introduced previously, can be used in reference to the sub-frameworks over which they are defined without ambiguity. Similarly, the graphs, the vertex, edge, and angle sets can be referenced.

Towards describing the available motions of frameworks characterized by heterogeneous

constraints, define f to be the constraint function generated by concatenating f_D, f_B, and f_S such that

$$f(x) = \begin{bmatrix} f_D(x) \\ f_B(x) \\ f_S(x) \end{bmatrix} \in \mathbb{R}^{|\mathcal{E}_D|+d|\mathcal{E}_B|+|\Theta_S|} \tag{7.20}$$

is the vector of distances, bearings, and angles corresponding with the particular sub-frameworks $G_D(x)$, $G_B(x)$, and $G_S(x)$ of $G(x)$.

As with the development of infinitesimal rigidity, bearing-rigidity, and shape-similarity, of central interest are those infinitesimal motions of the framework which maintain the heterogeneous constraints. Thus, consider motions for $f(x)$ is invariant, which using the background information in Chapter 2 on infinitesimal rigidity and infinitesimal bearing-rigidity, and the developments in Chapter 3 on infinitesimal shape-similarity, can be written in terms of the rigidity, bearing-rigidity, and shape-similarity matrices as follows:

$$\frac{d}{dt}f(x) = R(x)\dot{x} = \begin{bmatrix} R_D(x) \\ R_B(x) \\ \Gamma(x)R_S(x) \end{bmatrix} \dot{x} = 0, \tag{7.21}$$

where $R(x) \in \mathbb{R}^{(|\mathcal{E}_D|+|\mathcal{E}_B|+|\Theta_S|)\times nd}$ is henceforth referred to as the *constraint matrix*, which is the same terminology adopted by [83]. The expression in (7.21) yields the following result, which describes the available motions of formations characterized by heterogeneous constraints.

Theorem 7.6. *For frameworks $G(x) = G_D(x) \cup G_B(x) \cup G_S(x)$, the nullspace of the constraint matrix, $\ker(R(x)) = \ker(R_D(x)) \cap \ker(R_B(x)) \cap \ker(R_S(x))$ is the space of infinitesimal motions of the framework which render $f(x)$ invariant.*

To further characterize the types of formations that can be achieved while ensuring that the heterogeneous constraints represented by the constraint function are rendered invariant, the following framework property is defined.

Definition 7.1. *A framework $G(x)$ is* well-constrained *with respect to the constraint function $f(x)$ if and only if the rank of the constraint matrix $\frac{\partial f(x)}{\partial x}$ achieves its maximum.*

The definition of well-constrained frameworks bears a few noteworthy comments. First, for constraint functions which consist of the squared norms of inter-vertex positions, if the framework is well-constrained, then, equivalently, it is infinitesimally rigid; similarly, this holds for infinitesimally bearing-rigid and infinitesimally shape-similar frameworks with their corresponding constraint functions respectively—as such, the definition in Def. 7.1 is a generalized framework property. Second, well-constrained frameworks represent a large class of frameworks of interest. For example, a framework which is a maximally outerplane graph as in Chapter 5 is infinitesimally shape-similar, and thus well-constrained with respect to the angle-constraint function of the framework. Notably, if the constraint function of the maximally outerplane graph is taken to be the angle-constraint function together with a single squared norm between adjacent vertex positions in the framework, the framework remains well-constrained, but the available motions of the framework are reduced to infinitesimal translations and rotations. Because of the maintained distance, these motions do not include infinitesimal uniform scaling; this observation is central in the characterization of frameworks with heterogeneous constraints. With respect to the constraint function in (7.20), and with regards to the definition of well-constrained frameworks in Def. 7.1, the following theorem introduces a rank condition on the constraint matrix to characterize the available motions of frameworks with heterogeneous constraints.

Theorem 7.7. *A framework $G(x) = G_D(x) \cup G_B(x) \cup G_S(x)$ with constraint function $f(x) = [f_D^\top(x), f_B^\top(x), f_S^\top(x)]^\top$ is well-constrained if and only if*

$$\operatorname{rank}(R(x)) = nd - d.$$

Proof. The proof follows from Thm. 7.6 and from the properties of infinitesimal rigidity, bearing-rigidity, and shape-similarity. The least dimension of $\ker(R(x)) = \ker(R_D(x)) \cap$

$\ker(R_B(x)) \cap \ker(R_S(x))$ is d, corresponding with a framework in which infinitesimal translations are the only constraint satisfying motions. If the framework is well-constrained, then the rank of the constraint matrix is maximized, indicating that the nullspace achieves is minimum dimension, so $\text{rank}(R(x)) = nd - d$. Conversely, if the rank of the constraint matrix is given by $\text{rank}(R(x)) = nd - d$, then the nullspace of the constraint matrix has achieved its minimum, indicating that the rank of the constraint matrix is maximized; this completes the proof. □

Because it will be useful in the next section, which showcases formation control of frameworks characterized by different combinations of the heterogeneous constraints considered by this work, the following corollaries to Thm. 7.7 establish rank conditions on the constraint matrix under pairs of distance, bearing, and angle constraint functions. The proofs of these corollaries follow that of Thm. 7.7, and are omitted.

Corollary 7.7.1. *A framework $G(x) = G_D(x) \cup G_B(x)$ with constraint function $f(x) = [f_D^\top(x), f_B^\top(x)]^\top$ is well-constrained if and only if*

$$\text{rank}(R(x)) = nd - d.$$

Note that Cor. 7.7.1 is a recasting of the results of [83], which refers to well-constrained frameworks specified by distances and bearings as "stiff".

Corollary 7.7.2. *A framework $G(x) = G_D(x) \cup G_S(x)$ with constraint function $f(x) = [f_D^\top(x), f_S^\top(x)]^\top$ is well-constrained if and only if*

$$\text{rank}(R(x)) = nd - d - \binom{d}{2} + \binom{d-p}{2},$$

where $p = \dim(\text{aff}\{x\})$.

Corollary 7.7.3. *A framework $G(x) = G_B(x) \cup G_S(x)$ with constraint function $f(x) =$*

$[f_B^\top(x), f_S^\top(x)]^\top$ *is well-constrained if and only if*

$$\text{rank}(R(x)) = nd - d - 1.$$

The results of this section are summarized to highlight their use in formation control of frameworks characterized by heterogeneous constraints, which follows in Chapter 7.3. This section has presented a unified approach to considering formations characterized by heterogeneous constraints that consist of distance, bearing, and angle constraints. These constraints hold over sub-frameworks whose union is the entire framework. Characterization of the available motions of formations with heterogeneous constraints was a central part of this section. To determine the available motions of such frameworks, the constraint matrix was introduced; the nullspace of this matrix is a vector space that corresponds with infinitesimal motions that preserve the constraints. While frameworks with heterogeneous constraints may admit a number of different motions depending on the sub-frameworks over which the constraints are defined, well-constrained frameworks were defined to highlight frameworks with the least available constraint preserving motions; this property is a generalization of infinitesimal rigidity, bearing-rigidity, and shape-similarity. With respect to distance, bearing, and angle constraints, a rank condition was developed to certify frameworks that are well-constrained. In the following section, these results will be applied to achieve formation control of frameworks with heterogeneous constraints.

7.3 Controller Synthesis with Heterogeneous Constraints

In this section, the controller-synthesis approach to formation control of infinitesimally shape-similar frameworks presented in Chapter 4, and the controller-synthesis approach to control of infinitesimally rigid and bearing-rigid frameworks described previously in Chapter 7.1, are applied to frameworks characterized by heterogeneous constraints. As such, the developments of the previous section, which characterize the available motions

of such frameworks, are useful in understanding the ways in which frameworks can move while ensuring that certain constraint functions are invariant. The purpose of this section is to connect the individual synthesized controllers of infinitesimally rigid, bearing-rigid, and shape-similar frameworks such that controllers for frameworks with heterogeneous constraints can be synthesized; in this purpose, the significance of the trade-offs between network topology and the interaction modalities of a network team is featured, furthering the objective of this thesis.

To begin, the Lyapunov function used as the CLF inequality constraint in the QP yielding the synthesized controller is developed. In particular, consider a framework characterized by heterogeneous constraints, $G(x) = G_D(x) \cup G_B(x) \cup G_S(x)$, as described previously in Chapter 7.2. The constraint function of $G(x)$ is $f(x) = [f_D^\top(x), f_B^\top(x), f_S^\top(x)]^\top$, which represents a composition of distance, bearing, and angle constraints in the framework. From this constraint function, let $\hat{f}(x)$ be the *independent constraint function,* which includes the independent distance, bearing, and angle constraints for which, as described previously, the rank of the rigidity, bearing-rigidity, or shape-similarity matrices are reduced by removal of any constraint respectively. Define the *constraint-error function* $e(x)$ to be a vector of the distance-error, bearing-error, and angle-error functions; i.e.,

$$e(x) = \begin{bmatrix} e_D(x) \\ e_B(x) \\ e_S(x) \end{bmatrix} = \begin{bmatrix} f_D^* - \hat{f}_D(x) \\ f_B^* - \hat{f}_B(x) \\ f_S^* - \hat{f}_S(x) \end{bmatrix} \in \mathbb{R}^{|\hat{\mathcal{E}}_D| + d|\hat{\mathcal{E}}_B| + |\hat{\Theta}_S|},$$

where the desired distances $\hat{f}_D^*$, the desired bearings $\hat{f}_B^*$, and the desired angles $\hat{f}_D^*$ are assumed to be geometrically viable. The *constraint-error system* is given by

$$\dot{e}(x) = -\begin{bmatrix} \hat{R}_D(x) \\ \hat{R}_B(x) \\ \hat{R}_S(x) \end{bmatrix} u = -\hat{R}(x)u, \tag{7.22}$$

the origin of which corresponds with the desired configuration of the vertices as specified by the independent constraint function. Now, the define the CLF to be:

$$V(e(x)) = \frac{1}{2}\|e(x)\|^2 = \frac{1}{2}\|e_D(x)\|^2 + \frac{1}{2}\|e_B(x)\|^2 + \frac{1}{2}\|e_S(x)\|^2,$$

the time derivative of which is given by

$$\begin{aligned}\dot{V}(e(x)) &= \frac{\partial V(e(x))}{\partial x}u = -e^\top(x)\hat{R}(x)u \\ &= -(e_D^\top(x)\hat{R}_D(x) + e_B^\top(x)\hat{R}_B(x) + e_S^\top(x)\hat{R}_S(x))u.\end{aligned} \tag{7.23}$$

As in the previous presentations of asymptotic formation stabilizing controllers, the origin of the constraint-error system for frameworks with heterogeneous constraints can be made asymptotically stable by the following controller.

Theorem 7.8. *Let $G(x) = G_D(x) \cup G_B(x) \cup G_S(x)$ be a non-degenerate framework characterized by the independent constraint function $\hat{f}(x)$ for which $e(x) \in D$, where*

$$\begin{aligned}D = \{e(x) \in \mathbb{R}^{|\hat{\mathcal{E}}_D|+d|\hat{\mathcal{E}}_B|+|\hat{\Theta}_S|} \,\big|\, & e_D(x) \in \mathbb{R}^{|\hat{\mathcal{E}}_D|}; \\ & \hat{z}_b^\top \hat{e}_{B,b}(x) > -1, \forall b = 1, \ldots, |\hat{\mathcal{E}_B}|; \\ & e_S(x) \in (-2, 2)^{|\hat{\Theta}_S|}\};\end{aligned}$$

under the control input

$$u = \hat{R}^\top(x)e(x),$$

the origin of the constraint-error system in (7.22)*, $e(x) = 0$, is locally asymptotically stable.*

Proof. Substituting the controller into the time derivative of the Lyapunov function in (7.23)

yields

$$\begin{aligned}\dot{V}(e(x)) &= -e^\top(x)\hat{R}(x)\hat{R}^\top(x)e(x) \\ &= -\|\hat{R}_D^\top(x)e_D(x)\|^2 - \|\hat{R}_B^\top(x)e_B(x)\|^2 - \|\hat{R}_S^\top(x)e_S(x)\|^2,\end{aligned}$$

which is strictly less that zero according to the proofs of Thm.4.1, Thm. 7.1, and Thm. 7.4 for $e(x) \in D - \{0\}$, so the origin of the constraint-error system is locally asymptotically stable. □

While the controller in Thm. 7.8 provides a means of asymptotically stabilizing the origin of the constraint-error system, a more useful approach to formation control is controller synthesis because of the admission of the nominal control input. The synthesized formation controller is the solution to the following QP:

$$\begin{aligned}u^* = &\underset{u\in\mathbb{R}^{dn}}{\arg\min}\frac{1}{2}\|u - u^{\text{nom}}\|^2 \\ &\text{s.t.} \quad -e^\top(x)\hat{R}(x)u \leq -\frac{\rho}{2}\|e(x)\|^2,\end{aligned} \tag{7.24}$$

where $\rho \in \mathbb{R}_+$ is a parameter that can be chosen to affect the exponential convergence of the constraint-error to the origin. If they exist, solutions to (7.24) ensure that the origin of the constraint-error is locally exponentially stable, and as mentioned in previous descriptions of the controller-synthesis approach, the admission of the nominal control input allows high-level objectives to be addressed by the multi-robot formation, while the CLF inequality ensures that the desired distances, bearings, and angles are achieved.

Regarding the motions available under the controller-synthesis approach to formation control, the heterogeneous constraints dictate how these formations can move. In particular, a well-constrained framework as defined in Def. 7.1 executing the synthesized controller can be expected, according to Thm. 7.6, to asymptotically exhibit invariance only to translations. While well-constrained frameworks offer a clear idea of the available motions, frameworks

which are not well-constrained have, by definition, more available motions due to the relaxed nature of the constraints. To demonstrate the controller-synthesis approach to formation control with heterogeneous constraints, the following subsection describes a deployment of this method on a team of differential-drive robots.

7.3.1 Robotarium Demonstration

As suggested at the close of the previous paragraph, the controller-synthesis approach to formation control of teams of robots described by frameworks characterized by heterogeneous constraints can be applied to exploit the nature of the constraints to achieve desired motion of the team. Here, a demonstration of such a procedure highlights a significant limitation of well-constrained frameworks.

Shown along the numbered sequence of images in Figure 7.4, a team of nine differential-drive drive robots in the Robotarium executes the controller synthesized by solving (7.24). The framework is composed of four triangles: three smaller triangles connected by a large one. Distance constraints apply to the small triangles, while the angles of the large triangle are constrained. From the discussion in the previous section, it is clear that the framework in Figure 7.4 is not well-constrained, and it is neither infinitesimally rigid nor infinitesimally shape-similar; however, the nature of these constraints, examined extensively in this thesis, can be exploited to enable rich and predictable motion of the robots. Each of the small triangles is an infinitesimally rigid subframework, and the large triangle is an infinitesimally shape-similar subframework. As such, the available constraint preserving motions of the framework are myriad, including translation of the framework, uniform scaling of the central triangle, and rotations of the subframeworks.

Along the numbered images in Figure 7.4, the high-level motion of the robots is directed by a nominal controller which causes the three small triangles to individually rotate clockwise about its own centroid while simultaneously rotating about the centroid of the central triangle, which rotates and scales. Shown in bottom right image of Figure 7.4, the squared

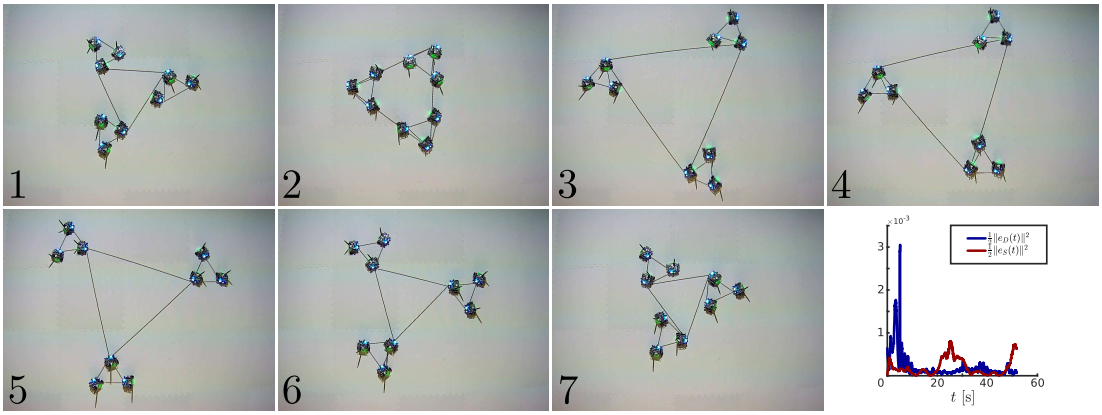

Figure 7.4: Along the numbered images, the controller synthesized by solving (7.24) is executed by a team of nine differential-drive robots in the Robotarium. The framework consists of three small triangles constrained by distances, and a large central triangle constrained by its angles. The synthesized controller stabilizes the origin of the constraint-error system, quantified by the graph in the bottom right image. The robots move such that the small triangles rotate about themselves and the centroid of the framework and the central triangle rotates and scales.

norms of the distance and angle errors are shown to approach zero and remain within acceptable tolerances given the limitations of the differential-drive robots, thus suggesting the efficacy of the controller-synthesis approach to formation control of multi-robot teams characterized by heterogeneous constraints.

As indicated in Cor. 7.7.2, the available motions of well-constrained frameworks with respect to distance and angle constraints include infinitesimal translation and rotation of the entire framework. The framework shown in the demonstration depicted in Figure 7.4 is not well-constrained, and so has many more constraint preserving motions; this demonstration supports the following claim. The available constraint preserving motions of well-constrained frameworks may not be rich enough to support the objectives of the team (e.g., the motions depicted in Figure 7.4 would not preserve the constraints of a corresponding well-constrained framework). While reducing the constraints in a framework increases the available motions, and thus may reduce the predictability of the motion of the multi-robot team, careful application of constraints, supported by the theoretical underpinnings of infinitesimal rigidity, bearing-rigidity, and shape-similarity, can enable the robots to execute complex maneuvers in predictable ways, which is a major advantage of

incorporating heterogeneous constraints by the method suggested in this chapter. Thus demonstrated, the controller-synthesis approach to formation control of multi-robot teams characterized by heterogeneous constraints is powerful in its extensibility, allowing various constraints to be transparently incorporated without undue effort in controller design.

7.4 Admitting Constraint Violation

In this section, the controller-synthesis approach to formation control, including the controller-synthesis approach to formation control of frameworks described by heterogeneous constraints as well as the controller-synthesis approach to formation control of infinitesimally rigid, bearing-rigid, and shape-similar frameworks, is reconsidered to examine situations in which it may be advantageous to violate the constraints that specify the formation. In particular, this section suggests a situation in which constraints should be violated, and modifies the controller-synthesis approach to formation control to handle this violation gracefully.

With regards to situations in which it may be necessary or advantageous not to insist that the distances, bearings, or angles of a multi-robot formation be maintained, an example that typically arises is that of navigation in the presence of obstacles in the environment. As such, one simple answer to the question of when formation constraints should be violated is: when it is necessary to safely navigate the environment. Having identified safe navigation as a use-case for constraint violation, the remainder of this section demonstrates the extensibility of the controller-synthesis approach to formation control in enabling safe navigation of teams of robots.

To achieve safe navigation, control barrier functions are introduced as further inequality constraints in the QP. As described in Chapter 2.3, CBFs have been used in the literature to achieve collision avoidance; the novelty in this presentation is not the incorporation of barrier functions for collision avoidance. Rather, its purpose is to consider trade-offs between the objectives of formation control, which bring to light those issues concerning

the interplay between network topology and interaction modalities in a multi-robot team, and broader objectives that a multi-robot team may be expected to address. As such, the incorporation of barrier functions will first begin with CBFs based on the distances between robots and obstacles and inter-robot distances.

To begin, consider the following barrier function based on the distances between robots and O points $p_o \in \mathbb{R}^d$, $o = 1, ..., O$, representing obstacles in the environment. Without loss of generality, assume that the points are stationary; if the velocities of the points are known or can be estimated, the following presentation can be modified appropriately. The barrier function based on the distances between robots and these points can be expressed as

$$h_{D,(i,o)}(x) = \frac{1}{2}\|x_i - p_i\|^2 - d_{io}^2,$$

where $d_{io} \in \mathbb{R}_+$ is the safe distance between robot i and the point o. The time derivative of this expression is given by

$$\dot{h}_{D,(i,o)}(x) = (x_i - p_o)^\top u_i. \tag{7.25}$$

Choosing u_i such that (7.25) is greater than $-h^3_{D,(i,o)}(x)$ ensures that the distance between robot i and obstacle o remains greater than the safe distance (see [73] for a thorough exposition of CBFs).

Perhaps more interesting in the context of this thesis, for reasons that will be made apparent shortly, consider the issue of collision avoidance between robots in formation, which could be achieved by the following CBF based on the inter-robot distances:

$$h_{D,(i,j)}(x) = \frac{1}{2}\|z_{ij}\|^2 - d_{ij}^2, \tag{7.26}$$

where $d_{ij} \in \mathbb{R}_+$ is the safe distance between robots i and j. Note that $h_{D,(i,j)}(x)$ is positive for inter-robot distances greater than d_{ij}, zero when the robots are exactly d_{ij} apart, and

negative otherwise. The time derivative of this barrier function is given by

$$\dot{h}_{D,(i,j)}(x) = z_{ij}^{\top} u_i + z_{ji}^{\top} u_j; \tag{7.27}$$

choosing u_i and u_j such that (7.27) is greater than $-h_{D,(i,j)}^3(x)$ results in collision avoidance between robots i and j. With regards to the complete framework $G^{\kappa}(x)$, consider the vector of barrier functions of the form in (7.26) between every pair of vertices in the framework

$$h_D^{\kappa}(x) = \begin{bmatrix} \vdots \\ h_{D,(i,j)}(x) \\ \vdots \end{bmatrix} \; \forall (i,j) \in \mathcal{V} \times \mathcal{V};$$

the time derivative of this expression is given by

$$\dot{h}_D^{\kappa}(x) = R_D^{\kappa}(x) u,$$

where $R_D^{\kappa}(x)$ is the rigidity matrix of the complete framework. By virtue of the component barrier functions of $h_D^{\kappa}(x)$ and the structure of $R_D^{\kappa}(x)$, satisfying the following inequality ensures that no two vertices collide:

$$R_D^{\kappa}(x) u \succeq -(h_D^{\kappa}(x))^3,$$

where $\succeq$ indicates the element-wise inequality, and $(h_D^{\kappa}(x))^3$ refers to the element-wise operation of cubing the elements; i.e,

$$(h_D^{\kappa}(x))^3 = \begin{bmatrix} \vdots \\ h_{D,(i,j)}^3(x) \\ \vdots \end{bmatrix} \; \forall (i,j) \in \mathcal{V} \times \mathcal{V}.$$

This set of control barrier functions is notable not only for its explicit utility, but for the role

that the rigidity matrix plays in these barrier functions based on the inter-robot distances. Apparent by the presentation, the rigidity matrix plays a role not only in the CLFs of the asymptotic formation-stabilization controller of (7.2) and the controller-synthesis method of (7.7), but in CBFs based on inter-robot distances.

Having described these CBFs, they can be incorporated as inequality constraints in the controller-synthesis approach to formation control. Here, the presentation of the QP assumes that the controller is being synthesized for a framework characterized by heterogeneous constraints, but the technique could also be applied to those characterized by homogeneous constraints as well. The formation controller, which ensures collision avoidance with respect to obstacles and inter-robot collisions, is synthesized by solving the following modification of the QP in (7.24):

$$\begin{aligned} u^* = &\underset{u\in\mathbb{R}^{dn}}{\arg\min}\frac{1}{2}\|u-u^{\text{nom}}\|^2+|\delta|^2 \\ &\text{s.t.} \quad -e^\top(x)\hat{R}(x)u-\delta\leq-\frac{\rho}{2}\|e(x)\|^2 \\ &\qquad \frac{\partial h_{D,(i,o)}(x)}{\partial x_i}u_i\geq -h^3_{D,(i,o)}(x) \quad \forall i=1,\dots,n, o=1,\dots,O \\ &\qquad R^\kappa_D(x)u\succeq-(h^\kappa_D(x))^3 \\ &\qquad \delta\geq 0, \end{aligned} \tag{7.28}$$

where δ is a slack variable which serves two important purposes. First, δ helps ensure feasibility of the problem. Second, and more significantly, δ determines the trade-off made between the collision avoidance constraints captured by the CBFs, and the formation-stabilization constraint captured by the CLF. The formation controllers synthesized by solving (7.28) address the issue of balancing the objective of maintaining the constraints specifying the formation against collision avoidance; as shown in the following demonstrations, this method enables the multi-robot team to accomplish a variety of objectives.

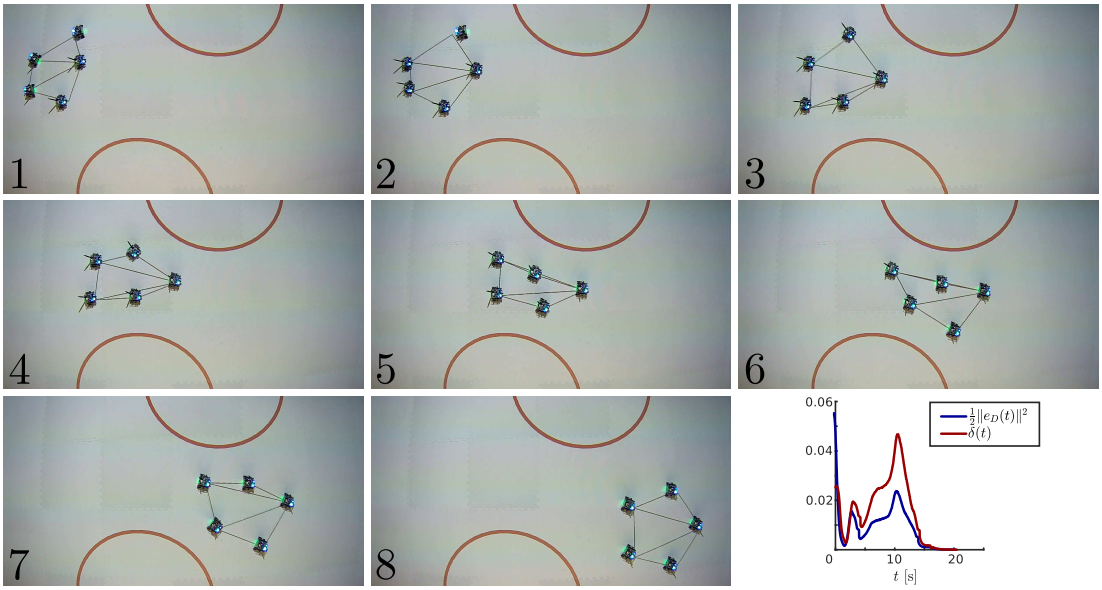

Figure 7.5: To demonstrate graceful constraint violation, a team of five differential-drive robots in the Robotarium described by an infinitesimally rigid framework executes the controller synthesized by solving (7.28). Along the numbered images, the robots are initialized and translate from the left of the testbed surface to the right. Quantified by the graph in the bottom right image, as the formation encounters obstacles in the environment, the distance CLF constraint is relaxed by increasing the value of the slack variable while the CBF collision avoidance inequality constraint is enforced. As a result, the formation distorts as the robots pass through the narrow passage before reforming on the other side, having safely navigated the environment.

7.4.1 Robotarium Demonstration

In contrast with previous sections, this section includes not one, but three demonstrations that highlight the utility of the approach to graceful constraint violation in (7.28) and the significant differences that arise in the application of this method to infinitesimally rigid and infinitesimally shape-similar frameworks.

To begin, the difference between constraint violation in the presence of obstacles is examined for infinitesimally rigid and shape-similar frameworks. Shown in the numbered images of Figure 7.5, a team of five differential-drive robots in an infinitesimally rigid framework executes the controller synthesized by solving (7.28). Quantified in the bottom right image of Figure 7.5, the distance error initially decreases rapidly as the distance CLF constraint is satisfied; however, when the obstacles are encountered as the formation moves through the environment, the slack variable is increased while the CBF collision avoidance constraints are enforced, relaxing the distance constraints and allowing the formation to

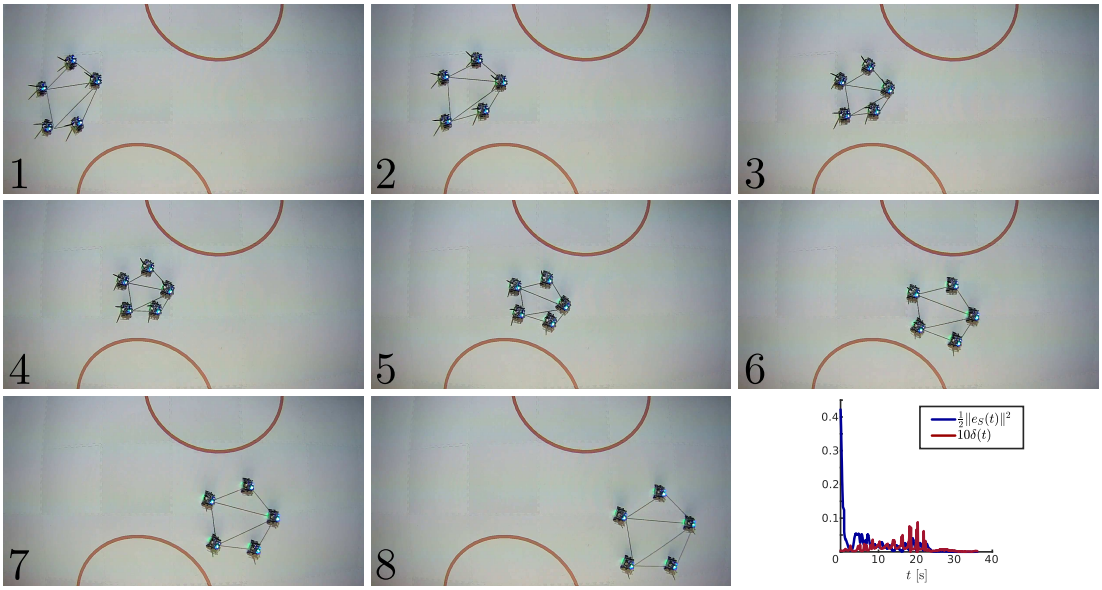

Figure 7.6: To demonstrate graceful constraint violation, a team of five differential-drive robots in the Robotarium described by an infinitesimally shape-similar framework executes the controller synthesized by solving (7.28). Along the numbered images, the robots are initialized and translate from the left of the testbed surface to the right. Quantified by the graph in the bottom right image, as the formation encounters obstacles in the environment, the angle CLF constraint is relaxed by increasing the value of the slack variable while the CBF collision avoidance inequality constraint is enforced. As a result, the formation contracts uniformly as the robots pass through the narrow passage before expanding on the other side, having safely navigated the environment.

safely navigate. After passing through the obstacles, the slack variable and squared norm of the distance error decrease as expected.

Now, consider the demonstration in Figure 7.6, in which the same framework of five differential-drive robots is characterized instead by angle constraints. In this case, when the robots encounter the obstacles and the angle CLF constraint is relaxed by increasing the value of the slack variable, the formation contracts uniformly; this, in contrast with the distortion when the distances between robots were constrained, highlights the practical differences between the angle and distance constraints and demonstrates the utility of uniform scaling as a constraint preserving motion for infinitesimally shape-similar frameworks.

In a final demonstration, Figure 7.7 shows two infinitesimally shape-similar frameworks of four differential-drive robots, which trade positions without collision. Along the numbered images, the robots are initialized and execute the controller synthesized by solving (7.28). The nominal controller for each formation directs the motion such that they encounter

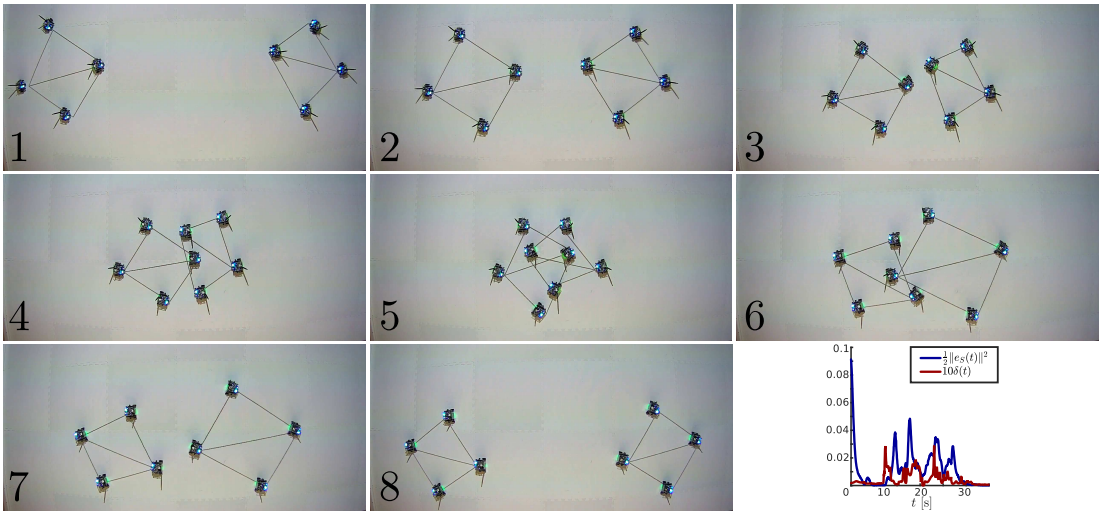

Figure 7.7: Shown along the numbered images, two teams of four differential-drive robots described by infinitesimally shape-similar frameworks are directed to trade places while executing the controller synthesized by solving (7.28). As they encounter each other, the formation stabilization inequality constraint is relaxed while the CBF inequality constraint is enforced. Each peak in the squared norm of the total angle error, as well as peaks in the slack variable value, shown in the bottom right image, corresponds with an encounter between robots. Once the formations pass through each other, the slack variable is reduced, and the angles converge to their desired values.

each other in the middle of the testbed surface. In order to avoid collisions, the formation stabilization CLF inequality constraint is relaxed by increasing the value of the slack variable, which is shown in the plot in the bottom right image of Figure 7.7. Shown in this plot, the peaks in the squared norm of the sum of the angle-errors for both formations increases when robots encounter one another and must avoid collision; corresponding with these peaks are increases in the value of the slack variable. Once the formations successfully pass through each other, the formation-stabilization constraint is enforced, and the angles return to desired values.

7.5 Summary of Conclusions

In this section, control of formations characterized by heterogeneous constraints was considered. In reference to understanding and exploring the interplay between network topology and the interaction modalities of a multi-robot team, this section examined frameworks characterized by heterogeneous constraints to determine the types of formations that can

be achieved and the available motions of such formations. Then, the controller-synthesis approach to formation control was applied to leverage the benefits of heterogeneity, which were demonstrated in numerous deployments on teams of differential-drive robots.

In this section, explicit reference was made to the controller-synthesis approach to formation control of infinitesimally shape-similar frameworks, and the section began by mirroring this approach to formation control for formations represented by infinitesimally rigid and bearing-rigid frameworks. After completing this presentation for formations characterized by homogeneous constraints, the frameworks described by heterogeneous distance, bearing, and angle constraints were characterized through the development of the constraint matrix, the nullspace of which corresponds with the available motions of the framework. Using the developments of infinitesimal shape-similarity in Chapter 3 and the background information on infinitesimal rigidity and bearing-rigidity in Chapter 2, a rank condition on the constraint matrix was introduced to explain that translations are the only available motions to frameworks that are well-constrained with respect to the heterogeneous distance, bearing, and angle constraints.

Not only was the constraint matrix important for characterizing the available motions of formations with heterogeneous constraints, the constraint matrix played an explicit role in the adaptation of the controller-synthesis approach to formation control of such frameworks, appearing in the CLF inequality constraint in the QP. In addition to the issue of formation stabilization captured by this CLF, graceful constraint violation was addressed in the context of safe navigation of the team through the incorporation of CBFs to enforce safety and a slack variable to determine the trade-off between avoiding collisions and maintaining the formation. Finally, this approach to formation control was demonstrated on a team of differential-drive robots to suggest the utility of the method.

CHAPTER 8
CONCLUSIONS AND FUTURE WORK

In this thesis, the interplay between network topology and the interaction modalities available in a multi-robot team were investigated in the context of formation control. Here, the main conclusions of this investigation, drawn from the chapters of this thesis, are collected and summarized; with respect to these conclusions, directions for future research are described. In particular, each chapter of this thesis was written to address a set of fundamental research questions designed to reveal the coupling between network topology and the interaction modalities in multi-robot teams—for clarity and convenience to the reader, these research questions have been posed plainly in Chapter 1, the introduction of this thesis. In the following paragraphs, the conclusions are stated by answering these research questions.

In Chapter 3, this thesis began by examining frameworks specified by the relative angles between robots to characterize and determine the available motions of these angle-constrained formations. In this examination, the framework property of infinitesimal shape-similarity, the principle theoretical development of this body of work, was defined to characterize frameworks where maintenance of the angles between robots renders the framework invariant to infinitesimal translations, rotations, and uniform scaling. With this characterization of the available motions of the frameworks of interest, tools for analyzing arbitrary frameworks for this property, namely conditions on the nullspace and rank of the shape-similarity matrix, were developed. In the process of developing these tools, both the network topology and the embedding of the framework were found to be intimately related through the shape-similarity matrix. Accounting for this relationship in specification and design of multi-robot formations is critical because: if the dimension of the affine hull of the vertex positions is not sufficiently high, then regardless of the network topology, the framework is pathological; similarly, if the vertices are positioned correctly, but the network

topology does not correctly constrain the motion, then the framework is not infinitesimally shape-similar.

After developing infinitesimal shape-similarity, design of formation controllers for infinitesimally shape-similar frameworks was the subject of Chapter 4. In this chapter, the objective was to leverage the developments concerning infinitesimal shape-similarity to achieve formation stabilization with particular attention paid to the induced sensing and communication requirements on robots in the team. With regard to this objective, the angle-error function was defined, and two approaches to formation control were presented. The first resulted in asymptotic stability of the origin of the angle-error system, which depends explicitly on the shape-similarity matrix; the second consisted of a controller-synthesis approach to formation control capable of incorporating high-level control objectives. Aside from the immediate utility of these formation controllers in leveraging the results of the previous chapter for control of infinitesimally shape-similar frameworks, examination of the partial derivatives of the angle-constraint function revealed that, in general, to stabilize the formation with these techniques, the robots needed distance and bearing information available locally and through communication with immediate neighbors. These requirements are founded and understood because the relative angles between robots explicitly require information from three robots, two of which may not be adjacent. Commenting on possible relaxations of these requirements, the chapter concluded by noting that restriction to the plane and particular network topologies might allow formations of robots to be controlled using fewer sensors, a subject that was explored in the following chapter. One avenue for future work is to consider further relaxations of these sensing and communication requirements to explore control of formations described by infinitesimally shape-similar frameworks in which communication is prohibited entirely.

After examining formation control of infinitesimally shape-similar frameworks at large, Chapter 5 considered self-assembly and control of a particular class of frameworks in order to explore the limited incorporation of heterogeneity in terms of the sensing capabilities

of the robots. To begin, triangulations were shown, using the tools of shape-similarity developed in Chapter 3, to be infinitesimally shape-similar. Self-assembly of maximally outerplane graphs, a class of triangulations, was then considered in two parts. First, a graph grammar was developed to assign the topology of the formation; second, a realizing controller was designed for robots equipped with bearing-only sensors so that triangular faces of the framework could be made equilateral. Through this self-assembly mechanism, the comments of the previous chapter were substantiated; because the robots were restricted to the plane, and because the robots were arranged with a particular network topology, it was possible to stabilize the formation without the use of distance information. To demonstrate the immediate utility of heterogeneous sensing capabilities, a single robot, designated the first follower, was equipped with distance sensors in addition to bearing sensors. Then, a leader-follower formation-control strategy was developed that used a leader to determine the position of the framework, the first follower to set the heading and scale of the formation with respect to the leader, and the remaining robots to maintain the desired relative angles between robots using the bearing-only controller. Ultimately, the limited addition of distance information had a dramatic impact on the capabilities of the formation, suggesting the utility of heterogeneity at large. Notably, the maintenance of the angles was applied along the weak dual graph of the maximally outerplane graph; in the future, identification of other network topologies where infinitesimally shape-similar subframeworks can be maintained serially may enable related formation-control strategies to be developed.

After the case-study in heterogeneity presented in the previous chapter, Chapter 6 exposed the underlying relationships between the framework properties of infinitesimal rigidity, bearing-rigidity, and shape-similarity. In particular, algebraic relationships between the rigidity, bearing-rigidity, and shape-similarity matrices were found, which allow the bearing-rigidity matrix to be written in terms of the rigidity matrix, and the shape-similarity matrix to be written in terms of the bearing-rigidity matrix. Using these algebraic relationships between the framework properties, the implications between them were considered. Hearken-

ing to the importance of the plane noted in Chapter 4, these three framework properties were shown to be equivalent for frameworks in two dimensions. However, in higher dimensions this was not the case. In fact, infinitesimal rigidity implies infinitesimal bearing-rigidity, and infinitesimal shape-similarity implies infinitesimal bearing-rigidity in greater than two dimensions. The provided counterexamples show that infinitesimal bearing-rigidity does not imply infinitesimal shape-similarity or infinitesimal rigidity in higher dimensions, and that infinitesimal shape-similarity does not imply infinitesimal rigidity in higher dimensions. Proving that infinitesimal rigidity implies infinitesimal shape-similarity is the subject of future work. With these relationships between the framework properties established, examination of frameworks characterized by heterogeneous constraints could be supported in the following chapter.

In the final chapter of this thesis, Chapter 7 considered frameworks described by heterogeneous sets of distance, bearing, and angle constraints to determine the available motions of such frameworks and to suggest the efficacy of the controller-synthesis approach to controlling them. To begin, and for completeness in the presentation, the approach to formation control of infinitesimally shape-similar frameworks in Chapter 4 was repeated for infinitesimally rigid and bearing-rigid frameworks; this presentation revealed a fundamental difference in the sensing and communication requirements of distance and bearing constrained frameworks as opposed to those of angle constrained frameworks arising from the pair-wise nature of the distances and bearings as compared to the triple-wise nature of angles. Then, frameworks with heterogeneous constraints were characterized using the constraint matrix, the nullspace of which describes the available motions of such frameworks. With a rank condition on the constraint matrix, well-constrained frameworks with respect to distances, bearings, and angles were shown to be invariant only to translations. With this characterization of frameworks with heterogeneous constraints, a controller-synthesis approach to formation control of such frameworks was presented, and demonstrations on teams of differential-drive robots show the utility of including heterogeneous constraints.

Future work will consider: the development of CBFs based on angles and bearings that ensure invariance of the region of attraction of the Lyapunov functions for the angle and bearing-error systems respectively, and the application of the controller-synthesis approach to formations of robots not modelled as unicycles.

Having summarized the objectives, contributions, and observations of this thesis, the following conclusions can be drawn with regard to understanding the interplay between network topology and the interaction modalities available in a multi-robot team. Substantiated by the results of this work, and in particular the results of Chapter 3 and Chapter 6, the network topology, the interaction modalities accompanying the particular constraints specifying the formation, and the embedding of the robots in space are all fundamentally coupled an should not be considered in isolation of each other. For example, when designing formation controllers for infinitesimally shape-similar frameworks, the position of the robots and the network describing their connectivity have a fundamental effect on how the robots can move while preserving measured angles. Furthermore, simply being equipped with sensors that can measure angles may not be sufficient to compute the control inputs necessary to maintain them. In fact, the sensing and communication modalities available to robots restrict the types of controllers that can be deployed, and there is a critical trade-off that must be made between communication and sensing which cannot be decoupled from the network topology of the framework. With regards to fielding multi-robot teams, this thesis has practical relevance to the design and outfitting of robotic platforms on which various formation controllers will be deployed. To effectively execute formation controllers, as evidenced by the results of Chapter 4, Chapter 5, and Chapter 7, the coupling of the underlying network topology and the sensing and communication capabilities of the robots should be accounted for explicitly in order to leverage the capabilities of formations described by homogeneous constraints and those greater capabilities afforded by formations in which the constraints are heterogeneous.

Appendices

APPENDIX A

AFFINE SETS

Here, a brief description of affine sets is included for convenience to the reader; a thorough exposition of affine sets and spaces is given in [79, Chapter 1].

The set $A \subseteq \mathbb{R}^n$ is *affine* if $\alpha x + \beta y \in A$ for $x, y \in A$ and $\alpha + \beta = 1$. The *affine hull* of a set $A \subseteq \mathbb{R}^n$ is the intersection of all affine sets containing A and is written $\mathrm{aff}\{A\}$; its dimension is denoted $\dim(\mathrm{aff}\{A\})$. The affine hull of the vertex positions of a framework is written $\mathrm{aff}\{x\} = \mathrm{aff}\{x_1, x_2, \ldots, x_n\}$.

An isometric transformation of $\mathbb{R}^n$ is a distance-preserving transformation $T : \mathbb{R}^n \to \mathbb{R}^n$ of the form $T = Mx + c$, where $M \in \mathbb{R}^{n \times n}$ is an orthogonal matrix and $c \in \mathbb{R}^n$. Affine sets are isometric if there is an isometry $T(A) = B$.

The following result will be useful for the development of tools for assessing frameworks for infinitesimal shape-similarity in Ch. 3. Note that [79] refers to affine sets as flats and isometries as congruencies.

Lemma A.1 ([79, Theorem 1.6.3, pg. 30])**.** *Let A and B be affine sets of dimension r in $\mathbb{R}^n$. Then A and B are isometric.*

APPENDIX B

NOTATION

For convenience to the reader, common notation between chapters of this thesis are listed in the order of appearance.

$\mathcal{G} = (\mathcal{V}, \mathcal{E})$	a graph
$\mathcal{V}$	the vertex set
$\mathcal{E}$	the edge set
n	the number of vertices
ϵ	the number of edges
H	the incidence matrix
L	the graph Laplacian
$\otimes$	the Kronecker products
I_d	the $d \times d$ identity matrix
$\mathrm{rank}(\cdot)$	the rank of the matrix
$\ker(\cdot)$	the nullspace of the matrix
$\mathrm{span}\{\cdot\}$	a set of spanning vectors
$x = [x_i^\top, \ldots, x_n^\top]^\top \in \mathbb{R}^{dn}$	the vector of vertex positions
$\dot{x}$	the infinitesimal motion of the vertices
d	the dimension of the vertices
$G(x) = (\mathcal{G}, x)$	the framework, a graph embedding
$\mathcal{G}^\kappa$	the complete graph
$G^\kappa(x)$	the complete framework
$g = (\mathcal{G}, \nu, \xi)$	a labeled graph
ν	the vertex labels of the labeled graph
ξ	the edge labels of the labeled graph
Φ	a graph grammar
$r = (g_l, g_r)$	a graph grammar rule

$\mathbb{R}_+$	the positive real numbers
$z_{ik} = x_i - x_k$	the difference of vertex positions
$\mathrm{vec}(z_b)$	the vector of the difference of vertex positions
$\mathrm{diag}(\cdot)$	a matrix with elements on the diagonal
$f_D(x)$	the distance-constraint function
$R_D(x)$	the rigidity matrix
$\mathrm{aff}\{x\}$	the affine hull of the vertices
$\dim(\mathrm{aff}\{x\})$	the dimension of the affine hull of the vertices
$\hat{z}_{ik} = z_{ik}/\|z_{ik}\|$	an inter-vertex bearing
$\mathrm{vec}(\hat{z}_b)$	the vector of inter-vertex bearings
$f_B(x)$	the bearing-constraint function
Q_{z_b}	the orthogonal projection matrix with respect to z_b
Θ_S	the angle set
m	the number of angles
θ_{ikj}	the angle between vertices i, k, and j centered on k
$\theta(x)$	the vector of angles of a framework
$\cos(\theta(x))$	the element-wise cosine of the vector of angles
$f_S(x)$	the angle-constraint function
$R_S(x)$	the shape-similarity matrix
$\Gamma_S = \mathrm{diag}(\ldots, \gamma_{ikj}, \ldots)$	the positive definite matrix of scalars γ_{ikj}
$S = \left[\begin{smallmatrix} 0 & 1 \\ -1 & 0 \end{smallmatrix}\right]$	a skew-symmetric matrix
$e_\alpha \in \mathbb{R}^d$	a standard basis vector
$S_\beta \in \mathbb{R}^{d\times d}$	a skew-symmetric matrix
V^t	a vector space of translations of x
V^r	a vector space of rotations of x
V^s	a vector space of uniform scaling of x
$G(x_{ijk})$	a subframework of $G(x)$
$e_D(x), e_B(x), e_S(x)$	the distance, bearing, and angle-error
$V_D(e_D(x)), V_B(e_B(x)), V_S(e_S(x))$	Lyapunov functions

REFERENCES

[1] G. Xu, W. Shen, and X. Wang, "Applications of wireless sensor networks in marine environment monitoring: A survey," *Sensors*, vol. 14, no. 9, pp. 16 932–16 954, 2014.

[2] S. Thrun, "Toward robotic cars," *Communications of the ACM*, vol. 53, no. 4, pp. 99–106, 2010.

[3] P. R. Wurman, R. D'Andrea, and M. Mountz, "Coordinating hundreds of cooperative, autonomous vehicles in warehouses," *AI Mag.*, vol. 29, no. 1, pp. 9–9, 2008.

[4] M. Dunbabin and L. Marques, "Robots for environmental monitoring: Significant advancements and applications," *Robot. & Autom. Mag.*, vol. 19, no. 1, pp. 24–39, 2012.

[5] D. Pickem, P. Glotfelter, L. Wang, M. Mote, A. Ames, E. Feron, and M. Egerstedt., "The Robotarium: A remotely accessible swarm robotics research testbed," in *Int. Conf. Robot. Autom.*, IEEE, May 2017.

[6] I. Buckley and M. Egerstedt, "Infinitesimally shape-similar motions using relative angle measurements," in *Int. Conf. Intell. Robot. Syst.*, IEEE, 2017, pp. 1077–1082.

[7] ——, "Self-assembly of a class of infinitesimally shape-similar frameworks," in *Int. Conf. Intell. Robot. Syst.*, IEEE, 2018, pp. 3751–3756.

[8] ——, "Infinitesimal shape-similarity for characterization and control of bearing-only multi-robot formations," *IEEE Trans. Robot. Autom.*, Submitted.

[9] ——, "Controller synthesis for infinitesimally shape-similar formations," in *Int. Conf. Robot. Autom.*, IEEE, 2020, To Appear.

[10] ——, "A decentralized heterogeneous control strategy for a class of infinitesimally shape-similar formations," in *Int. Conf. Robot. Autom.*, IEEE, 2019.

[11] D. P. Scharf, F. Y. Hadaegh, and S. R. Ploen, "A survey of spacecraft formation flying guidance and control. part II: Control," in *Proc. Amer. Control Conf.*, IEEE, vol. 4, 2004, pp. 2976–2985.

[12] K. Oh, M. Park, and H. Ahn, "A survey of multi-agent formation control," in *Automatica*, vol. 53, Mar. 2015, pp. 424–440.

[13] R. W. Beard, J. Lawton, and F. Y. Hadaegh, "A coordination architecture for spacecraft formation control," *IEEE Trans. Control Syst. Technology*, vol. 9, no. 6, pp. 777–790, 2001.

[14] T. Eren, W. Whiteley, B. D. O. Anderson, A. S. Morse, and P. N. Belhumeur, "Information structures to secure control of rigid formations with leader-follower architecture.," in *Proc. Amer. Control Conf.*, IEEE, 2005, pp. 2966–2971.

[15] Y. Wardi, C. Seatzu, M. Egerstedt, and I. Buckley, "Performance regulation and tracking via lookahead simulation: Preliminary results and validation," in *IEEE Conf. on Decision and Control*, IEEE, 2017, pp. 6462–6468.

[16] S. Dai, S. He, H. Lin, and C. Wang, "Platoon formation control with prescribed performance guarantees for USVs," *IEEE Trans. Ind. Electron.*, vol. 65, no. 5, pp. 4237–4246, 2018.

[17] H. Du, W. Zhu, G. Wen, Z. Duan, and J. Lü, "Distributed formation control of multiple quadrotor aircraft based on nonsmooth consensus algorithms," *IEEE Trans. Cybern.*, vol. 49, no. 1, pp. 342–353, 2019.

[18] S. Shashwat, I. Buckley, Y. Wardi, C. Seatzu, and M. Egerstedt, "Tracking control by the newton-raphson flow: Applications to autonomous vehicles," in *European Control Conf.*, IEEE, 2019.

[19] J. R. T. Lawton, R. W. Beard, and B. J. Young, "A decentralized approach to formation maneuvers," *IEEE Trans. Robot. Autom.*, vol. 19, no. 6, pp. 933–941, Dec. 2003.

[20] T. H. A. van den Broek, N. van de Wouw, and H. Nijmeijer, "Formation control of unicycle mobile robots: A virtual structure approach," in *IEEE Proc. Conf. Decision and Control*, Dec. 2009, pp. 8328–8333.

[21] F. Zhang, M. Goldgeier, and P. S. Krishnaprasad, "Control of small formations using shape coordinates," in *Int. Conf. Robot. Autom.*, IEEE, 2003, pp. 2510–2515.

[22] M. A. Hsieh, V. Kumar, and L. Chaimowicz, "Decentralized controllers for shape generation with robotic swarms," *Robotica*, vol. 26, no. 5, pp. 691–701, 2008.

[23] F. Zhang, "Geometric cooperative control of particle formations," *Trans. Automatic Control*, vol. 55, no. 3, pp. 800–803, 2010.

[24] J. A. Fax and R. M. Murray, "Information flow and cooperative control of vehicle formations," *IFAC World Congress*, vol. 35, no. 1, pp. 115–120, 2002.

[25] A. Jadbabaie, J. Lin, and A. S. Morse, "Coordination of groups of mobile autonomous agents using nearest neighbor rules," in *Proc. Conf. Decision Control*, IEEE, vol. 3, 2002, pp. 2953–2958.

[26] W. Ren, R. W. Beard, and T. W. McLain, "Coordination variables and consensus building in multiple vehicle systems," in *Cooperative control*, Springer, 2005, pp. 171–188.

[27] M. Mesbahi and M. Egerstedt, "Graph theoretic methods in multiagent networks," in. 2010.

[28] E. Montijano, E. Cristofalo, D. Zhou, M. Schwager, and C. Sagüés, "Vision-based distributed formation control without an external positioning system," *IEEE Trans. Robot.*, vol. 32, no. 2, pp. 339–351, 2016.

[29] M. Ye, B. D. O. Anderson, and C. Yu, "Bearing-only measurement self-localization, velocity consensus and formation control," *IEEE Trans. Aerosp. Electron. Syst.*, vol. 53, no. 2, pp. 575–586, 2017.

[30] F. Bullo, J. Cortéz, and S. Martínez, "Distributed control of robotic networks: A mathematical approach to motion coordination algorithms," in. 2009.

[31] W. Ren, R. W. Beard, and E. M. Atkins, "A survey of consensus problems in multi-agent coordination," in *Proc. Amer. Control Conf.*, IEEE, 2005, pp. 1859–1864.

[32] R. Olfati-Saber and R. M. Murray, "Distributed cooperative control of multiple vehicle formations using structural potential functions," in *IFAC World Congress*, vol. 15, 2002, pp. 242–248.

[33] Z. Lin, L. Wang, Z. Chen, M. Fu, and Z. Han, "Necessary and sufficient graphical conditions for affine formation control," *IEEE Trans. Autom. Control*, vol. 61, no. 10, pp. 2877–2891, 2016.

[34] J. Bondy and A. Murty, "Graph theory," in. 2008.

[35] S. M. Hedetniemi, A. Proskurowski, and M. M. Sysło, "Interior graphs of maximal outerplane graphs," *J. Combinatorial Theory*, vol. Series B 38, no. 2, pp. 156–167, 1985.

[36] E. Klavins, R. Ghrist, and D. Lipsky, "Graph grammars for self assembling robotic systems," in *Int. Conf. Robot. Autom.*, IEEE, vol. 5, 2004, pp. 5293–5300.

[37] ——, "A grammatical approach to self-organizing robotic systems," *IEEE Trans. Autom. Control*, vol. 51, no. 6, pp. 949–962, 2006.

[38] J. Graver, B. Servatius, and H. Servatius, "Combinatorial rigidity," in. 1993.

[39] G. Laman, "On graphs and rigidity of plane skeletal structures," *J. Eng. Math.*, vol. 4, pp. 331–340, 4 1970.

[40] H. Gluck, "Almost all simply connected closed surfaces are rigid," *Lecture Notes in Math*, vol. 438, pp. 225–239, 1975.

[41] L. Asimow and B. Roth, "The rigidity of graphs," in *Trans. Amer. Math. Soc.*, vol. 245, 1978, pp. 249–289.

[42] ——, "The rigidity of graphs II," *J. Math. Anal. Applicat.*, vol. 68, no. 1, pp. 171–190, 1979.

[43] B. Roth, "Rigid and flexible frameworks," *The Amer. Math. Monthly*, vol. 88, no. 1, pp. 6–21, 1981.

[44] B. Hendrickson, "Conditions for unique graph realizations," *SIAM J. Computing*, vol. 21, no. 1, pp. 65–84, 1992.

[45] B. D. O. Anderson, C. Yu, B. Fidan, and J. M. Hendrickx, "Rigid graph control architectures for autonomous formations," *IEEE Control Syst. Mag.*, vol. 28, no. 6, pp. 48–63, 2008.

[46] T. Eren, P. N. Belhumeur, B. D. O. Anderson, and A. S. Morse, "A framework for maintaining formations based on rigidity," *IFAC Proc. Volumes*, vol. 35, no. 1, pp. 499–504, 2002.

[47] T.-S. Tay and W. Whiteley, "Generating isostatic frameworks," *Structural Topology*, 1985.

[48] Z. Sun, S. Mou, B. D. O. Anderson, and M. Cao, "Exponential stability for formation control systems with generalized controllers: A unified approach," *Syst. Control Lett.*, vol. 93, pp. 50–57, 2016.

[49] R. Olfati-Saber and R. M. Murray, "Graph rigidity and distributed formation stabilization of multi-vehicle systems," in *Conf. Decision and Control*, IEEE, vol. 3, 2002, pp. 2965–2971.

[50] Z. Sun, U. Helmke, and B. D. O. Anderson, "Rigid formation shape control in general dimensions: An invariance principle and open problems," in *Conf. Decision Control*, IEEE, 2015, pp. 6095–6100.

[51] D. Zelazo, A. Franchi, F. Allgöwer, H. H. Bülthoff, and P. R. Giordano, "Rigidity maintenance control for multi-robot systems," in *Robotics: Sci. Syst.*, 2012, pp. 473–480.

[52] D. Zelazo, A. Franchi, H. H. Bülthoff, and P. Robuffo Giordano, "Decentralized rigidity maintenance control with range measurements for multi-robot systems," *Int. J. of Robotics Research*, vol. 34, no. 1, pp. 105–128, 2015.

[53] S. Zhao and D. Zelazo, "Bearing-based formation maneuvering," in *Int. Symp. Intell. Control*, IEEE, 2015, pp. 658–663.

[54] M. H. Trinh, K.-K. Oh, K. Jeong, and H.-S. Ahn, "Bearing-only control of leader first follower formations," *IFAC-PapersOnLine*, vol. 49, no. 4, pp. 7–12, 2016.

[55] N. Shiell and A. Vardy, "A bearing-only pattern formation algorithm for swarm robotics," in *Int. Conf. Swarm Intell.*, Springer, 2016, pp. 3–14.

[56] D. Zelazo, A. Franchi, and P. R. Giordano, "Rigidity theory in SE(2) for unscaled relative position estimation using only bearing measurements," in *European Control Conf.*, IEEE, 2014, pp. 2703–2708.

[57] S. Zhao and D. Zelazo, "Bearing rigidity and almost global bearing-only formation stabilization," in *Trans. Autom. Control*, vol. 61, IEEE, 2016, pp. 1255–1268.

[58] G. Michieletto, A. Cenedese, and A. Franchi, "Bearing rigidity theory in SE(3)," in *Conf. Decision and Control*, IEEE, 2016, pp. 5950–5955.

[59] T. Eren, W. Whiteley, A. S. Morse, P. N. Belhumeur, and B. D. O. Anderson, "Sensor and network topologies of formations with direction, bearing, and angle information between agents," in *Conf. Decision and Control*, IEEE, vol. 3, 2003, pp. 3064–3069.

[60] F. Schiano and P. R. Giordano, "Bearing rigidity maintenance for formations of quadrotor UAVs," in *Int. Conf. Robot. Autom.*, IEEE, 2017, pp. 1467–1474.

[61] T. Eren, "Formation shape control based on bearing rigidity," *Int. J. of Control*, vol. 85, no. 9, pp. 1361–1379, 2012.

[62] A. Franchi and P. R. Giordano, "Decentralized control of parallel rigid formations with direction constraints and bearing measurements," in *Conf. Decision Control*, IEEE, 2012, pp. 5310–5317.

[63] D. Zelazo, P. R. Giordano, and A. Franchi, "Bearing-only formation control using an SE(2) rigidity theory," in *Conf. Decision Control*, IEEE, 2015, pp. 6121–6126.

[64] S. Zhao and D. Zelazo, "Bearing-based distributed control and estimation of multi-agent systems," in *European Control Conf.*, IEEE, 2015, pp. 2202–2207.

[65] E. Klavins, "Automatic synthesis of controllers for distributed assembly and formation forming," in *Int. Conf. Robot. Autom.*, vol. 3, IEEE, 2002, pp. 3296–3302.

[66] M. Sharf and D. Zelazo, "A network optimization approach to cooperative control synthesis," *IEEE Control Syst. Lett.*, vol. 1, no. 1, pp. 86–91, 2017.

[67] V. Gupta, B. Hassibi, and R. M. Murray, "A sub-optimal algorithm to synthesize control laws for a network of dynamic agents," *Int. J. Control*, vol. 78, no. 16, pp. 1302–1313, 2005.

[68] Y. Liu and Z. Geng, "Finite-time formation control for linear multi-agent systems: A motion planning approach," *Syst. Control Lett.*, vol. 85, pp. 54–60, 2015.

[69] J. Alonso-Mora, S. Baker, and D. Rus, "Multi-robot formation control and object transport in dynamic environments via constrained optimization," *Int. J. Robot. Research*, vol. 36, no. 9, pp. 1000–1021, 2017.

[70] Z. Li, W. Yuan, Y. Chen, F. Ke, X. Chu, and C. L. P. Chen, "Neural-dynamic optimization-based model predictive control for tracking and formation of nonholonomic multirobot systems," *IEEE Trans. Neural Netw. Learn. Syst.*, vol. 29, no. 12, pp. 6113–6122, 2018.

[71] T. H. Summers, C. Yu, S. Dasgupta, and B. D. Anderson, "Control of minimally persistent leader-remote-follower and coleader formations in the plane," *Trans. Autom. Control*, vol. 56, no. 12, pp. 2778–2792, 2011.

[72] A. D. Ames and M. Powell, "Towards the unification of locomotion and manipulation through control lyapunov functions and quadratic programs," in *Control Cyber-Physical Systs.* Springer, 2013, pp. 219–240.

[73] A. D. Ames, J. W. Grizzle, and P. Tabuada, "Control barrier function based quadratic programs with application to adaptive cruise control," in *Conf. Decision Control*, IEEE, 2014, pp. 6271–6278.

[74] X. Xu, T. Waters, D. Pickem, P. Glotfelter, M. Egerstedt, P. Tabuada, J. W. Grizzle, and A. D. Ames, "Realizing simultaneous lane keeping and adaptive speed regulation on accessible mobile robot testbeds," in *Conf. Control Tech. Applicat.*, IEEE, 2017, pp. 1769–1775.

[75] P. Glotfelter, I. Buckley, and M. Egerstedt, "Hybrid nonsmooth barrier functions with applications to provably safe and composable collision avoidance for robotic systems," *Robot. Autom. Lett.*, vol. 4, no. 2, pp. 1303–1310, 2019.

[76] G. Notomista and M. Egerstedt, "Constraint-driven coordinated control of multi-robot systems," in *Amer. Control. Conf.*, IEEE, 2019.

[77] R. Olfati-Saber, "Near-identity diffeomorphisms and exponential epsilon-tracking and epsilon-stabilization of first-order nonholonomic SE(2) vehicles," in *Amer. Control Conf.*, IEEE, vol. 6, 2002, pp. 4690–4695.

[78] G. Jing, G. Zhang, H. W. J. Lee, and L. Wang, "Angle-based shape determination theory of planar graphs with application to formation stabilization," *Automatica*, vol. 105, pp. 117–129, 2019.

[79] R. Webster, "Convexity," in. 1994.

[80] T. Biedl, "On triangulating k-outerplanar graphs," *Discrete Appl. Math.*, vol. 181, pp. 275–279, 2015.

[81] H. J. Fleischner, D. P. Geller, and F. Harary, "Outerplanar graphs and weak duals," *J. Indian Math. Soc.*, vol. 38, no. 1-4, pp. 215–219, 1974.

[82] J. McNew, E. Klavins, and M. Egerstedt, "Solving coverage problems with embedded graph grammars," in *Int. Workshop Hybrid Syst.: Comput. Control*, Springer, 2007, pp. 413–427.

[83] B. Servatius and W. Whiteley, "Constraining plane configurations in computer-aided design: Combinatorics of directions and lengths," *SIAM J. Discrete Math.*, vol. 12, no. 1, pp. 136–153, 1999.

[84] A. N. Bishop, T. H. Summers, and B. D. O. Anderson, "Stabilization of stiff formations with a mix of direction and distance constraints," in *Int. Conf. Control Appl.*, IEEE, 2013, pp. 1194–1199.

[85] A. N. Bishop, M. Deghat, B. D. O. Anderson, and Y. Hong, "Distributed formation control with relaxed motion requirements," *Int. J. Robust Nonlinear Control*, vol. 25, no. 17, pp. 3210–3230, 2015.

[86] K. Fathian, D. I. Rachinskii, M. W. Spong, and N. R. Gans, "Globally asymptotically stable distributed control for distance and bearing based multi-agent formations," in *Amer. Control Conf.*, IEEE, 2016, pp. 4642–4648.